From the Surgical Department of the Medical Faculty Mannheim
(Director: Prof. Dr. med. Christoph Reissfelder)

Proteome Profiling of Pancreatic Ductal Adenocarcinoma and Specific Detection of Kallikrein Proteases -6 and -10 by Targeted and Explorative Mass Spectrometry

Inaugural Dissertation
For the Award of the Doctoral Degree in Medicine
of the
Medical Faculty Mannheim
of the Ruprecht-Karls-University
at
Heidelberg

Submitted by
Janina Juliette Werner

from
Munich
2023

Dean: Prof. Dr. med. Sergij Goerdt
Referent: Prof. Dr. med. Felix Rückert

Table of Contents

Page

1 LIST OF ABBREVIATIONS

AC	Ampullary cancer
ACN	Acetonitrile
AGC	Automatic gain control
BCA	Bicinchoninic acid
BPE	Bovine pituitary extract
CA 19-9	Carbohydrate antigen 19-9
CCM	Cell conditioned medium
CID	Collision-induced dissociation
CP	Chronic pancreatitis
DDA	Data-dependent acquisition
DIA	Data-independent acquisition
DMEM	Dulbecco's modified eagle medium
DPBS	Dulbecco's phosphate buffered saline
DTT	Dithiothreitol
ECM	Extracellular matrix
EDTA	Ethylenediamine tetraacetic acid
EGF	Epidermal growth factor human recombinant
ELISA	Enzyme-linked immunosorbent assay
EMT	Epithelial mesenchymal transition
ER	Endoplasmic reticulum
ESI	Electrospray-ionization
FA	Formic acid
FBS	Fetal bovine serum
FDR	False discovery rate
FFPE	Formalin-fixed paraffin-embedded
GAPDH	Glyceraldehyde-3-phosphate dehydrogenase
GPF	Gas-phase fractionation
HE	Hematoxylin and eosin
HEPES	4-(2-hydroxyethyl)-1-piperazineethanesulfonic acid
IAA	Iodoacetamide
iRT	Indexed retention time
KLK	Kallikrein
KSFM	Keratinocyte-serum-free medium

LC	Liquid chromatography
m/z	Mass-to-charge ratio
MALDI	Matrix-assisted laser desorption/ionization
MEG	Monoethylene glycol
MES	2-Morpholinoethanesulfonic acid monohydrate
MS	Mass spectrometry
NCE	Normalized collision energy
NMAP	Non-malignant adjacent pancreas
NNMC	Normal non-malignant control
NP	Normal pancreas
P/S	Pen strep
PaCaDD	Pancreatic cancer dresden
PDAC	Pancreatic ductal adenocarcinoma
PRM	Parallel reaction monitoring
PSA	Prostate-specific antigen
RG	RapiGest
RPMI	Roswell park memorial institute
RT	Retention time
SDS	Sodium dodecyl sulfate
SFM	Serum-free medium
SP3	Single-pot solid-phase-enhanced-enhanced sample preparation
sPLS-DA	Sparse partial least squares discriminant analysis
SRM	Selected reaction monitoring
TCEP	Tris(2-carboxyethyl)phosphine hydrochloride
TFA	Trifluoroacetic acid
TRIS	Tris(hydromethyl)aminomethan
TSQ	Triple-stage quadrupole
vs.	Versus

2 INTRODUCTION

2.1 Pancreatic Ductal Adenocarcinoma (PDAC)

Pancreatic ductal adenocarcinoma (PDAC) originates from the pancreas' exocrine glands and represents the most common type of pancreatic cancer, counting for more than 90 % of cases [1]. There are many risk factors for developing PDAC, one of which is chronic pancreatitis, where recurrent, highly inflammatory episodes in the pancreatic tissue are present [2]. PDAC is associated with an abysmal prognosis, resulting in a 5-year-survival rate of only 2-9 % [3, 4]. Due to the lack of early symptoms and therefore a late presentation of the disease, merely 20 % of patients are suitable for surgical resection at the time of diagnosis, which is the only possible curative approach by now [5]. Whilst upfront resection followed by adjuvant chemotherapy represents the current standard of care, it could be shown that adjuvant chemotherapy improves the median overall survival, although remaining at an inferior survival of 28 months [6]. Patients diagnosed with borderline resectable PDAC are recommended to undergo neoadjuvant chemotherapy in order to initially decrease the tumor size and to improve negative resection margin rates (R0) during surgery [7, 8]. Nevertheless, neoadjuvant treatment is still not commonly applied [8]. However, most patients receive palliative treatment because they already present a metastatic stage [4].

The most widely used conventional biomarker for PDAC is carbohydrate antigen 19-9 (CA 19-9), which plays a vital role for follow-up after therapy. However, CA 19-9 is not appropriate for screening a general population or individuals [9]. These findings indicate an urgent need for further research and identification of new biomarkers which enable early diagnosis.

2.2 The Human Tissue Kallikrein Family

One example for a well-established protein biomarker is the prostate-specific antigen (PSA) in prostate cancer, which has already been routinely applied for decades [10]. Due to its increased serum levels in prostate cancer patients, it serves as a powerful diagnostic marker and as an essential follow-up parameter during monitoring. PSA represents one member of the human tissue kallikrein family and is also known as human kallikrein 3 (KLK3). Because of multiple functional similarities between KLK3/PSA and other kallikreins of the family, it is suggested that some of the remaining KLKs may also be valuable as a potential biomarker [10]. Including KLK3/PSA, the

kallikrein family consists of 15 secreted serine proteases, appearing in several different tissues and biological fluids [11]. Some kallikreins are known to participate in multiple physiological processes as the regulation of blood pressure, electrolyte balance, tissue remodeling and skin desquamation. As KLKs are also key players in essential cellular functions such as tissue remodeling, migration, proliferation and angiogenesis, dysfunction and dysregulation of kallikreins may lead to major implications and pathological conditions such as hypertension and inflammatory cascades or even cancer [12, 13].

All human kallikreins are intracellularly produced as preproenzymes, which are further processed to secreted proenzymes by proteolytically removing the signal peptide. The catalytically inactive proenzymes are then converted into the active, mature form of the protease by an additional proteolysis step in the extracellular space [11, 14]. It is suggested that some kallikreins (KLK4, 5, 11, 12, and 14) can activate almost all residuary members of the family. Hence, they could be seen as “general activators” of the whole kallikrein family [14]. Whilst some KLKs show potential to activate each other, some are implicated in auto-activation or may be involved in cross-talks with other serine proteases or metalloproteases (see **Figure *1***). Vitally important is the fact, that all findings concerning the “KLK activome” are deriving from *in vitro* research [13]. Hence, by gaining more information about the *in vivo* activome of kallikreins and their substrates, more detailed knowledge about physiological and pathological roles of kallikreins needs to be provided.

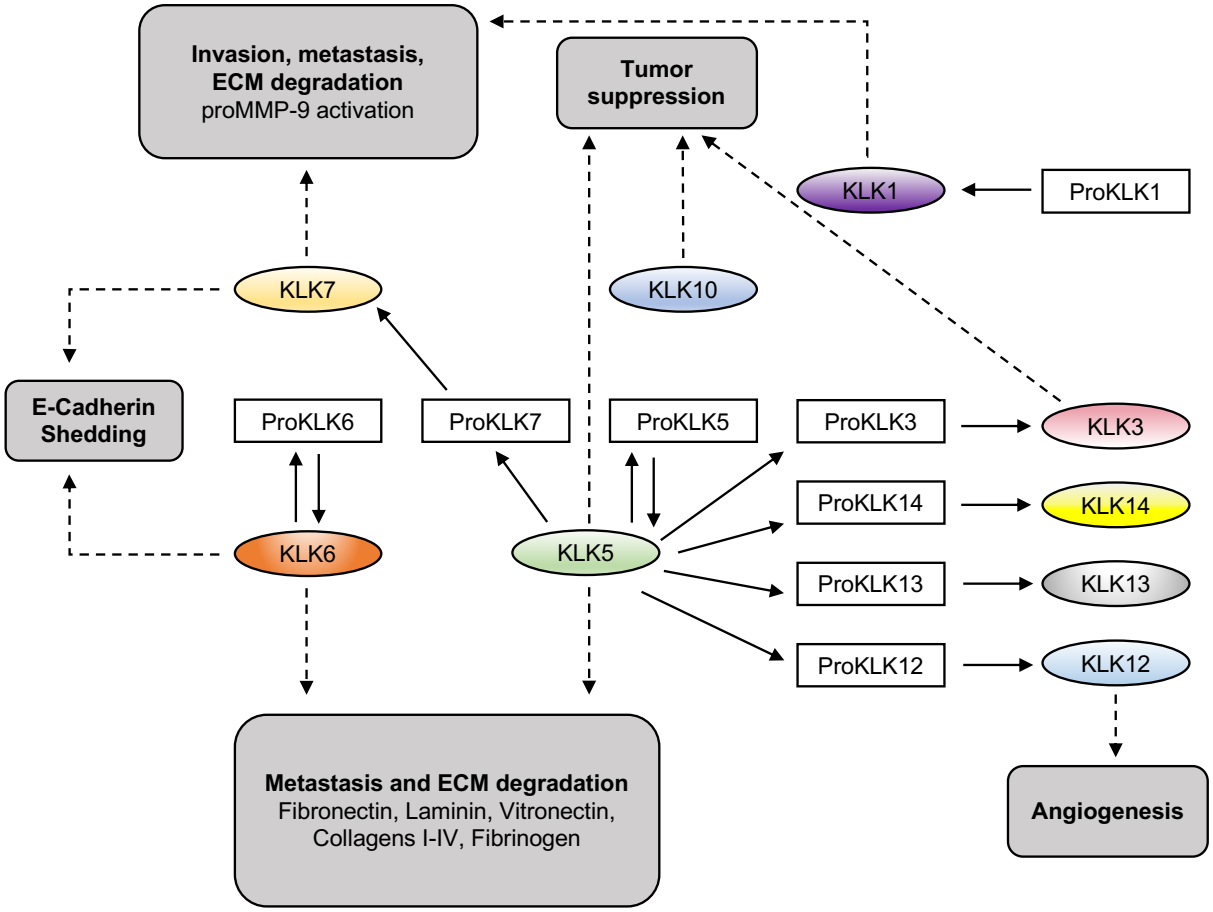

Figure 1: Simplified Overview of proposed KLK Activation and Involvement in Cancer. Some KLKs mostly activate residuary members of the family, as others can execute auto-activation. Certain KLKs seem to be involved in several pathways leading to different processes, for example extracellular matrix (ECM) degeneration and invasion/metastasis (KLK1, KLK5, KLK6, KLK7), tumor suppression (KLK3, KLK5, KLK10), promoting angiogenesis (KLK12). Continuous lines represent activation processes, whereas doted lines show pleiotropic effects of KLKs. Figure was adapted from [15].

2.3 Kallikrein Expression and Function in PDAC

Interestingly, the name “kallikrein” derives from the greek word for pancreas (“Kallikreas”), owing to the original finding of human kallikrein 1 (KLK1) as an abundant protein in the pancreas [16] KLK1 is expressed in normal pancreatic tissue, and it could be shown that expression levels of KLK1 are comparable between normal pancreatic tissue and cancerous tissue [17, 18]. Nevertheless, other members of the kallikrein family have been found to be highly overexpressed in pancreatic cancer at the transcriptomic and proteomic level. Among the most upregulated genes within pancreatic cancer are KLK6 and KLK10, both of which show high expression in PDAC compared to normal and benign pancreatic tissues [17, 19-22]. Besides the significant upregulation of KLK6 and KLK10 in pancreatic cancer, elevated levels of KLK6, KLK7, KLK8, KLK10 and KLK11 seem to correlate with a significant poorer overall survival of patients diagnosed with

PDAC [20, 21, 23, 24]. The combination of both KLK upregulation linked to poor prognosis suggests these kallikreins to be an essential protein for cancer progression and thereby represents a promising diagnostic or even therapeutic target for PDAC patients.

Regarding one of the most upregulated kallikreins in pancreatic cancer, namely KLK10, a study found that immunohistochemical KLK10 expression of human PDAC tissue was significantly higher in a group of patients with metastasis as in the metastasis-free group, assuming an aberrant expression pattern of KLK10 within malignant transformation of PDAC (Cao et al. 2018). In the literature, however, KLK10 has been attributed a possible role as a tumor suppressor [25]. It was demonstrated that KLK10 is downregulated in most breast cancer and prostate cancer cell lines, giving strong evidence that KLK10 may play a role as a tumor suppressor in these cancer entities [11, 13, 26, 27]. Nevertheless, despite all efforts concerning structural characteristics, natural substrates, and the exact function of KLK10, its specific roles in physiological and pathological pathways and the contribution to pancreatic carcinogenesis remain mostly unexplained.

With regard to the other kallikrein which is highly overexpressed in pancreatic cancer, KLK6 mRNA expression appears to be dependent on tumor areas within a PDAC tissue section, with higher KLK6 levels in invasive tumor areas, while non-invasive tumor areas have significantly lower KLK6 mRNA levels [24]. This observation strongly leads to the suggestion of KLK6 contributing to the invasiveness of PDAC. As an upregulation of several kallikreins (KLK5, KLK6 and KLK7) could also be observed within colon cancer tissue compared to its normal counterpart [17], a recent study investigated the cellular functions of KLK6 in colon adenocarcinoma, revealing that its proteolytic activity was directly related to the invasiveness of the cells [28]. Although the exact role of KLK6 in tumorigenesis has not been discovered yet, these findings strongly implicate a contribution of KLK6 to the invasiveness and progression of both colon and pancreatic adenocarcinoma.

In vitro studies further suggested KLK6 to be implicated in the degradation of several proteins of the extracellular matrix (ECM), such as fibrinogen and collagen type I, as well as collagen type IV, the latter representing a major part of the basement membrane [29]. In addition, KLK6 was further described to be able to rapidly degrade rat plasma fibronectin; likewise, mouse laminin showed rapid degradation upon prolonged

incubation with KLK6 [30]. This strongly suggests that KLK6 might facilitate tumor cell migration.

It is widely accepted, that cleaving components of the ECM facilitates tumor cell growth and malignant transformation. KLK6 is therefore considered to be actively involved in tissue remodeling, tumor invasion and metastasis [12, 29]. Consistent with the assumption that KLK6 is involved in cancer progression, Klucky et al. showed that E-cadherin levels are dependent on KLK6 expression, leading to the suggestion of KLK6 cleaving E-cadherin either directly or indirectly [31]. Interestingly, the same observation was made for KLK7, as it could be shown to proteolytically cleave E-cadherin using *in vitro* assays [32]. As E-cadherin represents one of the most essential junction molecules, its loss on the cell surface results in less cell-cell adhesion, thus promoting cell proliferation, migration, and invasion [31]. These findings strongly suggest E-cadherin being a potential substrate for KLK6 and KLK7 and facilitating tumor invasiveness in pancreatic cancer through disruption of cell-cell junctions.

Besides the aim of identifying novel diagnostic and/or prognostic biomarkers for pancreatic cancer, there is a great need for more effective treatment options, which still require improvement. Due to the upregulation of several kallikreins in PDAC, some of them were not only suggested as a tumor marker, but also as new therapeutic targets. KLK7 could represent such novel chemotherapeutic target for pancreatic cancer, due to the finding of KLK7 (mRNA and protein levels) being strongly upregulated in pancreatic cancer compared to normal and adjacent tissue [32, 33]. The fact that KLK7 was not detectable in tissue sections of normal pancreatic tissue could also be confirmed in previous reports [23, 34]. Interestingly, another study even reported a correlation between increased KLK7 expression and shorter overall survival of patients, suggesting KLK7 to play an active role in the development of pancreatic cancer [23]. Due to the observation of KLK7 being significantly upregulated in pancreatic cancer and its correlation with a shorter overall survival, KLK7 represents a promising therapeutic target for PDAC. Nevertheless, even though KLK7 could be shown to belong, besides KLK6 and KLK10, to the most highly upregulated kallikreins within pancreatic cancer, PDAC is still lacking a specific and sensitive tumor marker for clinical use, as well as effective therapeutic strategies.

The above-mentioned reports were partly carried out at the transcriptome level. In contrast to the transcriptome, however, proteins carry out the actual function. Since

they further provide essential structural and functional duties as they are responsible for cell movement, communication, reproduction, and other vitally important pathways, cellular life is depending on intact protein activity and their correct function [35]. Dysfunction of proteins or disturbed protein expression may therefore lead to defective signaling cascades and protein pathways, representing a major cause of disease development. The entirety of proteins encoded by the genome expressed in a biological system to a certain time point is described as the “proteome” [36]. In contrast to genomic information which doesn’t vary substantially over time, the proteome of an organism is dynamically changing at different stages of activity or development [37]. Besides the fact, that the number of proteins within a proteome of an organism highly outreaches the number of genes within an organism, it thereby represents a far more complex research field of research and provides great potential in discovering proteins used for drug targets or novel protein markers for diagnostic or prognostic purpose [35, 38]. In addition, since information on protein expression has been described to be more valuable than that of mRNA expression [39], it is important to research directly at the level of the proteome.

Moreover, all the above-mentioned reports about KLK protein detection in pancreatic cancer were performed with either Western Blot or immunohistochemistry analysis. Since, to our knowledge, there is no report yet on the detection of KLK proteins in PDAC by mass spectrometry, the current study includes mass spectrometric analyses of both cell conditioned medium (CCM) of pancreatic cancer cells and PDAC FFPE tissue at the protein level.

2.4 Mass Spectrometry-based Proteomics

Mass spectrometry (MS) represents a very powerful and versatile tool in large-scale proteomic analysis [40]. Therefore, the aim of global MS-based proteomics is to get an overview of a large set of proteins expressed within a functional context [41]. Its technology is based on the measuring of precise molecular masses of ionized peptides in relation to their charge (m/z), which further enables protein identification, characterization, and quantification [40]. To distinguish between proteins with the same masses, or to find isoforms of a protein, there have been two approaches established: The “top-down” method describes the direct measuring of intact proteins. The “bottom-up” method analyses peptides obtained from proteolytic digestion of proteins, which

further allow to make suggestions about the initial protein behind it [42]. In this project, we used the “bottom-up” approach for proteomic analyses.

2.5 Standard MS-proteomics Experiment

The standard MS-proteomics experiment consists of several stages (see **Figure 2**) [41]. First, the proteins of interest need to be extracted from the sample. Hence, the proteins are undergoing proteolytical digestion, mostly by using trypsin [42]. Subsequently, the peptide mixture is separated by reversed phase liquid chromatography (LC) in order to reduce the complexity of the peptide mixture reaching the detector at each time point. The separation of peptides is based on their hydrophobicity by applying an increasing acetonitrile gradient, forcing the digested peptides to elute at different retention times from the hydrophobic matrix. To ensure and monitor the reproducibility of the liquid chromatography, commercially available spiked-in indexed retention time (iRT) reference peptides are used, which elute at predefined time points over the whole chromatographic gradient [43]. For peptide ionization, the most commonly used method is electrospray ionization (ESI), where individual ionized peptides are ready to enter the mass spectrometer [44]. Once the ionized peptides reached the mass spectrometer, the peptide ions (so-called precursor ions) are separated dependent on their m/z value. The precursor ions are now guided through a first mass filter (e.g. a quadrupole), which only selects individual precursor ions of a certain m/z value. By scanning through the whole m/z-range, a mass spectrum of all present precursor ions (MS1) is captured [45]. One specific precursor or a small group of precursors is further selected for subsequent fragmentation in a gas-filled collision cell. Here, the precursor ions undergo random fragmentation due to colliding with gas particles, mostly helium. This technique is referred to as collision-induced dissociation (CID), which is the most commonly used method for peptide fragmentation [46]. Subsequently, the resulting fragments, representing the peptide sequence, were analyzed again based on their m/z values, thereby generating an MS2 spectrum. Such an ability to capture two mass spectra is commonly referred to as “tandem mass spectrometry” (MS/MS), including the mass spectrum of the precursor ion, MS1, and its fragments, MS2 [45].

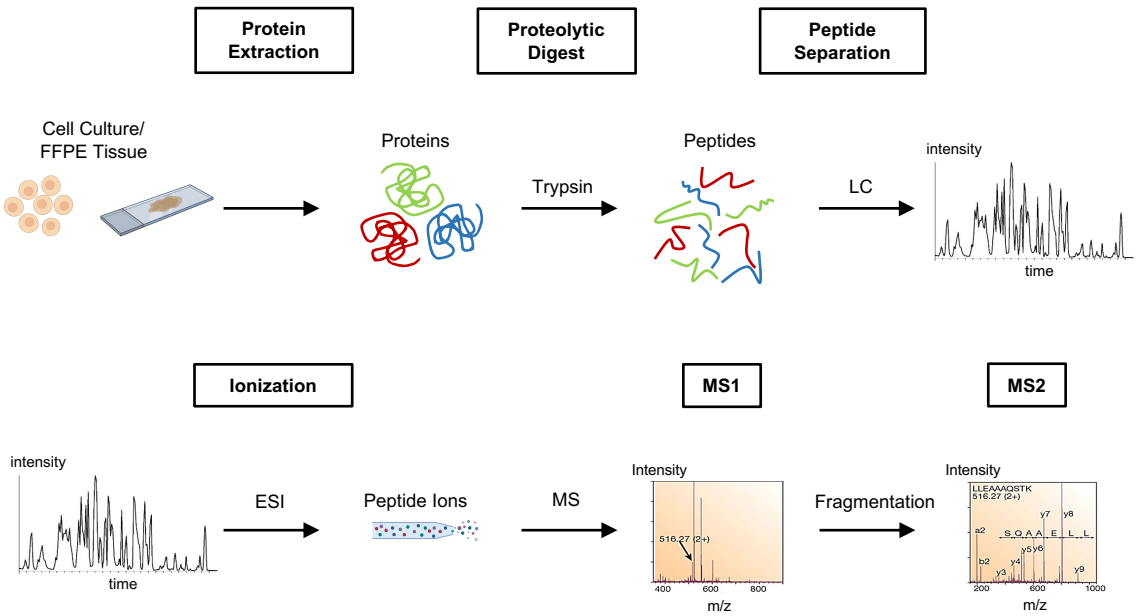

Figure 2: General Mass Spectrometric Workflow of Bottom-up Protein Analysis. Proteins of interest are extracted from cells or FFPE tissue. After proteolytic digest (most commonly by trypsin), the generated peptides are subjected to Liquid chromatography (LC) and are separated based on their hydrophobicity in order to reduce sample complexity. The specific peptides eluting at the corresponding retention times (RT) are undergoing electrospray ionization (ESI) and enter the mass spectrometer. Subsequently, MS1 spectrum is generated by analyzing the m/z values of the specific precursor ions. Further selection and fragmentation of a certain precursor ion reveals the MS2 spectrum. Figure was adapted from [47] and [41]. Parts of the Figure were created with the publicly accessible website biorender.com.

2.6 Targeted Proteomics versus Explorative Proteomics

Mass spectrometry is the method of choice for identifying, characterizing and quantifying either individual proteins or the entire proteome of an organism, whereby there are two approaches facing these investigations [42]. In targeted proteomics, the proteins of interest and their amino acid sequence needs to be already known. Therefore, this strategy requires a pre-defined list of proteolytical peptides representing the proteins to be analyzed [45]. Furthermore, prior to each MS measurement, heavy isotope-labelled synthetic peptide standards are added to the samples to account for any technical variances of MS performance. This heavy isotope-labelling of peptides enables differentiation from the unlabeled, endogenous peptide, which is important for subsequent data analysis and correct chromatographic peak picking. By adding the same amount of heavy labelled peptides to all samples, they can further be used to normalize the abundance of the same endogenous peptide between samples. The other approach is called explorative or shotgun proteomics, which is not looking at predefined, individual proteins, but rather at the entirety of proteins within one sample [48]. As targeted proteomics requires information about the proteins of interest before each measurement, no prior knowledge (except of the

organism the sample derives from) is necessary for explorative proteomics [45]. Furthermore, targeted MS shows the potential to enable the detection of lower abundant proteins in a complex sample, since it specifically focuses on the pre-defined proteins. As explorative proteomics is measuring the whole proteome within one sample, this high complexity leads to a reduced sensitivity and thereby less abundant proteins may not be caught [45]. As both methods have their advantages and disadvantages and are applied in different settings, it becomes clear that mass spectrometry is a broadly versatile field of research and does not consist of one monolithic method.

For targeted MS, the triple quadrupole mass spectrometer monitors pairs of precursor-fragment ions, which is referred to as transition. Hereby, the list of transitions needs to be determined prior to analysis. Since there are several precursors owing the identical or very similar m/z values, the precursor selection in the first quadrupole may not be sufficient for unambiguous identification. By applying a second m/z filter and therefore detecting both the precursor ion and its specific fragment ion, the sensitivity and selectivity are substantially increased [38]. Since only the selected peptides are subjected to analysis, this method is referred to as selected reaction monitoring (SRM) [49].

Unlike SRM, which only detects one transition at a time, another method called parallel reaction monitoring (PRM) is able to simultaneously analyze the entirety of fragment ions passing the last m/z filter (see **Figure *3***). It therefore performs a parallel monitoring of all fragment ions deriving from the corresponding precursor ion [49]. Although both methods require prior definition of which precursor peptides need to be selected, PRM does not need specifications of the selected fragments, as it monitors all fragment ions.

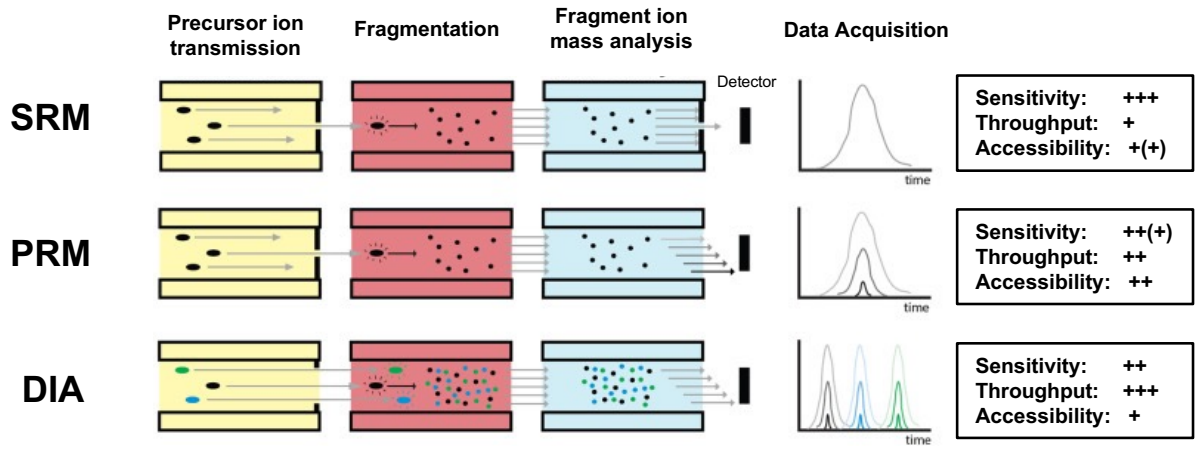

Figure 3: Comparison of SRM, PRM and DIA Analysis. The principle of all three methods is consistent: After transmission of specific precursor ions, they are undergoing fragmentation before further mass analysis of the fragments and subjecting them to the detector. SRM acquisition mode is mostly using features of a triple quadrupole instrument (Q1-Q3). The first quadrupole (Q1) is transmitting a specific precursor ion for further fragmentation in Q2, followed by another mass filter (Q3) only transmitting a fragment with a certain m/z to the detector. As for SRM, the PRM method selects precursor ions of interest by the first mass filter, which are then fragmented and accumulated in an ion trap before subjecting them to analysis in the orbitrap mass analyzer. In contrast to SRM and PRM, the DIA mode does not select specific precursor ions but instead measures all precursors in predefined m/z windows in the first mass analyzer/filter, which are all undergoing further fragmentation, and, like PRM, are subjected to an ion trap followed by analysis in the orbitrap. Scoring for sensitivity, throughput, and accessibility is depicted in the right boxes. Figure was adapted from [50].

With respect to targeted acquisition strategies, both the SRM and PRM method have contributed to an enormous success in the field of protein identification [51]. Nevertheless, both SRM and PRM require prior knowledge about the proteins of interest, whereas gaining information about other targets is not intended. An acquisition method based on explorative (shotgun) MS, which enables the quantification of a larger set of proteins, is the so-called data-dependent acquisition (DDA) method. Here, the top *n* highest signal intensities in MS1 are selected for subsequent fragmentation and further analysis (MS2) [52]. Although the DDA mode enables the identification of a significant number of proteins, it also has several limitations. One major disadvantage is the exclusive consideration of the most abundant peptides, whereas only a certain number of low abundant peptides are being identified. This huge drawback of DDA makes it challenging to identify rarely abundant proteins, as for example members of the kallikrein family. To overcome these limitations, alternative data acquisition methods, like the data-independent acquisition (DIA), have emerged. In contrast to DDA, DIA is based on predetermined specific mass windows, in which all ionized peptides are further being fragmented and analyzed (see **Figure *3***) [52]. This results in the ability to not only cover the most abundant proteins, as referred to in DDA measurements, but to cover a larger extent of the proteome of the measured samples. Besides the improved proteome coverage, accuracy of peptide

identification is increased by cross-reference with a spectral library, composed of pooled samples from the cohort [52]. In the end of either acquisition mode, the generated tandem mass spectra (MS/MS) including information about peptide sequence and abundance are generally matched against a proteome sequence database, to map these sequences to the corresponding proteins. The resulting list, which consists of numerous identified proteins and their signal intensities corresponding to their abundance, is then used for further data analysis.

For quantification, the most commonly used approach is relative protein quantification [53]. By summarizing all quantitative protein information during the entire LC-MS run, statistical analysis can be performed, giving us further information about differentially expressed proteins between the samples analyzed [53]. As different conclusions about protein abundance can be drawn, however, no information about absolute quantification is being obtained, as therefore an absolutely quantified reference would be needed.

2.7 MS-based KLK Detection in Pancreatic Cancer

To date, up to our knowledge, there are no reports existing about targeted MS analysis of secreted kallikrein proteins in CCM of pancreatic cancer cell lines. A previous study using KLK-specific ELISAs found elevated levels of KLK5, KLK6, KLK7, KLK8, KLK9, KLK10 and KLK13 in CCM of the pancreatic cancer cell line MiaPaCa-2, which was also included in our project [54]. Interestingly, among these constitutively secreted kallikreins, KLK5 and KLK6 showed relatively high protein levels, closely followed by KLK7. Although human cell lines represent a great possibility to simulate the tumor microenvironment *in vitro*, working with formalin-fixed paraffin-embedded (FFPE) tissue provides us with a more valuable resource for biomedical research [55]. Due to a superior preservation of proteins, FFPE samples can be stored for decades and are still suitable for clinical research [56]. To date, MS-based proteomic studies of FFPE tissues are commonly used in the biomedical research field, aiming to identify new biomarkers which are convenient for clinical use. A proteomic comparison using explorative (shotgun) MS to compare the proteomes of benign and malignant pancreatic tissues showed several candidate proteins to be exclusively expressed within the distinct entities, however, among these proteins, no kallikreins were detected [57]. This finding goes in line with a study comparing the expression profiles of PDAC FFPE tissues with tissues of non-malignant adjacent pancreas and benign

pancreatic cystadenoma by using tandem MS [58]. However, they reported a similar profile expression pattern for both benign tissues pancreatic cystadenoma and non-malignant adjacent pancreas, compared to the proteome of PDAC [58]. This interesting fact is suggesting a substantial separation of proteomes from benign and malignant pancreatic diseases.

Up to now, very few studies regarding MS-based proteomic analysis of conditioned pancreatic cancer cell media and PDAC FFPE tissues have been reported. This emphasizes the necessity to look more closer into the KLK expression in pancreatic cancer, which we aim to pursue with this thesis.

2.8 Aim of Project

As some KLKs seem to play a role in pancreatic carcinogenesis, the aim of this project is to detect KLKs in CCM of pancreatic cancer cell lines as well as in patient-derived tissues of PDAC. Thereby, we mainly focus on KLK6 and KLK10, as they are the most commonly known upregulated KLKs in PDAC. Nevertheless, we are also interested in the other kallikreins of the family, as some of them seem to be overexpressed within PDAC as well. Many reports on KLK research refer to kallikrein transcriptomics or KLK protein expression investigated via methods such as Western Blot and immunohistochemistry analyses. In this project, however, we focus on the detection and relative quantification of KLK proteins by both targeted and explorative (shotgun) MS in CCM of pancreatic cancer cell lines as well as in FFPE tissue samples.

As part of the protocol optimization, we aim to establish a robust and reproducible sample preparation workflow enabling the maximal signal for KLK proteins. Using the single-pot solid-phase-enhanced sample preparation (SP3) bead method, we can simultaneously work with both high volumes and low protein concentrations, which is suitable for MS preparation of CCM as well as FFPE tissue samples. In addition, we examine the optimal bead type and amount to ensure the best possible KLK enrichment and detection of KLKs by MS. An SRM assay for all fifteen KLKs was established, including isotope-labelled reference peptides and an internal protein standard to account for technical variance.

The second aim is to simulate the tumor microenvironment *in vitro* by culturing of pancreatic cancer cell lines. To compare the KLK secretion levels of different pancreatic cancer cell lines, we include cell lines from different origins, as well as

primary cell lines, the latter most closely representing the tissue of origin. Here, we apply targeted MS analysis of all fifteen kallikreins in CCM of the different pancreatic cancer cell lines.

Due to the superior preservation of proteins and vital structures in FFPE tissue, another aim of this project is to examine KLK detection within FFPE patient tissue samples by applying PRM as an alternative targeted MS approach. Besides the comparison of PDAC tissue to its normal counterpart, our cohort includes some additional tissue entities, such as chronic pancreatitis, non-malignant adjacent pancreas and ampullary cancer. To our knowledge, this would be the first targeted MS detection of KLKs in PDAC FFPE tissue samples. Aside from KLK detection in the different tissue entities, we aim to perform a global proteome comparison between the FFPE samples named above by applying explorative (shotgun) MS.

3 MATERIALS AND METHODS

3.1 Materials

3.1.1 Chemicals, Buffers and Enzymes

Table 1: Used Chemicals and their Manufacturers

Name	Manufacturer
4-(2-hydroxyethyl)-1-piperazineethanesulfonic acid (HEPES)	Sigma-Aldrich, St. Louis, USA
Acetonitrile (ACN)	Merck, Darmstadt, Germany
Ammonia solution 25 % (NH4OH)	Merck, Darmstadt, Germany
Aqua Ad Iniectabilia Braun	B. Braun Melsungen AG, Melsungen, Germany
Avidin from egg white	Sigma-Aldrich, St. Louis, USA
Dithiothreitol (DTT)	AppliChem GmbH, Darmstadt, Germany
Dulbecco`s Modified Eagle`s Medium, high glucose, GlutaMAX™ Supplement (DMEM)	Gibco, Thermo Fisher Scientific, Waltham, USA
Dulbecco`s Phosphate-Buffered Saline (DPBS)	Gibco, Thermo Fisher Scientific, Waltham, USA
Ethanol absolute	VWR International SAS, Fontenay sous Bois, France
Iodoacetamide (IAA)	Sigma-Aldrich, St. Louis, USA
Isopropyl alcohol (Isopropanole)	VWR International SAS, Fontenay sous Bois, France
MES monohydrate	Sigma-Aldrich, St. Louis, USA
Sodium 3-[(2-methyl-2-undecyl-1,3-dioxolan-4-yl)methoxy]-1-propanesulfonate (RapiGest)	Synthesized by laboratory of Professor H. Jessen
Sodium dodecyl sulfate (SDS), 10% in ddH2O	AppliChem GmbH, Darmstadt, Germany
SpeedBead Magnetic Carboxylate Modified Particles (Hydrophilic)	GE Healthcare UK Limited, Chalfont St Giles Buckinghamshire, UK
SpeedBead Magnetic Carboxylate Modified Particles (Hydrophobic)	GE Healthcare UK Limited, Chalfont St Giles Buckinghamshire, UK
Trifluoroacetic acid (TFA)	Thermo Scientific, Rockford USA
Tris(hydromethyl)aminomethan (TRIS)	United States Biochemical Corporation, Cleveland, USA
Tris(2-carboxyethyl)phosphine hydrochloride (TCEP)	Sigma-Aldrich, St. Louis, USA
Xylol (Xylene)	Carl Roth GmbH & Co.KG, Karlsruhe, Germany
Penicillin Streptomycin (Pen Strep)	Gibco, Thermo Fisher Scientific, Waltham, USA
Supplements for Keratinocyte-SFM	Gibco, Thermo Fisher Scientific, Waltham, USA
FBS Supreme, Fetal bovine serum	PAN-Biotech GmbH, Aidenbach, Germany
Roswell Park Memorial Institute (RPMI) Medium 1640	Gibco, Thermo Fisher Scientific, Waltham, USA

Keratinocyte-SFM with L-glutamine	Gibco, Thermo Fisher Scientific, Waltham, USA
MEM NEAA, Non-Essential Amino Acid Solution (100x) w/o: L-Glutamine for cell culture	PAN-Biotech GmbH, Aidenbach, Germany
EDTA solution pH 8.0 (0,5 M)	AppliChem GmbH, Darmstadt, Germany
PMSF BioChemica	AppliChem GmbH, Darmstadt, Germany

Table 2: Used Buffers and their Composition

Name	Composition
Denaturation Buffer (Cell Line Comparison Protocol) pH 8,5	2 % SDS, 400 mM TRIS
Elution Buffer (PreOmics Kit)	2 % NH4OH, 80 % ACN in H2O
Lysis Buffer (FFPE protocol) pH 8,0	0,1 % SDS in 0,1 M Hepes
RapiGest Lysis Buffer (FFPE Protocol)	0,1 % RapiGest in 0,1 M Hepes
Wash Buffer I (PreOmics Kit)	1 % TFA in Isopropanole
Wash Buffer II (PreOmics Kit)	0,2 % TFA in H2O

Table 3: Used Enzymes and their Manufacturers

Name	Manufacturer
Lysyl Endopeptidase®, Mass Spectrometry Grade (Lys-C)	Fujifilm Wako Pure Chemical Corpoaration, Osaka, Japan
TrypLE Express Enzyme, Trypsin for cell culture	Gibco, Thermo Fisher Scientific, Waltham, USA
Benzonase	Sigma-Aldrich, St. Louis, USA

3.1.2 Consumables, Kits, Instruments and Software

Table 4: Used Consumables and their Manufacturers

Material	Manufacturer
1,5 ml Protein LoBind tubes	Eppendorf AG, Hamburg, Germany
1,5 ml Safe lock tubes	Eppendorf AG, Hamburg, Germany
15 ml Falcon tubes	Greiner Bio-One AG, Kremsmünster, Austria
2 ml Protein LoBind tubes	Eppendorf AG, Hamburg, Germany
2 ml Safelock tubes	Eppendorf AG, Hamburg, Germany
50 ml Falcon tubes	Greiner Bio-One AG, Kremsmünster, Austria
96-well plate	Greiner Bio-One AG, Kremsmünster, Austria
Adhesion Microscope Slides Superfrost Plus	R.Langenbrinck, Emmendingen, Germany
epT.I.P.S. 0.5 µl to 10 µl	Eppendorf AG, Hamburg, Germany
epT.I.P.S. 10 µl to 100 µl	Eppendorf AG, Hamburg, Germany
epT.I.P.S. 100 µl to 1000 µl	Eppendorf AG, Hamburg, Germany
Feather® disposable scalpel, No. 11	Graham Field, Atlanta, USA

Eppendorf Research® Plus 2,5 µl, 10 µl, 100 µl, 1000 µl (Hand pipets)	Eppendorf AG, Hamburg, Germany
pH indicator strips 0-6, 5-10	Merck, Darmstadt, Germany
Stripette® Serological Pipets for cell culture, 5 ml, 10 ml, 25 ml, 50 ml	Corning Incorporated, Corning, NY, USA
Cell Culture Flasks, 50 ml, 25 cm^2, PS, red standard screw cap, sterile	Greiner Bio-One AG, Kremsmünster, Austria
Cell Culture Flasks, 250 ml, 75 cm^2, PS, red standard screw cap, sterile	Greiner Bio-One AG, Kremsmünster, Austria
Cell Culture Dishes, 145/20 mm, vents, Advanced TC™, sterile	Greiner Bio-One AG, Kremsmünster, Austria

Table 5: Used Kits and their Manufacturers

Name	Manufacturer
BCA Protein Assay Kit	Thermo Scientific, Rockford USA
PreOmics Phoenix Peptide Clean-up	PreOmics GmbH, Planegg/Martinsried, Germany

Table 6: Used Instruments and their Manufacturers

Name	Manufacturer
Bioruptor® plus (Sonication device)	Diagenode s.a. Belgium Europe, Seraing, Berlgium
Concentrator 5301 (Speed vac)	Eppendorf AG, Hamburg, Germany
Easy nanoLC 1000 (LC system)	Thermo Fisher Scientific™, Waltham, USA
Eve Automatic Cell Counter	NanoEnTek, Waltham, USA
Heracell 240i CO2 Incubator	Thermo Fisher Scientific™, Waltham, USA
Incubation bath 1013 (Waterbath)	GFL Gesellschaft für Labortechnik mbH, Burgwedel, Germany
Liebherr comfort (- 20°C freezer)	Liebherr-International Deutschland GmbH, Biberach an der Riß, Germany
DynaMag™-2 Magnet	Thermo Fisher Scientific™, Waltham, USA
Leica RM2255	Leica Microsystems, Wetzlar, Germany
LSE Mini Microcentrifuge	Corning Incorporated, NY USA
Pfm waterbath 1000 (Microtome waterbath)	Pfm AG, Köln, Germany
FiveEasy pH meter F20-Std-Kit	Mettler-Toledo GmbH, Gießen, Deutschland
Q Exactive™ plus hybrid Quadropol-Orbitrap™	Thermo Fisher Scientific™, Waltham, USA
Thermoshaker TS1 (Heating block)	Biometra GmbH, Goettingen, Germany
Tissue Stainer COT 20 (Tissue stainer and deparaffinization device)	Medite Medizintechnik, Burgdorf, Germany
Transsonic 310/H (Ultrasonic bath)	Elma Hans Schmidbauer, GmbH & Co.KG, Singen, Germany

TSQ Vantage™	Thermo Fisher Scientific™, Waltham, USA
HERAfreeze HLE series (-80 freezer)	Thermo Fisher Scientific™, Waltham, USA
VortexGenie 2 (Vortexer)	Scientific Industries Inc., Bohemia, USA
Pipetgirl Pipette Controller	Intergra Biosciences, Biebertal, Germany
Heraeus Megafuge 40R Centrifuge	Thermo Fisher Scientific™, Waltham, USA
Leica Microscope Type 090-135.001	Leica Microsystems, Wetzlar, Germany

Table 7: Used Software and their Manufacturers

Name	Manufacturer
MaxQuant, v.1.6.17.0	Max Planck Institute for Biochemistry
Prism V9	GraphPad Software, San Diego, USA
Xcalibur V2.0	Thermo Electron Corporation
Skyline V19.1	MacCoss Lab Software. Washington, USA
DIA-NN V1.7.12	[59]
RStudio (V 1.3.1093)	Rstudio, Boston, USA

3.2 Methods

The proteomic studies were performed at the Institute for Surgical Pathology at the University of Freiburg, Faculty of Medicine in collaboration with Professor Dr. Oliver Schilling, head of the research group.

3.2.1 Cell Culture of MiaPaCa-2 and AsPC-1

The two human pancreatic cancer cell lines MiaPaCa-2 and AsPC-1 (DSZM, Braunschweig) were received from cell line services and were cultured within T-25 (25 cm^2, Greiner) or T-75 (75 cm^2, Greiner) cell culture flasks. MiaPaCa-2 cells were grown in Dulbecco´s Modified Eagle Medium (DMEM, Thermo Fisher Scientific) supplemented with 10 % (v/v) fetal bovine serum (FBS) and 1 % (v/v) Pen Strep (P/S, 10 mg/ml), whereas AsPC-1 cell culture was grown in RPMI (Thermo Fisher Scientific) supplemented with 10 % (v/v) FBS and 1 % (v/v) P/S. The two cell lines were cultured at 37 °C in a humidified atmosphere of 5 % CO2 and were regularly subcultured to adjust cell confluency to 70-90 %. They showed an absence of mycoplasma during the whole study. When passaging the cells, the medium was removed, and cells were washed with 1-3 ml Dulbecco's Phosphate Buffered Saline (DPBS). 2-4 ml Trypsin was applied to the adherent cell layer, and cells were incubated at 37 °C for 4-6 minutes in order to detach the cells from the ground. After quenching trypsinization with 2-4 ml of DMEM or RPMI (depending on which cell line), cells were centrifuged for 3 minutes at 500 g. The supernatant was removed, and cells were resuspended in 2-6 ml DMEM or RPMI. An appropriated volume of the resuspended cells was then transferred to a new flask according to the cell density required (ratios 1:2 to 1:12).

Cryopreserved cell aliquots were taken out the liquid nitrogen tank and warmed by hand until cells have been thawed. The cells were immediately transferred to prewarmed DMEM or RPMI medium. After centrifuging the cells, the supernatant was removed, and the cell pellet was resuspended in 5 ml of prewarmed DMEM or RPMI and transferred into a T25-flask.

3.2.2 Cell Culture of PaCaDD-165, PaCaDD-159 and MaPaC-107

Three primary human pancreatic cancer cell lines have been kindly provided by the surgical department of the University of Heidelberg, Faculty of Mannheim [60]. During the study, the cells were cultured in Dresden-medium, which consist of two different media: First, DMEM was prepared containing 10 % (v/v) FBS and 1 % (v/v) P/S.

Second, KSFM (Keratinocyte-Serum-free medium, Thermo Fisher Scientific) was supplemented with EGF and BPE (Epidermal Growth Factor Human Recombinant and Bovine Pituitary Extract, both provided in the kit). When performing cell culture, the two media were mixed at the ratio of 2:1 (DMEM:KSFM) by frequently change of the Dresden-medium. We produced fresh Dresden-medium prior to each experiment. The cell lines were maintained at 37 °C in a humidified atmosphere of 5 % CO2 and were mycoplasma free at all times.

3.2.3 SFM Harvesting and CCM Production

Cells were cultured in Advanced TC cell culture dishes (145/20 mm, Greiner). When confluency of cells was about 70-90 %, cells were washed three times with 10 ml of SFM (Serum-free medium, supplemented with 1 % (v/v) P/S, 1x Minimum Essential Medium and 1x Non-essential Amino Acid Solution). Another 22 ml of SFM was then applied to the cells and was incubated for 24 h at 37 °C. After incubation, SFM was transferred to Falcon Tubes before adding EDTA to a final concentration of 10 mM and PMSF to a final concentration of 0,1 mM. The so-called CCM (cell conditioned medium) was then further centrifuged for 10 minutes at 4000 rpm, and the supernatant was transferred into new falcons. CCM was stored at -80 °C. For determining the total cell number on the dishes, the cells were washed with 10 ml Dulbecco`s Phosphate-Buffered Saline (DPBS). DPBS was discarded, and cells were trypsinized with 4 ml trypsin for 4-6 minutes. To stop trypsinization, another 4 ml of medium was applied to the cells, and cell suspension was transferred into a 15 ml falcon. Cells were counted by mixing 10 µl of the cell suspension with 10 µl of trypan blue staining and measuring with a cell counter (EVE Automatic cell counter, NanoEnTek).

3.2.4 CCM-Protein-Enrichment with SP3 Beads

For protein-enrichment, 5 ml CCM were prepared in the presence or absence of 1 µg Avidin (Sigma) solved in water. A denaturation buffer was prepared containing 2 % (v/v) SDS-solution and 400 mM TRIS (pH 8,5). Denaturation buffer and benzonase were then added to each sample to a final concentration of 0,2 % (v/v) SDS, 36 mM TRIS and 9 U/ml benzonase, respectively. After an incubation of 15 minutes at room temperature, TCEP was added to a final concentration of 2 mM in order to reduce cysteine-residues, followed by a 30-minute incubation in a water bath heated to 80 °C. After cooling down to room temperature, iodoacetamide as an alkylation reagent was added to a final concentration of 5 mM to all samples and incubated in the dark for

30 minutes at room temperature. Subsequently, MES (2-Morpholinoethanesulfonic acid monohydrate) was added to a final concentration of 83 mM and samples were gently mixed. At that point, the pH should be between 6,5-7,0. SP3 beads were quickly vortexed and sonicated for 30 seconds before pipetting them. Finally, SP3 beads (mixture of equal volumes of Sera-Mag Magnetic hydrophilic and hydrophobic SpeedBeads, previously washed three times with water) were added to a final concentration of 0,2 µg/µl to each falcon. After adding 6 ml of Acetonitrile (ACN) to the samples and gently inverting the falcons, samples were incubated at room temperature for 10 minutes. After incubation, the samples were centrifuged for 8 minutes at 800 g and supernatants were removed. The Bead-Pellet was resuspended in 500 µl of 80 % (v/v) Ethanol, and the solutions were pipetted into LoBind Eppendorf tubes. The last step was repeated, and the Eppendorf tubes were put into the magnetic rack until the beads have settled to the tube wall. The supernatant was discarded, and the washing step was repeated with 1000 µl of 80 % (v/v) Ethanol. Eppendorf tubes were placed in the magnetic rack, supernatants were removed, and Beads were resuspended with 1000 µl of ACN. After putting the Eppendorf tubes in the rack and removing the supernatant, samples were dried in SpeedVac at 45 °C. A general overview of the SP3 bead workflow can be seen in **Figure *4***.

3.2.5 Protein-Elution from SP3 Beads and Digest

Protein-Elution of SP3 Beads was performed by resuspending the beads in 50 µl 0,1 % (w/v) RapiGest in 0,1 M Hepes, sonicating the samples for 10 minutes and applying another 10 minutes heating step at 95 °C, 400 rpm. The Eppendorf tubes were then placed in the magnetic rack, and the supernatants were transferred into new LoBind Eppendorf tubes. All steps were repeated, and supernatants were combined in the same LoBind Eppendorf tubes. After protein elution, a BCA was performed in duplicates in order to digest 10-70 µg of protein. Sample pre-digestion took place by adding Lysyl Endopeptidase in an enzyme:protein mass ratio of 1:50 and then incubating the samples for 2 h at 42 °C. Digestion with Trypsin was performed at an enzyme:protein mass ratio of 1:50 and samples were incubated overnight at 37 °C.

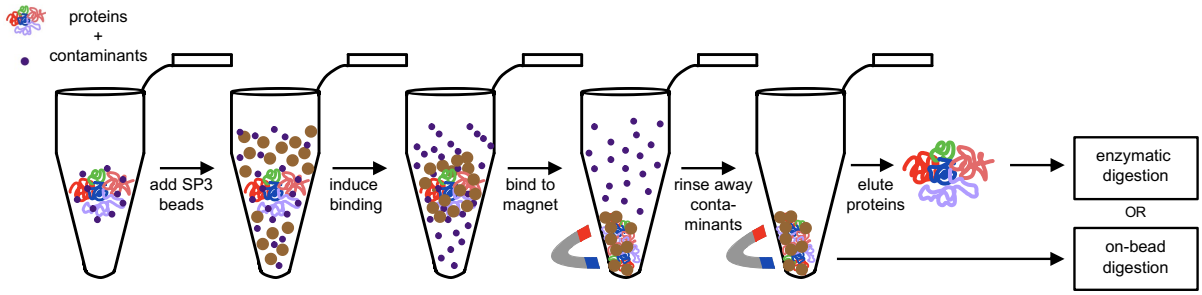

Figure 4: Schematic Illustration of Standard SP3 Bead Workflow for both CCM and FFPE Tissue. The magnetic beads are added to a sample containing proteins and unwanted contaminants. The beads bind to the proteins via a hydrophilic/hydrophobic interaction mechanism. When approaching a magnet, SP3 beads with their bound proteins are attracted towards it. Unwanted contaminants can further be rinsed away. Purified proteins can either be eluted directly and then enzymatically digested, or on-bead digestion is performed followed by elution of the resulting peptides. Figure adapted from [61].

3.2.6 PreOmics Peptide Clean-Up

For PreOmics Clean-Up the digestion reaction was stopped by acidifying the samples to a pH < 2 through the addition of Trifluoroacetic acid (TFA) to a final concentration of 2 % (v/v). Subsequently, samples were incubated at 37 °C and 400 rpm for 30 minutes. To remove unsolved material, samples were centrifuged for 5 minutes at maximum speed at room temperature and the supernatant was loaded on top of the PreOmics columns placed in 1,5 ml LoBind Eppendorf tubes. The reaction tubes containing the columns were centrifuged for 15 minutes between 300-1500 g to get the supernatant through the column. The loading step was repeated to ensure complete binding of peptides to the PreOmics columns. Samples were further washed two times with 200 µl of 1 % (v/v) TFA in 2-propanole (washing buffer 1) followed by two washing steps with 200 µl 0,2 % (v/v) TFA in distilled water (washing buffer 2). After each washing step, samples were centrifuged at 1000 g for 2 minutes. Afterwards, peptides were eluted two times with 100 µl elution buffer including 2 % (v/v) ammonia in 80 % (v/v) ACN. In order to get rid of ACN, the samples were dried in the SpeedVac at 45 °C, and finally resuspended in 60 µl of distilled water. After sonicating the samples for 5 minutes, a BCA of the elutions was performed in duplicates with 5 µl of each sample for peptide quantitation. 3 µg of each sample was transferred to fresh 0,5 ml LoBind Eppendorf tubes, evaporated at 45 °C until dryness and stored at -80 °C until MS-measurement.

3.2.7 Formalin-Fixed Paraffin-Embedded Tissue

Proteomic analyses were performed from 45 formalin-fixed paraffin-embedded (FFPE) tumor tissue, which derived from the surgical department of the University of Heidelberg, Faculty of Mannheim, as well as the University of Freiburg, Institute for Surgical Pathology. Involved were tissues of PDAC (n=14), chronic pancreatitis (n=7), ampullary cancer (n=3), adjacent non-malignant pancreatic tissue (n=16), and normal pancreatic tissue (n=5). The latter group was obtained from the pancreas of 5 autopsy cases (median age 63 years; range 43 ± 84). All samples were kindly approved by the Ethics Committee (file number: 2012-293N-MA).

3.2.8 Light Microscopy of Hematoxylin and Eosin (HE) stained Slides

FFPE blocks of each tissue entity were cut with varying thickness using a microtome and routine hematoxylin and eosin (HE) stains were performed. In order to determine which tissue sections would be suitable for proteomic analyses, the tissue slides were evaluated under a light microscope. Criteria for exclusion were tissue sections containing neither tumor tissue nor normal pancreatic tissue, as well as tissue sections containing too little tumor cells which would not be suitable for macrodissection. Consequently, the area for subsequent macrodissection was marked on stained tissue sections to distinguish malignant tissue from the adjacent non-malignant tissue.

3.2.9 Deparaffinization and Macrodissection of FFPE Tissue Slides

Unstained tissue slides suitable for macrodissection were deparaffinized by immersing the glass slides with the tissue into increasing concentrations of xylol followed by decreasing concentrations of ethanol (xylol 4x, alcohol absolute, alcohol 96 %, alcohol 70 %, aqua distilled 2x). Using a light microscope and a scalpel, the selected tissue areas were scratched from each slide and were transferred into individual Eppendorf tubes. Samples were then stored at -80 °C until preparation for MS analysis.

3.2.10 Sample Preparation for Mass Spectrometry (MS)

Denaturation buffer was freshly prepared containing 0,1 % (v/v) SDS in 0,1 M Hepes (pH 8). The tissue used for MS analyses were resuspended in 100 µl denaturation buffer. In order to extract the proteins, tissue samples were heated for 2 h at 95 °C, 500 rpm. Directly after, samples were stored on ice and were then ultrasonicated for 10 minutes to shear DNA and further homogenize the tissue-lysis buffer mixture (10 cycles x 45 seconds of sonication followed by a 15 second break, Bioruptor,

Diagenode). After sonication, samples were centrifuged for 10 minutes at maximum speed at room temperature. Subsequently, the protein concentration in the supernatants was determined by a BCA assay. A maximum of 100 µg of protein (according to the BCA results) was reduced with a final concentration of 5 mM DTT (37 °C, 30 minutes, 400 rpm) and alkylated with a final concentration of 15 mM IAA (in the dark at room temperature, 30 minutes). After reduction and alkylation, the pH was tested to ensure an alkaline pH. To separate the beads, the pre-washed SP3 bead mix was sonicated for 30 seconds. 10 µl of the bead mix was added to each sample, which was subsequently mixed. To encourage protein binding to the beads, a 1:1 ratio of ACN was added to each sample before letting them incubate at room temperature, 10 minutes, 500 rpm. After incubation, samples were put into the magnetic rack for 2 minutes to separate beads from the clear supernatant, whereas the latter was removed. Subsequently, the beads were washed twice with 200 µl 70 % (v/v) Ethanol, followed by a washing step with 180 µl 100 % (v/v) ACN, each time using the magnetic rack to separate the beads and discard the supernatant. To eliminate any remaining ACN, samples were dried in SpeedVac for 5 minutes without heating. Beads were then resuspended in 100 µl of digest buffer containing 0,1 % RG in 0,1 M Hepes and sonicated for 30 seconds in order to separate the beads.

3.2.11 Digestion (on-bead)

Sample pre-digestion took place by adding Lysyl Endopeptidase in an enzyme:protein mass ratio of 1:100 and then incubating the samples for 2 h at 42 °C, 500 rpm. Digestion with Trypsin was performed at an enzyme:protein mass ratio of 1:50 and samples were incubated overnight at 37 °C, 500 rpm.

3.2.12 PreOmics Peptide Clean-Up

After incubation overnight samples were sonicated for 30 seconds and put into the magnetic rack for 2 minutes to separate beads from the peptide containing supernatant. The supernatant was then transferred into a new 1,5 ml LoBind Eppendorf tube and was acidified by adding TFA to a final concentration of 2 %. pH was checked to ensure an acidic pH below 2. Samples were incubated for 30 minutes, 37 °C at 500 rpm to precipitate RapiGest and then centrifuged for 10 minutes at max. speed. Supernatant, containing digested peptides, was desalted by using the PreOmics MS sample preparation Kit as described above. Samples were stored at -80 °C until MS measurement.

3.2.13 LC-MS/MS-Measurements for Pancreatic Cancer Cell Line Comparison

For SRM Measurement, the dried samples containing 3 µg of peptide each were resuspended in Buffer A (0,1 % (v/v) FA in H2O), and 600 fmol of iRT peptides and 300 fmol of heavy peptides (KLK and Avidin) were added to the samples. After sonication for 5 minutes, samples were transferred to MS measurement tubes (WICOM). 1 µg of each peptide sample was analyzed on the TSQ by applying an MRM assay with the use of a nanoflow LC system (Proxeon Easy-nLC II). The nLC contained a trapping column (Fused Silica Capillary, 5 cm length, 100 µm inner diameter (ID), VICI Jour, Schenkon, Switzerland) as well as an analytical column (Selfpack PicoFrit column, 35 cm length, 75 µm ID, New Objective, Woburn, MA) both of which were in-house packed with C18 particles (Dr. Maisch, ReproSil-Pur 120 C18-AQ, 3 µm C18 particle size, 120 Å pore size). The samples were captured at 220 bars with 100 % Buffer A (0,1 % (v/v) FA) and separated with the use of a reverse phase C18 column, the analytical column temperature was set to 60 °C. The samples were separated on the nLC at a flow rate of 250 nl/min with a linear increasing concentration of buffer B (50 % (v/v) ACN in 0,1 % (v/v) FA in H2O) in buffer A from 8-56 % (v/v) B in 60 minutes. An additional washing of the column to 8 % buffer B after 83 minutes followed (detailed gradient information see **Table *S 14***). The analytical column was equipped with an integrated uncoated pre-cut emitter (Silica Tip, 10 µm tip inner diameter, New Objective, Woburn, MA) with a voltage of 2,7 kV for electrospray ionization. Measurement on the TSQ Vantage (ThermoFisher Scientific) took place by applying a randomized sample order, samples were scanned with a dwell time of 15 ms.

3.2.14 PRM-Measurement

Regarding the PRM measurement, the vacuum dried peptides were resolubilized in 0,1 % (v/v) TFA to a final concentration of 0,2 µg/µL, sonicated for 5 minutes, centrifuged at 20,000 g for 10 minutes, and the supernatant was transferred to the measurement tube. 800 ng of each sample, together with 100 fmol of stable-isotope labelled heavy peptides and 150 fmol of iRT-Peptides, were applied to a nanoflow LC system, Easy-nLC 1000 (Thermo Scientific) containing a trapping column (50 cm µPac™ trapping column, PharmaFluidics, Ghent, Belgium) as well as an analytical column (200 cm µPac™ analytical column, PharmaFluidics, Ghent, Belgium).

Samples were captured at 250 bars with 100 % buffer A (0,1 % v/v FA) followed by separation with the use of a reverse phase C18 column with the analytical column

temperature set at 45 °C and at a flow rate of 350 nL/min. A multistep gradient of 8 % to 55 % buffer B (80 % v/v ACN, 0,1 % v/v FA, 1 % v/v MEG) in buffer A was used for separation, followed by subsequent washing (100 % B) and reconditioning of the column to 8 % B (see **Table *S 15*** for detailed gradient overview).

The Easy-nLC 1000 system was online coupled to a Q-Exactive plus (Thermo Scientific) mass spectrometer through a Nanospray Flex Ionsource (Thermo Scientific). For electrospray injection, a voltage of 2,1 kV was applied. The analytical column was connected to a pulled and uncoated ESI emitter (10 µm tip inner diameter, 20 µm inner diameter, 7 cm length, CoAnn Technologies, Richland, USA) through a µPac™ Flex iON Connect ESI-MS interface (PharmaFluidics, Ghent, Belgium).

The unscheduled parallel reaction monitoring (PRM) acquisition mode was used for the operation of the mass spectrometer device. M2 scans (1 µscan) of doubly-charged precursor ions were performed applying an isolation window size of 1,2 m/z. The MS2 resolution was set to 35,000, automatic gain control (AGC) to 3e6 and the maximum injection time was fixed to 150 ms with the use of stepped normalized collision energy (NCE) of 25 and for fragmentation 30.

Data analyses were performed using Skyline (version 19.1), a publicly available software tool application for proteomic analysis [62]. To guarantee correct peak detection and integration, the entirety of integrated peaks was manually inspected. A two-sample t-test was carried out using Benjamini-Hochberg for multiple testing correction. Volcano plots were used to picture the adjusted p-values and the corresponding fold changes. Differentially expressed proteins were defined by having a significant abundance change (adjusted p-value ≤ 0,05) as well as an absolute log2 fold change ≥ 1 (corresponds to 2-fold abundance change).

3.2.15 DIA Measurement

Vacuum dried peptides for DIA measurement were resolubilized in 0,1 % (v/v) TFA to a final concentration of 0,2 µg/µL. The samples were then sonicated for 5 minutes followed by centrifugation at 20,000 g for 10 minutes. The supernatant was then transferred to the measurement tube. A nanoflow LC system, Easy-nLC 1000 (Thermo Scientific) containing a trapping column (50 cm µPac™ trapping column, PharmaFluidics, Ghent, Belgium) as well as an analytical column (200 cm µPac™

analytical column, PharmaFluidics, Ghent, Belgium) was used for analysis with each sample containing 800 ng and 100 fmol of iRT-Peptides.

Subsequent to separation of peptides using a reverse phase C18 column (analytical column temperature 45 °C, flow rate 350 nL/min) the samples were caught at 250 bars with 100 % buffer A (0,1 % v/v FA). A multistep gradient of 8 % to 55 % buffer B (80 % v/v ACN, 0,1 % v/v FA, 1 % v/v MEG) in buffer A was used for separation, followed by washing (100 % B) and reconditioning of the column to 8 % B (see **Table *S 15*** for detailed gradient overview).

The Easy-nLC 1000 system was online coupled to a Q-Exactive plus (Thermo Scientific) mass spectrometer via a Nanospray Flex Ionsource (Thermo Scientific) and a voltage of 2,1 kV was applied for electrospray injection. The analytical column was coupled to a pulled, uncoated ESI emitter (10 µm tip inner diameter, 20 µm inner diameter, 7 cm length, CoAnn Technologies, Richland, USA) via a µPac^{TM} Flex iON Connect ESI-MS interface (PharmaFluidics, Ghent, Belgium).

A data independent acquisition (DIA) mode was used for each DIA-sample. Two cycles of 24 m/z broad windows (range 400 to 1000 m/z and a 50 % shift between the cycles; staggered window scheme [63]) was applied, resulting in an overall isolation window size of 12 m/z. Additionally, the following settings were selected: MS2 resolution 17,500, automatic gain control (AGC) 1e6, maximum injection time 80 ms (stepped NCE of 25 and 30). Following 25 repeated MS2 scans, a MS1 survey scan was generated at the identical range but increased resolution of 70,000, an AGC target of 3e6 and the maximal injection time was fixed at 50 ms.

Comparable amounts of samples were mixed resulting in one masterpool sample used for GPF-library measurements. For sample measurement, the total mass scan range of 400 to 1,000 m/z was separated into 6 single measurements (mass scan range 100 m/z, overall isolation window size 4 m/z). With this exception the same settings were used.

DIA-NN (1.7.12) was used with the recommended settings [59] for DIA analysis. A human proteome database covering reviewed UniProt sequences without isoforms was downloaded from Uniprot on 14th June 2021 (20856 entries) and was used for peptide identification. The GPF-measurement was then used for the refinement of this database. The library was refined by activating deep learning-based spectra and RTs

prediction. The allowed peptide length was set between 7-30 amino acids. Tryptic cleavage specificity (Trypsin/P) was set to 1 missed cleavage. Additionally, N-terminal M excision, C carbamidomethylation, retention time (RT) profiling as well as RT-dependent cross-normalization options were permitted. Decoys of the database entries were routinely produced by DIA-NN, and precursor FDR was fixed at 1,0 %. Identical settings except deactivated deep learning-based spectra as well as RTs prediction option were performed concerning the *in silico* predicted library search. Subsequently, the DIA-NN output was processed in R (V 4.1.0) which included RStudio (V 1.3.1093) as an integrated development environment. Subsequent to filtering for unique proteins, the DIANN package (V 1.0.1) [59] was used to perform the log2-transformation. In order to perform sparsity reduction, the dataset was filtered for proteins with at minimum 80 % valid values per protein per condition. ComBat batch correction was then performed with the use of the sva (V 3.40.0) package. The partial least squares discriminant analysis (PLS-DA) as well as the extraction of protein representatives was accomplished by the use of the mixOmics package (V 6.16.3). Using the Clust algorithm (V 1.10.10) [22] in Python (V 3.8.9) with a Z-score normalization prior to k-means clustering with seed number k=8 and tightness weight=0,5, the cluster of proteins which are continuously co-expressed were identified. The limma (V 3.48.3) package was further used to perform differential expression analysis, and the gene Ontology annotation as well as the gene enrichment analysis of protein subsets were accomplished with the use of the topgo (V 2.44.0), clusterprofiler (V 4.0.5) and ReactomePA (V 1.36.0) packages.

4 RESULTS

4.1 Protocol Optimization

The aim of this project is to study kallikrein protein levels in CCM of pancreatic cancer cell lines as well as in patient-derived tissues via targeted and explorative (shotgun) MS. In order to detect the maximum amount of identified KLK proteins, different optimization steps needed to be performed to ensure a robust and reproducible sample preparation workflow. In addition, an SRM assay for all fifteen KLKs was established, including isotope-labelled reference peptides and Avidin as internal protein standard to account for any technical variance during sample preparation and MS-measurements.

4.1.1 Single-Pot Solid-Phase-Enhanced Sample Preparation (SP3)

The main question of the following optimization part was how to obtain the best possible enrichment and detection of KLKs. Therefore, we needed a sample preparation workflow suitable for low protein concentrations like the KLK protein family, as well as a method which enables working with high volumes applying to the CCM of the pancreatic cancer cell lines. One way to enclose both at the same time is the so called single-pot solid-phase-enhanced sample preparation (SP3) bead method, which is adequate for MS sample preparation of CCM as well as FFPE tissue samples. The beads consist of two magnetic layers which ensures an improved separation from suspensions within a magnetic field. Additionally, the encapsulation of the beads is corrugated so that the overall surface area available for protein binding is strongly increased. As the surface of the magnetic beads is covered with carboxyl groups, biomolecules in the sample can bind to the hydrophilic surface to form amide bonds and thus attaching the proteins and peptides of interest to the particles (see **Figure *5***). By increasing the amount of hydrophobic solvent (e.g. acetonitrile) to more than 50 % (v/v), the desired protein or peptide binding is initiated. Moreover, the magnetic beads can be acquired in different levels of surface hydrophilicity/hydrophobicity. Thus, depending on the different surfaces of the beads, they can act either more hydrophilic or more hydrophobic. To detect the maximum amount of KLKs in our samples, we evaluated the different types of magnetic beads (hydrophilic, hydrophobic, and a 1:1 mixture of both hydrophilic and hydrophobic) as well as different bead amounts (0,25 mg, 1 mg, 40 mg).

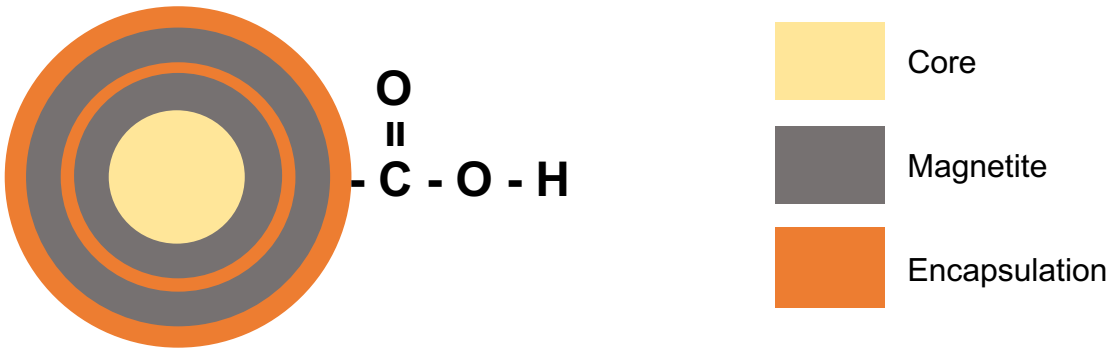

Figure 5: Schematic overview of the inner composition of Sera-Mag Carboxylate-modified Magnetic SpeedBeads. The inner core consists of two magnetic layers to ensure maximum speed in response to the magnetic field. The surface of the beads is covered with carboxyl groups, resulting in a surrounding hydrophilic layer. Figure adapted from Sigma-Aldrich.

4.1.2 Comparing different Bead *Types* by using the SP3 Bead Protocol

Depending on the surface of the SP3 beads, particles may vary in their hydrophilicity/hydrophobicity. Thus, three sample preparation protocols were compared in triplicates, testing 1 mg of either hydrophilic, hydrophobic or a 1:1 (v/v) mixture of both magnetic bead types. Aim of this optimization part was to determine which bead type is most specifically attracting and binding our proteins of interest, thus the kallikreins. Therefore, CCM samples of the pancreatic cancer cell line MiaPaCa-2 were prepared with the SP3 bead protocol and measured by targeted MS, including all 15 KLKs in the SRM assay (see **Figure *6***).

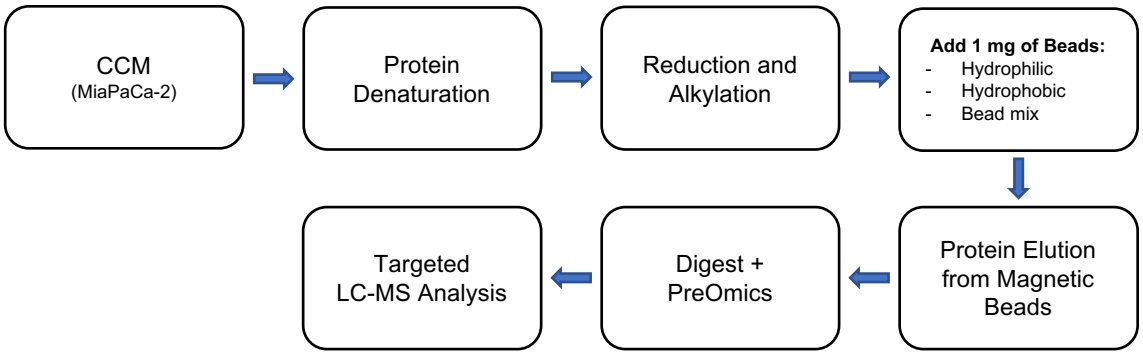

Figure 6: Schematic Workflow for the Bead Type Comparison. Secreted proteins in CCM of pancreatic cancer cell line MiaPaCa-2 are denatured in an SDS-containing buffer. By adding different types of magnetic beads in combination with acetonitrile, proteins are forced to bind to the surface of the respective bead types, which vary in their hydrophilicity/hydrophobicity. Proteins are further eluted from magnetic beads by adding an elution buffer, followed by a tryptic digest. Peptide clean-up (PreOmics) was performed before subjecting the samples to SRM analysis.

KLK5, KLK6 and KLK7 have been detected in all samples. MS data analysis in Skyline revealed comparable peak areas of the three tested bead types for all detected KLK peptides in the SRM assay (see **Figure 7**).

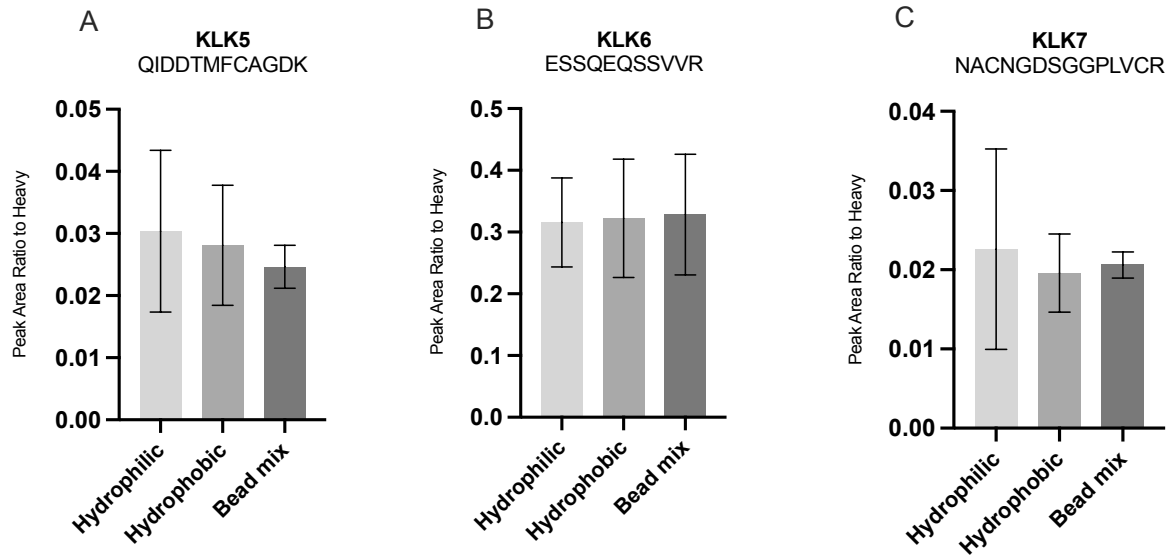

Figure 7: Peak Area Comparison of the three tested Bead Types, illustrated for peptides of KLK5, KLK6 and KLK7. CCM of the pancreatic cancer cell line MiaPaCa-2 was prepared with the SP3 bead protocol as described above whilst using different types of magnetic beads (hydrophilic, hydrophobic and a 1:1 mixture of hydrophilic and hydrophobic beads). All samples were analyzed as technical triplicates of the measurement and were measured in a randomized sample order. The bar plots show the average KLK peak areas of the replicates for each bead type. The peak areas were normalized to heavy peptides as global standard, which showed stable signals throughout the measurements. The error bars correspond to the standard deviation.

Although the different bead types provide minor variances in their surface hydrophilicity, no clear differences in KLK detectability could be observed between the three bead types. Therefore, an equal mix of hydrophilic and hydrophobic beads was further used for this project, which is in line with previous publications using the SP3 bead protocol [61, 64-67].

4.1.3 Comparing different Bead *Amounts* by using the SP3 Bead Protocol

In addition to the optimal bead type for this project, we further tried to optimize the used bead amount to ensure the best possible KLK enrichment and detection of KLKs by MS. As our previously chosen value (1 mg for 5 ml of sample volume) was obtained from an SP3 protocol optimized for urine samples, we wanted to test different bead amounts which could possibly turn out to be more suitable for the kallikrein project. Here, triplicates of MiaPaCa-2 CCM were tested with different amounts of the bead mix (0,25 mg, 1 mg, and 40 mg) prepared with the same SP3 protocol as for the bead type comparison. Samples were then measured via targeted MS, monitoring all 15 KLKs in the SRM assay (see **Figure *8***).

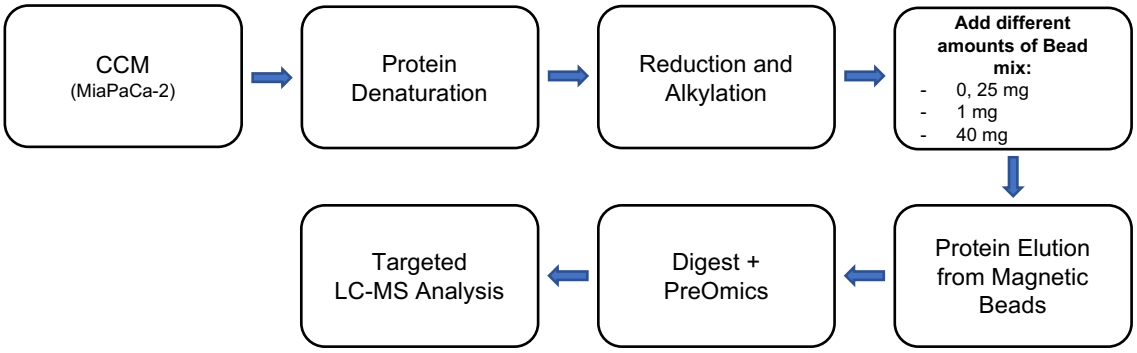

Figure 8: Schematic Workflow for the Bead Amount Comparison. CCM samples of the pancreatic cancer cell line MiaPaCa-2 were prepared following the same SP3 bead protocol as described above, using different amounts (0,25 mg, 1 mg, and 40 mg) of a 1:1 mixture of hydrophilic and hydrophobic magnetic beads. After tryptic digest and peptide clean-up (PreOmics), LC-MS Analysis was performed using the same SRM assay like for the bead type comparison.

Kallikreins which have been detected include KLK5, KLK6, KLK7, and KLK10.

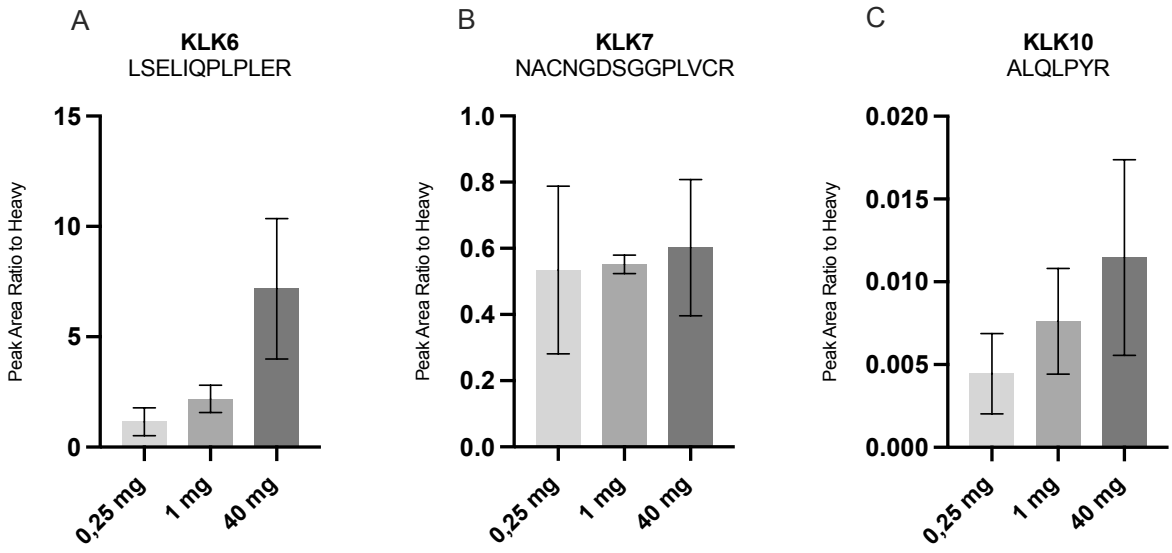

Figure 9: Peak Area Comparison of the three tested Bead Amounts for KLK6, KLK7 and KLK10. CCM of the pancreatic cancer cell line MiaPaCa-2 was prepared with the SP3 bead protocol as described above whilst using different bead amounts (0,25 mg, 1 mg, and 40 mg). All samples were analyzed as technical triplicates of the measurement and were measured in a randomized sample order. The bar plots show the average KLK peak areas of the replicates for each bead amount. The peak areas were normalized to heavy peptides as global standard, which showed stable signals throughout the measurements. The error bars correspond to the standard deviation.

As expected, MS data analysis in Skyline showed an increase for the peak area of KLK6 and KLK10 when using 40 mg compared to 0,25 mg and 1 mg SP3 beads per sample (see **Figure *9 A and C***). KLK peak areas of 0,25 mg and 1 mg samples are comparable, applying to all peptides of the mentioned KLKs. However, for KLK7, all three tested bead amounts show similar peak areas (see **Figure *9 B***). The same effect

could be observed for the detected kallikreins KLK5, KLK7 and KLK15 (data not shown).

Although there is an increase in KLK signals observable by using 40 mg of the bead mix, this difference is only marginal and comes along with a much more complicated handling, resulting in a lower reproducibility of the overall sample preparation workflow. As there is no substantial difference between the KLK signals of 0,25 mg and 1 mg of the bead mix, and the latter represents our previously chosen value, we decided to continue working with 1 mg of the bead mix for further measurements.

4.1.4 Avidin as Internal Standard

GAPDH and Tubulin are housekeeping proteins commonly used as internal controls. As we are working with CCM of pancreatic cancer cell lines and are therefore interested in the secreted kallikreins in the extracellular space, intracellular standards as GAPDH and Tubulin are not appropriate for this project. Hence, a glycoprotein obtained from egg white was used as internal control, namely Avidin, to eliminate any handling variances during sample preparation. In order to determine an appropriate amount of Avidin as internal standard to ensure sufficient detectability on the one hand and to prevent shadowing of the actually interesting KLKs on the other hand, different amounts of Avidin (absence, 1 µg, 5 µg, 50 µg and 100 µg) were added to the CCM of pancreatic cancer cell lines before performing the previously optimized SP3 bead protocol (see **Figure 10**).

The samples were prepared in triplicates and the SRM assay included seven peptides of Avidin and a selection of kallikreins (KLK6, KLK7, KLK10, KLK11), which have already been detected in previous measurements and pilot experiments.

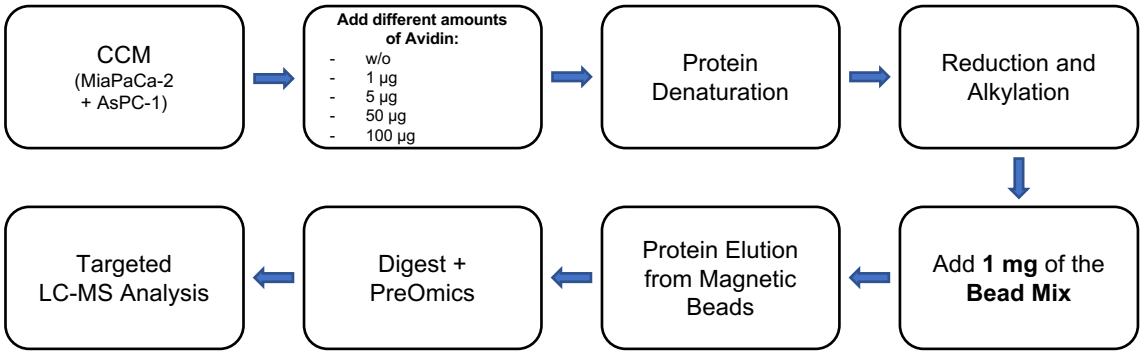

Figure 10: Schematic Workflow for the Avidin Amount Comparison. Different amounts of Avidin were added to the pooled CCM of the pancreatic cancer cell lines MiaPaCa-2 and AsPC-1, together with one sample without Avidin. Samples were prepared in triplicates before following the same SP3

bead protocol as described above, using 1 mg of the bead mix. After tryptic digest and peptide clean-up (PreOmics), targeted LC-MS Analysis was performed using the same SRM assay as for the bead type and bead amount comparison.

The results showed clearly detectable peaks with several transitions in all seven Avidin peptides (no heavy peptides for peak comparison were available). As expected, there were higher signal intensities of Avidin peptides observable with increasing amounts of initially added Avidin (see **Figure *11***). On the other hand, error bars were increasing as well, resulting in a lower reproducibility of the sample preparation workflow. In addition, samples with 50 µg and 100 µg Avidin showed signals which were not entirely accurate and were “tailing” due to the high amounts of Avidin, whereas the samples with 1 µg and 5 µg Avidin showed nice and sharp peaks. We further observed that in some cases, samples without Avidin showed weak signals of Avidin due to carry over. Despite adding different amounts of Avidin to the samples, no signal compression of the KLK peptides was observable (see **Figure *12***).

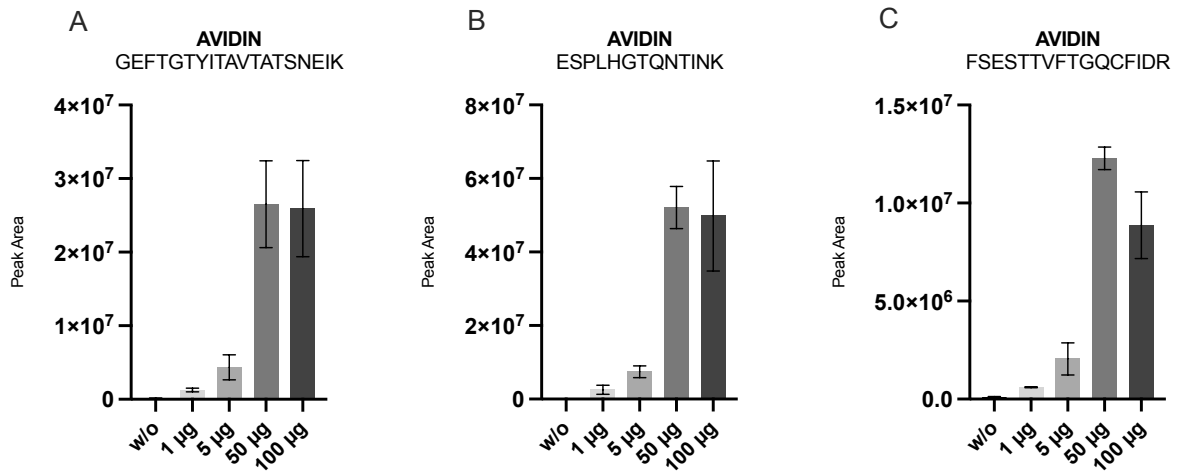

Figure 11: Peak Areas of different Avidin Amounts. CCM of the pancreatic cancer cell line MiaPaCa-2 was supplemented with different amounts of Avidin (w/o, 1 µg, 5 µg, 50 µg and 100 µg) before preparing the samples with the optimized SP3 bead protocol as described above. All samples were analyzed as technical triplicates of the measurement and were measured in a randomized sample order. The bar plots show the unnormalized average Avidin-peak areas of the replicates for each Avidin amount after evaluation in Skyline. The error bars correspond to the standard deviation.

The results revealed the unsuitability of higher Avidin amounts as internal controls, due to an overloading of the chromatographic system resulting in higher error bars and a reduced reproducibility in sample preparation. The main criteria when choosing the optimal Avidin amount as internal control is the exclusion of a potential signal suppression of KLK peptides. As the 1 µg and 5 µg Avidin samples show sufficient

signal intensities for both Avidin and KLK peptides, and we aimed to use as less Avidin as possible, we decided to choose 1 µg Avidin for this project.

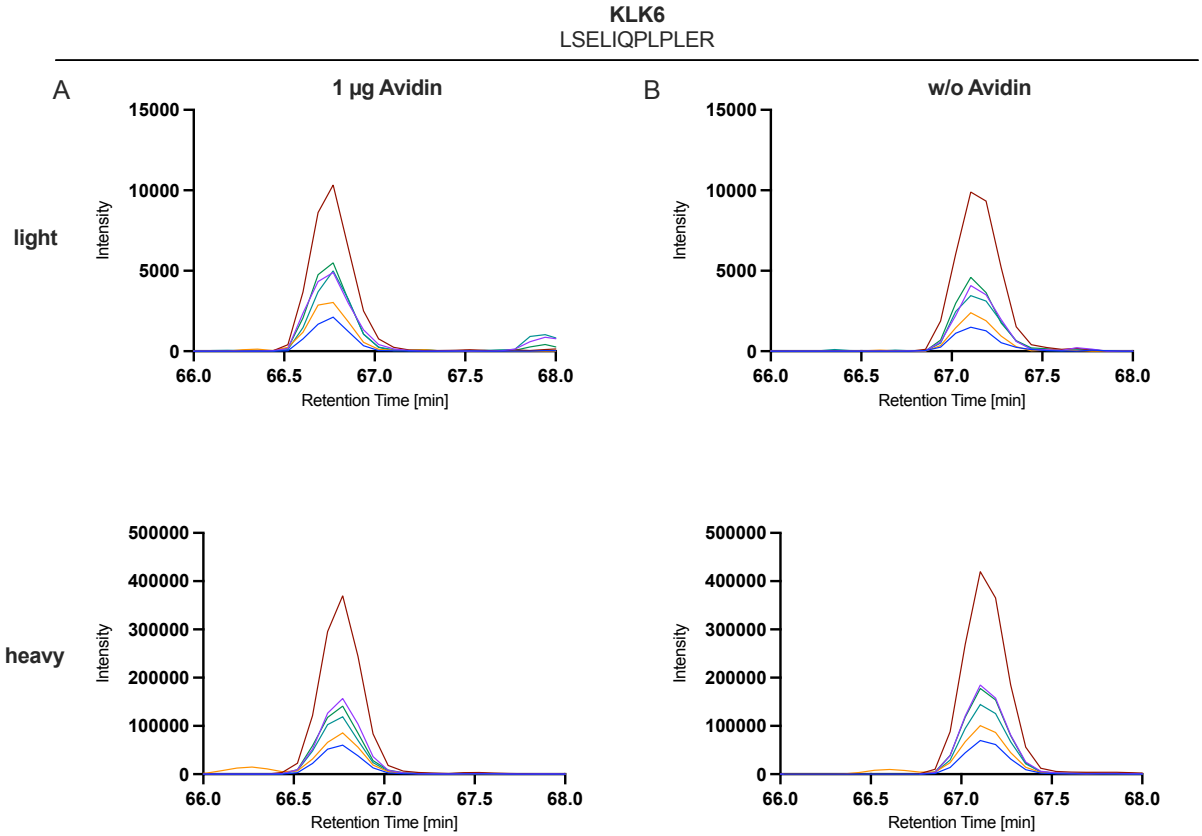

Figure 12: Detectability of KLK6 peptides in the presence or absence of Avidin. Different Avidin amounts were tested in technical triplicates of CCM deriving from pancreatic cancer cell lines. To ensure that Avidin does not interfere with the KLK signals and causes a suppression in KLK detection, samples without Avidin were carried along the measurement as reference. The resulting extracted ion chromatograms for the exemplary peptide LSELIQPLPLER from KLK6 separately illustrate light and heavy signals for the measurement in the presence (A) or absence (B) of Avidin. Lines of different color represent the different transitions.

4.1.5 SRM Assay Refinement

The optimization steps described above were performed in order to obtain a sample preparation workflow adjusted to the kallikrein proteins and thus suitable for our project. Based on the results described above we were able to establish a highly sensitive MS-based selected reaction monitoring (SRM) assay, including peptides of all fifteen kallikreins. Furthermore, the SRM assay was extended by several reference proteins as for example isotope-labelled reference peptides and the internal protein standard Avidin, which can be used for subsequent data normalization to account for biological variance between different cell lines. The established SRM assay was used for further measurements.

4.2 Cell Line Comparison

In order to investigate the pathophysiology and functional characteristics of pancreatic cancer, it is important to consider several biological models. Thereby, human cell lines represent a great biological resource for *in vitro* research of cancer and various diseases and are commonly used in the field of biomedical research. The data available in the literature about KLK secretion or expression in pancreatic cancer cell lines are almost completely based on genomic data, Western Blot analyses, or KLK-specific ELISAs [21, 54], however, only sparsely using MS as a highly sensitive and high-throughput detection method.

Therefore, the aim of this part was to use MS to compare various pancreatic cancer cell lines regarding their KLK secretion pattern in order to simulate the tumor microenvironment *in vitro*. Here, five pancreatic cancer cell lines of different types and origins were chosen, including two well-established cell lines (MiaPaCa-2 and AsPC-1) and three recently cultivated and characterized cell lines (PaCaDD-165, PaCaDD-159 and MaPaC-107), which have been kindly provided by Prof. Dr. med. Felix Rückert and his group (see **Table *8***).

Table 8: Human Pancreatic Cancer Cell Lines included in the KLK Secretion Comparison. Cell lines are deriving from different origins (PDAC, ascites from PDAC) and were either immortalized or taken directly from the primary tumor of the patient. The chosen cell lines vary in their sex, age at sampling, histology, metastatic characteristics, and their differentiation. The table was adapted from Werner et al., 2023 [68].

Tumor Cell Line	Origin of Cells	Type of Cell Line	Sex of Patient	Age at Sampling	Citation
MiaPaCa-2	Primary tumor	Immortalized cells	Male	65	https://web.expasy.org/cellosaurus/CVCL_0428
AsPC-1	Metastasis (Ascites)	Immortalized cells	Female	62	https://web.expasy.org/cellosaurus/CVCL_0152
PaCaDD-165	Metastasis (Ascites)	Primary cell culture	Male	54	[69]
PaCaDD-159	Primary tumor	Primary cell culture	Male	78	[69]
MaPaC-107	Metastasis (Ascites)	Primary cell culture	-	-	Provided by Dr. Felix Rückert

Pancreatic cancer cell lines were cultured in the respective specific medium (see Methods 5.2.1 and 5.2.2). From each of the mentioned cell lines, CCM was harvested in triplicates and processed by following the previously optimized SP3-protocol. All samples were analyzed using the SRM assay, including all 15 KLKs.

4.2.1 Peak Area Normalization to Avidin and Cell Number

Before final data analysis, detected peak areas of the KLKs needed to be normalized to correct for technical variations between different MRM measurements. Therefore, dual normalization was further applied, according to formula (1).

$$Normalised\ Peak\ Area\ Ratio = \frac{\left(\frac{Peak\ Area\ KLK}{Peak\ Area\ Avidin}\right)}{Cell\ number} \qquad (1)$$

First, unnormalized peak areas of KLKs were normalized to the internal standard Avidin in order to eliminate any handling variations between the triplicates of one cell line. Therefore, the Avidin peptide ESPLHGTQNTINK was used, which showed the most reproducible signals throughout the measurements. Second, the normalized KLK peak area of each sample was further divided by the total cell number of the corresponding cell culture dish, which was determined directly after CCM harvesting of the dishes. This last normalization step accounts for the elimination of any variations in KLK secretion between the cell lines simply caused by varying cell amounts on the dishes (see **Figure *13***). Subsequently, the mean values of the double normalized KLK peak areas and the standard deviation were calculated for each cell line.

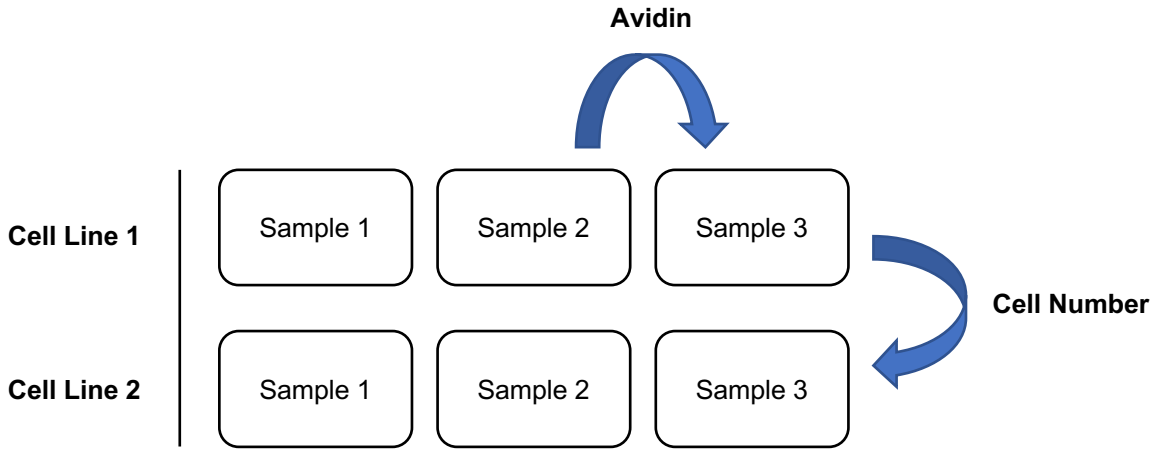

Figure 13: Normalization to Avidin and Cell Number. The spiked-in glycoprotein Avidin was used as internal standard to eliminate any variations between the triplicates during sample preparation. After harvesting the CCM from one dish, cells left on the dish were trypsinated and counted, the resulting cell numbers were compared for normalization in order to eliminate any cell-number-deriving differences between the cell lines.

To illustrate the effect of this double normalization, the signals for an exemplary peptide of the KLK6 protein are shown in **Figure *14***. The three diagrams show the different stages of the normalization steps and their effect on the peak area error. In the first

diagram, unnormalized peak areas of KLK6 for the peptide ESSQEQSSVVR are shown for the five different cell lines (MiaPaCa-2, AsPC-1, PaCaDD-165, PaCaDD-159 and MaPaC-107). By dividing the unnormalized peak area of KLK by the peak area of Avidin, followed by a division by the cell number of the corresponding cell culture dish, a decrease of the respective peak area error is revealed. Furthermore, the double normalization led to a decrease in signal values, as expected.

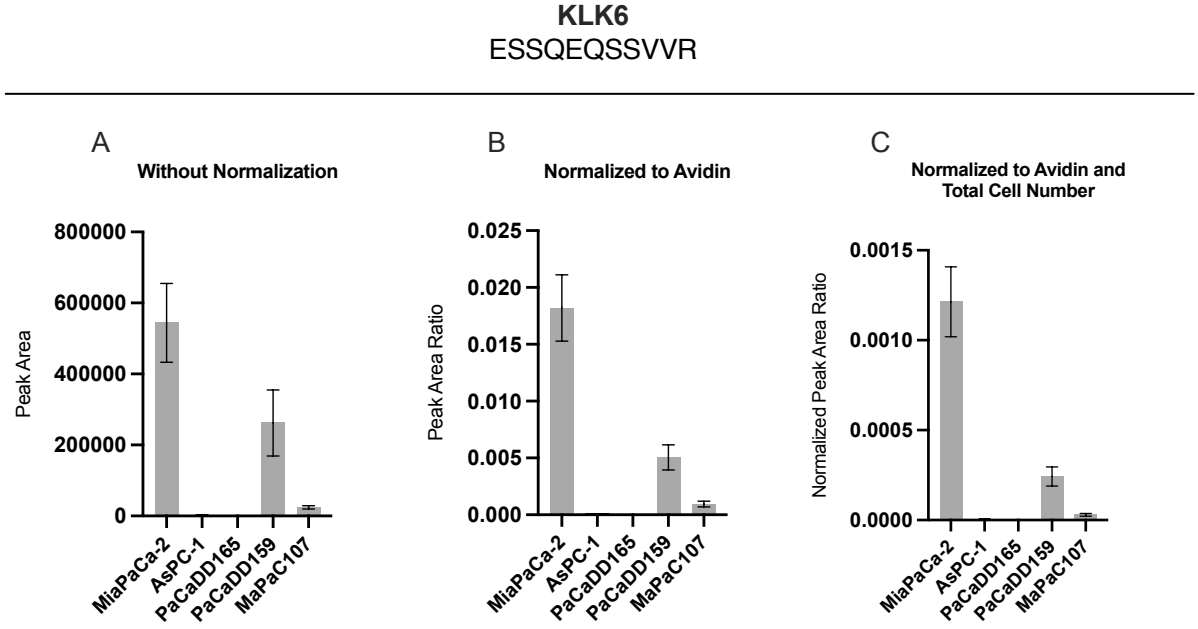

Figure 14: Effect of Avidin and Cell Number Normalization on the Peak Area of KLK6. Peak area of KLK6 (peptide ESSQEQSSVVR) is divided by the peak area of Avidin (ESPLHGTQNTINK). The resulting value is divided by the cell number of the according dish. Error bars represent the standard deviation.

4.2.2 KLK Detection in CCM of Pancreatic Cancer Cell Lines

In this part, KLK secretion levels in CCM of different pancreatic cancer cell lines were compared. All 15 KLKs of the protein family were analyzed, with particular focus on KLK6 and KLK10. Hereby, KLK3, KLK5, KLK6, KLK7 and KLK10 could be reproducibly detected in certain cell lines. The data revealed the highest level of KLK6 in CCM of the MiaPaCa-2 cell line compared to the other pancreatic cancer cell lines (see **Figure *15 A***), although the CCM of the cell line PaCaDD-159 also showed low levels of KLK6. In contrast, no KLK6 was detectable in CCM of the cell lines AsPC-1, PaCaDD-165 and MaPaC-107. The highest KLK10 secretion could be detected for the cell line AsPC-1, whereas no KLK10 was detectable in CCM of the MiaPaCa-2 cell line (see **Figure *15 B***). The three primary cell lines PaCaDD-165, PaCaDD-159 and MaPaC-107 showed lower KLK10 levels than AsPC-1. Besides KLK6 and KLK10, we were also

able to detect KLK3/PSA, KLK5 and KLK7 in several pancreatic cancer cell lines (see **Figure *15 C-E***). For all these additional KLKs, its secretion was the highest in CCM of the MiaPaCa-2 cell line.

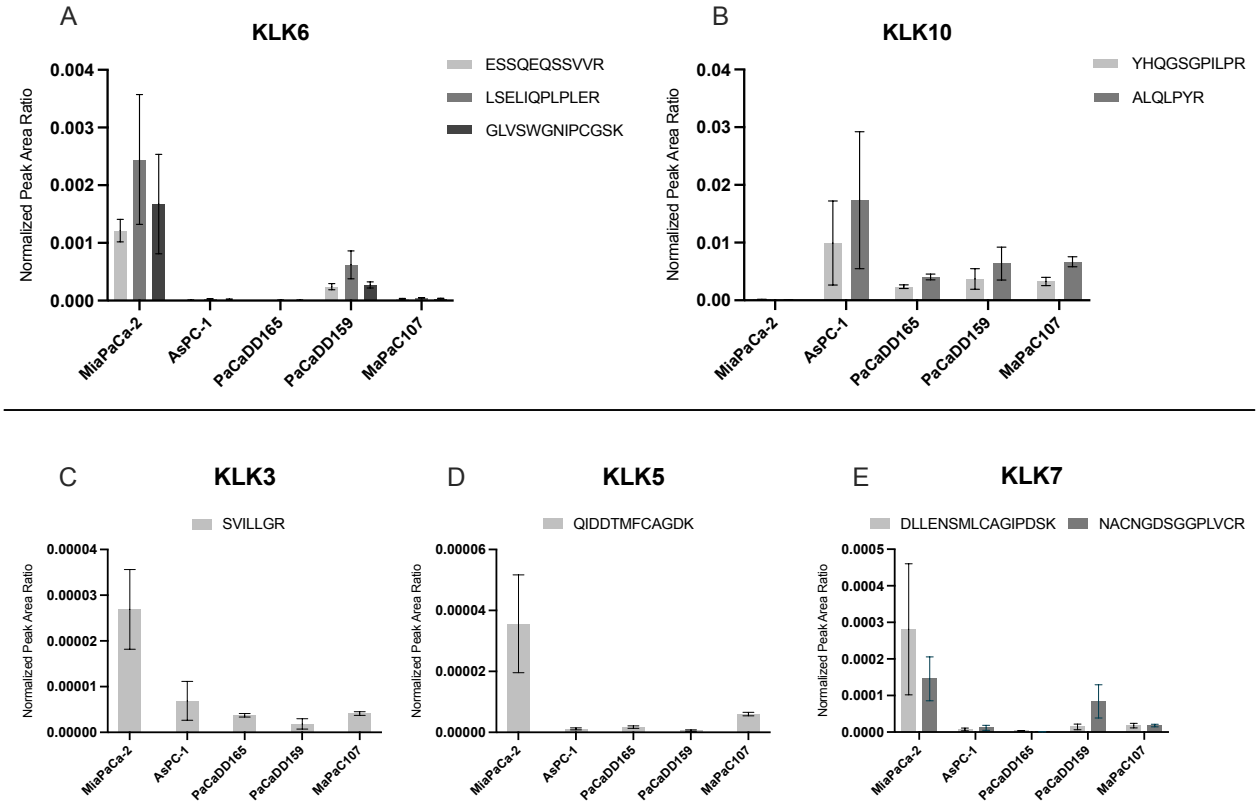

Figure 15: KLK Secretion in different Pancreatic Cancer Cell Lines. CCM of five different pancreatic cancer cell lines was tested for KLK detectability by SRM analysis. The graphs show the detected peptides for KLK3, KLK5, KLK6, KLK7 and KLK10 among the different cell lines. The peak areas of the KLKs were normalized to Avidin and the total cell number of the according dishes, as described above. Error bars represent the standard deviation. Adapted from figure 1 of Werner et al., 2023 [68].

4.3 FFPE Cohort

The main objective of the last part of the thesis was to perform both targeted and explorative MS based analyses of patient-derived FFPE tissues. As FFPE tissues represent one of the most valuable sources for clinical research, tissues of PDAC (n=14), normal pancreas (n=5), non-malignant adjacent pancreas (n=11), chronic pancreatitis (n=7) and ampullary cancer (n=3) were chosen for the present study, resulting in a patient cohort of 40 samples (see **Table *9***).

Table 9: Patient Cohort for Targeted and Explorative Analysis. Samples were kindly provided by the University of Heidelberg, Faculty of Mannheim, and the Institute for Surgical Pathology, Freiburg.

Tissue entity	PDAC	Normal Pancreas	Non-malignant Adjacent Pancreas	Chronic Pancreatitis	Ampullary Cancer
Number of patients	14	5	11	7	3

As part B of the thesis compared the KLK secretion of different pancreatic cancer cell lines, we further aimed to investigate the KLK protein expression in patient-derived FFPE tissues, again by applying targeted MS. Secondly, the cohort samples were subjected to explorative MS, aiming to compare the different tissue proteomes regarding specific characteristics or commonalities between their protein expression independent of the KLK proteins. To our knowledge, these would be the first targeted and explorative MS approaches of tissues from PDAC, chronic pancreatitis, ampullary cancer, as well as normal and non-malignant pancreas.

4.3.1 Pilot PRM Measurement of Patient Cohort

FFPE tissues included in the cohort were undergoing deparaffinization, macrodissection and subsequent preparation with the optimized SP3 bead protocol, before subjecting the samples to PRM analysis. First, a rough overview about the qualitative KLK expression was gained, in order to choose the most promising KLKs for the second and final measurement. This was achieved by including all 15 KLKs in the PRM assay, as well as the housekeeping protein GAPDH, which was suggested to serve as a potential reference protein for future data analysis. Regarding the normalization of the generated data, three options were taken into consideration: normalization to GAPDH, iRT spike-in peptides and normalization to heavy reference peptides. GAPDH expression varied among the different entities, resulting in higher GAPDH levels in malignant tumors such as PDAC and ampullary cancer and

substantially lower levels in non-neoplastic tissues. Due to the unequal expression of GAPDH in tumorous and non-tumorous tissue, in this study, GAPDH was not considered as a normalization protein. Furthermore, several iRT spike-in peptides did not constantly show stable signals throughout the measurement (measurement time was over one week) and were therefore also not suitable as a possible normalization basis. This specific effect could also be observed for certain KLK heavy peptides, leading to the conclusion that neither iRT peptides nor KLK heavy peptides could be used as normalization references. As none of the potential normalization sources seemed to be in line with the data and the latter only represented a pilot study prior to our final PRM measurement, we decided to leave this data set unnormalized. Therefore, this approach has been limited to qualitative information about KLK protein expression.

The data revealed GAPDH expression in all samples of the five tissue entities (no heavy peptides as reference) (see **Table 10**). Furthermore, KLK1 was detected in tissues of both normal and non-malignant adjacent pancreas. KLK14 showed expression in PDAC, in line with KLK7, whereas KLK6 and KLK10 both showed expression in PDAC as well as in tissues of ampullary cancer. KLK6 was additionally detected in 3/14 samples in tissues of non-malignant adjacent pancreas, however, the tissue of these three samples was scraped off directly next to the marked tumor areas, which might explain KLK detectability. Kallikreins not detected in any of the five conditions included KLK2, KLK3, KLK4, KLK5, KLK8, KLK9, KLK11, KLK12, KLK13 and KLK15. Due to the expression of KLK6 and KLK10 in both malignant entities PDAC and ampullary cancer, these two KLKs were chosen to be further included in the final PRM measurement assay. In addition, KLK7 was included in the final PRM assay as it showed several promising signals throughout the PDAC samples, in contrast to KLK14, which was only detectable in 1/14 PDAC samples. Moreover, since increased protein levels of KLK7 have already been reported within pancreatic cancer [23], we aimed to validate this finding.

Table 10: KLK and GAPDH Detectability in PDAC, Normal Pancreatic Tissue, Non-Malignant Adjacent Pancreatic Tissue, Chronic Pancreatitis, and Ampullary Cancer by PRM Measurement. The PRM assay included all 15 KLKs and the commonly used internal standard GAPDH as a potential reference protein for future data normalization. Tissues included in the cohort were PDAC (n=14), normal pancreas (n=5), non-malignant adjacent pancreas (n=11), chronic pancreatitis (n=7) and ampullary cancer (n=3), whereas individual samples per condition were combined in this table. To validate the correct peak picking, heavy peptides were used as positive control/reference source. Data was not subjected to any normalization processes

	PDAC	Normal Pancreas	Non-malignant Adjacent Pancreas	Chronic Pancreatitis	Ampullary Cancer
KLK1	-	+	+	-	-
KLK2	-	-	-	-	-
KLK3	-	-	-	-	-
KLK4	-	-	-	-	-
KLK5	-	-	-	-	-
KLK6	+	-	+	-	+
KLK7	+	-	-	-	-
KLK8	-	-	-	-	-
KLK9	-	-	-	-	-
KLK10	+	-	-	-	+
KLK11	-	-	-	-	-
KLK12	-	-	-	-	-
KLK13	-	-	-	-	-
KLK14	+	-	-	-	-
KLK15	-	-	-	-	-
GAPDH	+	+	+	+	+

Consequently, the final PRM analysis of the cohort was performed focusing on KLK6, KLK7 and KLK10. The reduced number of proteins-of-interest allows the inclusion of more peptides of the respective proteins to the PRM assay, increasing the probability for KLK detection.

4.3.2 Final PRM Measurement of Patient Cohort

To ensure the most optimized final PRM measurement of the cohort, further improvement steps needed to be performed. First, heavy labelled peptide standards of GAPDH were added to each sample in order to confirm the presence of GAPDH by correct chromatographic peak picking. Concerning the stability of iRT and heavy peptides and in order to reduce peptide degeneration, aliquots of both iRT and heavy labelled peptides were prepared in advance and were added to the sample immediately before MS measurement. Samples were measured in less than two hours after sample preparation to again avoid rapid peptide degeneration.

The results of the final PRM measurement revealed stable signals of heavy labelled (KLK) reference peptides throughout the measurement, which could then be further used as normalization source for the generated data. Interestingly, GAPDH expression

showed the same effect as it could already be observed in the previous measurement, with elevated levels in PDAC and ampullary cancer compared to the residuary benign tissues (see **Figure *16***).

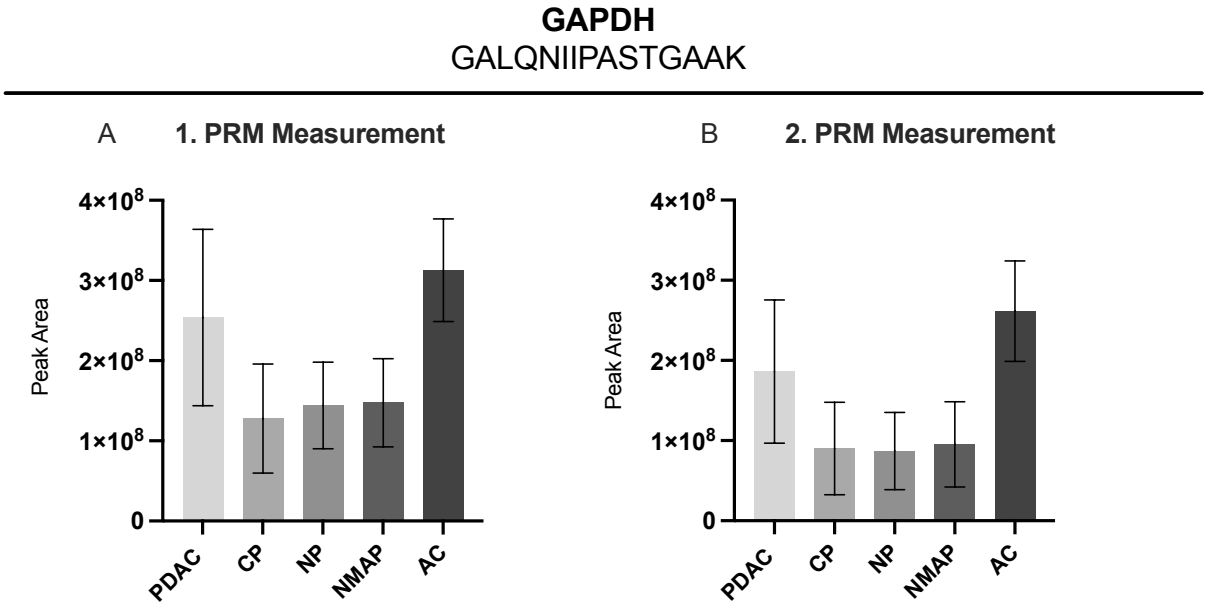

Figure 16: GAPDH Expression in different Tissue Entities in the first and second PRM Measurement, illustrated for the exemplary peptide GALQNIIPASTGAAK. The two diagrams show the detected GAPDH peak areas in tissues of pancreatic ductal adenocarcinoma (PDAC), chronic pancreatitis (CP), normal pancreas (NP), non-malignant adjacent pancreas (NMAP), and ampullary cancer (AC) in the first PRM measurement (A) and in the second PRM measurement (B). The represented data is unnormalized, error bars represent the standard deviation. (B) was adapted from figure 2 of Werner et al., 2023 [68].

In addition to GAPDH detection, KLK detection could be shown in several samples of the different conditions (see **Table *11***). KLK6 showed expression in 11/14 PDAC samples, whereas KLK10 was detected in 12/14 PDAC tissues. With respect to ampullary cancer, both KLK6 and KLK10 showed expression in all samples (n=3). Furthermore, KLK6 was detected in 1/11 samples deriving from non-malignant adjacent pancreatic tissues, whereas KLK10 additionally showed expression in 1/7 samples of chronic pancreatitis. In tissues of normal pancreas, no KLK detectability was observed, consistent with a missing detectability of KLK7 in all samples of the cohort.

Table 11: Endogenously detected KLK6, KLK7 and KLK10 in PDAC, Normal Pancreatic Tissue, Non-Malignant Adjacent Pancreatic Tissue, Chronic Pancreatitis, and Ampullary Cancer by PRM Measurement. The PRM assay included KLK6, KLK7 and KLK10. Tissues included in the PRM analysis were PDAC (n=14), normal pancreas (n=5), non-malignant adjacent pancreas (n=11), chronic pancreatitis (n=7) and ampullary cancer (n=3), whereas each sample per condition is shown in the table. Data was normalized to heavy labelled reference peptides. Adapted from table 2 of Werner et al., 2023 [68].

Tissue Entity	KLK6	KLK10	KLK7
PDAC (n=14)	+	+	-
	+	-	-
	-	-	-
	+	+	-
	-	+	-
	+	+	-
	+	+	-
	-	+	-
	+	+	-
	+	+	-
	+	+	-
	+	+	-
	+	+	-
	+	+	-
Ampullary Cancer (n=3)	+	+	-
	+	+	-
	+	+	-
Normal Pancreas (n=5)	-	-	-
	-	-	-
	-	-	-
	-	-	-
	-	-	-
Non-malignant Adjacent Pancreas (n=11)	-	-	-
	-	-	-
	-	-	-
	-	-	-
	+	-	-
	-	-	-
	-	-	-
	-	-	-
	-	-	-
	-	-	-
	-	-	-
Chronic Pancreatitis (n=7)	-	-	-
	-	-	-
	-	+	-
	-	-	-
	-	-	-
	-	-	-
	-	-	-

Since we gained valuable information about KLK protein expression in PDAC, ampullary cancer, normal pancreas, non-malignant adjacent pancreas and chronic pancreatitis, a further quantitative comparison regarding KLK upregulation was performed between the different tissue entities. Hereby, we focused on comparisons between PDAC and the benign tissues (see **Figure *17***).

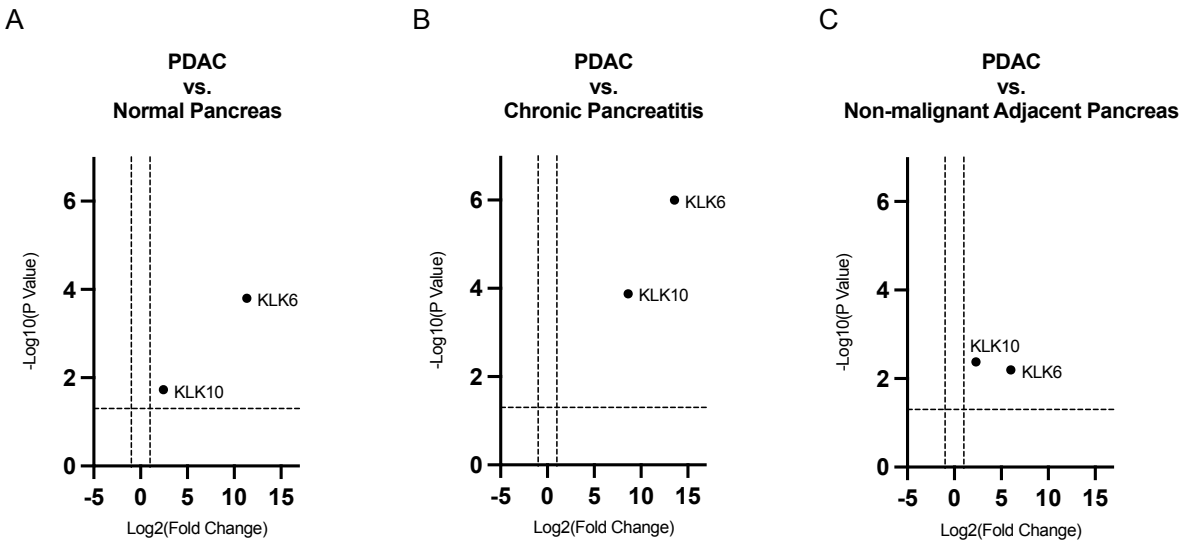

Figure 17: Volcano Plots on KLK protein level comparing PDAC with tissues of Normal Pancreas, Non-malignant Adjacent Pancreas, and Chronic Pancreatitis. Results of pairwise quantitative comparisons (two-sample t-test) of KLK6 and KLK10 between PDAC and the respective controls. The data is normalized to heavy labelled reference peptides. Black dots represent KLK6 or KLK10 protein. X-axis shows the Log2 Fold Chance in protein expression and y-axis represents the adjusted p-value in -log10 scale. Horizontal dashed line represents the adjusted p-value threshold of P value=0,05, whereas the vertical dashed line represents a Fold Change threshold for 2-fold abundance change. Adapted from figure 2 of Werner et al., 2023 [68].

All three diagrams show a significant upregulation of both KLK6 and KLK10 in PDAC when compared to various non-neoplastic tissues. In general, KLK6 seems to be higher upregulated in PDAC than KLK10, applying to all three comparisons. Additionally, in comparison to normal pancreatic tissue and to chronic pancreatitis, KLK6 in PDAC shows a more significant upregulation than KLK10. Interestingly, the same effect of KLK6 and KLK10 being upregulated in cancer tissue in comparison to benign tissues could also be shown when plotting ampullary cancer against tissues of normal pancreas, non-malignant adjacent pancreas, and chronic pancreatitis (see **Figure *S 26***).

In conclusion, we observed high protein levels of KLK6 and KLK10 in PDAC and ampullary cancer compared to normal pancreas, non-malignant adjacent pancreas, and chronic pancreatitis.

4.3.3 DIA Measurement

As the targeted approach aimed to gain information specifically about KLK expression in samples of PDAC, normal and non-malignant adjacent pancreas, chronic pancreatitis as well as ampullary cancer, the following explorative analysis aims to describe and compare the overall proteome biology of the above-named tissue entities.

Here, the patient cohort used for the PRM approach was measured again, this time by applying the DIA mode (see **Figure *18***).

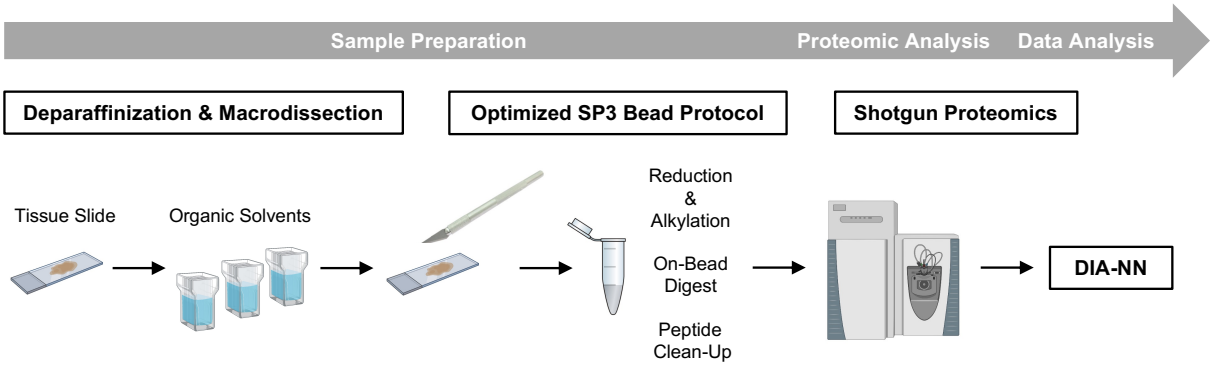

Figure 18: **Experimental Design of DIA measurement regarding the FFPE Patient Cohort.** Sample preparation included deparaffinization and macrodissection of FFPE tissue slides, followed by application of the optimized SP3 bead protocol. Subsequent to proteomic analysis of the samples, a gas phase fractionation (GPF) library was generated, important for future data analysis. Lastly, data analysis was performed using the platform DIA-NN.

4.3.4 Library Generation, Measurement of Cohort, and sPLS-DA

For appropriate peptide and protein identification, a spectral library was generated, which ideally represents the totality of peptides contained in the cohort. The library derived from an equal mixture of all cohort samples, which was online gas phase fractionated during subsequent measurement before the spectral library was generated using DIA-NN. The resulting spectral library contained 7307 proteins, with a total number of 42636 peptides. Unique Peptide and Protein IDs are represented in **Figure *19***.

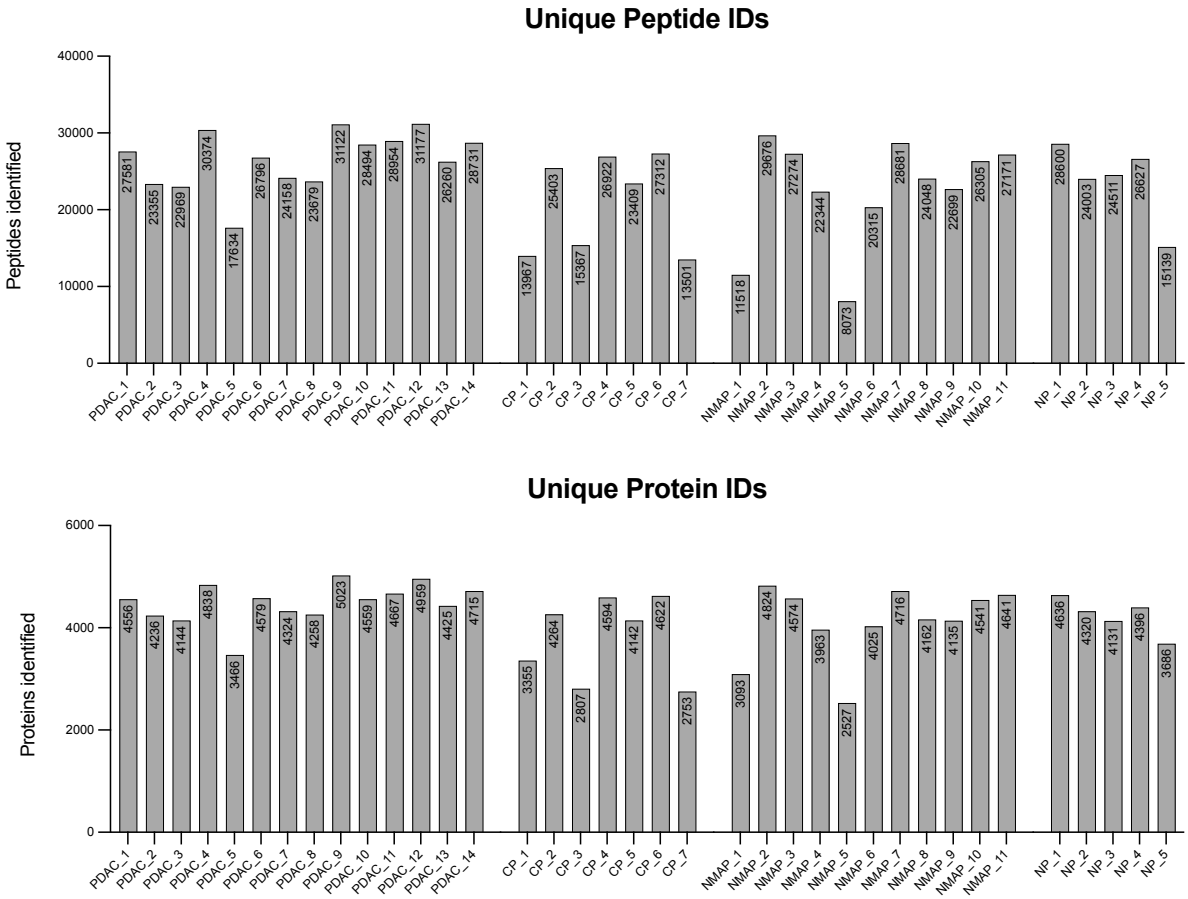

Figure 19: Unique Peptide and Protein IDs in cohort samples. Results of data-independent acquisition (DIA) measurement of cohort using the Q Exactive mass spectrometer. The cohort included samples of PDAC (n=14), chronic pancreatitis (CP) (n=7), non-malignant adjacent pancreas (NMAP) (n=11) and normal pancreas (NP) (n=5). Values were obtained from a report generated by the platform DIA-NN. A 1 % false discovery rate (FDR) was used. Y-axis represents the peptides/proteins identified. Adapted from figure 3 of Werner et al., 2023 [68].

After subsequent DIA measurement of cohort samples, the resulting DIA dataset contained 5936 identified and quantified proteins. In order to ensure a high-quality dataset for further analysis and to avoid misinterpretations due to a high number of missing values, only proteins were kept which provide at least 80 % valid values per condition. This filtering led to 2279 remaining proteins with a total of 2,1 % missing values in the overall dataset. After performing batch correction using ComBat, the generated data was subjected to sparse partial least squares discriminant analysis (sPLS-DA), which enables a visual comparison between the different proteome profiles of the included conditions. An overlap of the calculated 95 % confidence intervals (visualized by ellipses) indicates that the affected conditions share one or more differentially expressed proteins. The initial sPLS-DA revealed a complete overlap of malignant proteomes of PDAC and ampullary cancer (see **Figure *S 24***). Unfortunately, further in-depth analysis of the ampullary cancer condition had to be skipped due to

the small number of samples (n=3). sPLS-DA additionally showed an almost complete overlap between the conditions normal pancreas (NP) and non-malignant adjacent pancreas (NMAP). This indicates multiple similarities in their global proteomic profile, which was initially expected as the two conditions almost represent the same tissue identities. For further studies, they were therefore no longer considered as two single conditions and were consequently pooled to form the new condition normal non-malignant control (NNMC). The subsequent sPLS-DA was hence performed with the three conditions PDAC, chronic pancreatitis and NNMC (see **Figure *S 25***). Here, we observed one outlier of the NNMC condition, namely cohort sample NMAP_11. However, as the sample is located outside of the calculated NNMC 95 % confidence interval, which ensures a certain consistency of the generated data, as well as due to the former very close location of the macrodissected adjacent tissue to the contiguous tumorous tissue, the sample NMAP_11 has therefore been removed from the NNMC condition. Further in-depth analysis was redone, now including the three conditions PDAC, chronic pancreatitis and NNMC, the latter without cohort sample NMAP_11 (see **Figure *20***). The final sPLS-DA shows a distinct clustering of all three conditions, however, with partial overlapping regions. Furthermore, benign entities NNMC and CP show a larger overlap compared to the malignant entity PDAC.

Final sPLSDA of the Conditions CP, NNMC and PDAC

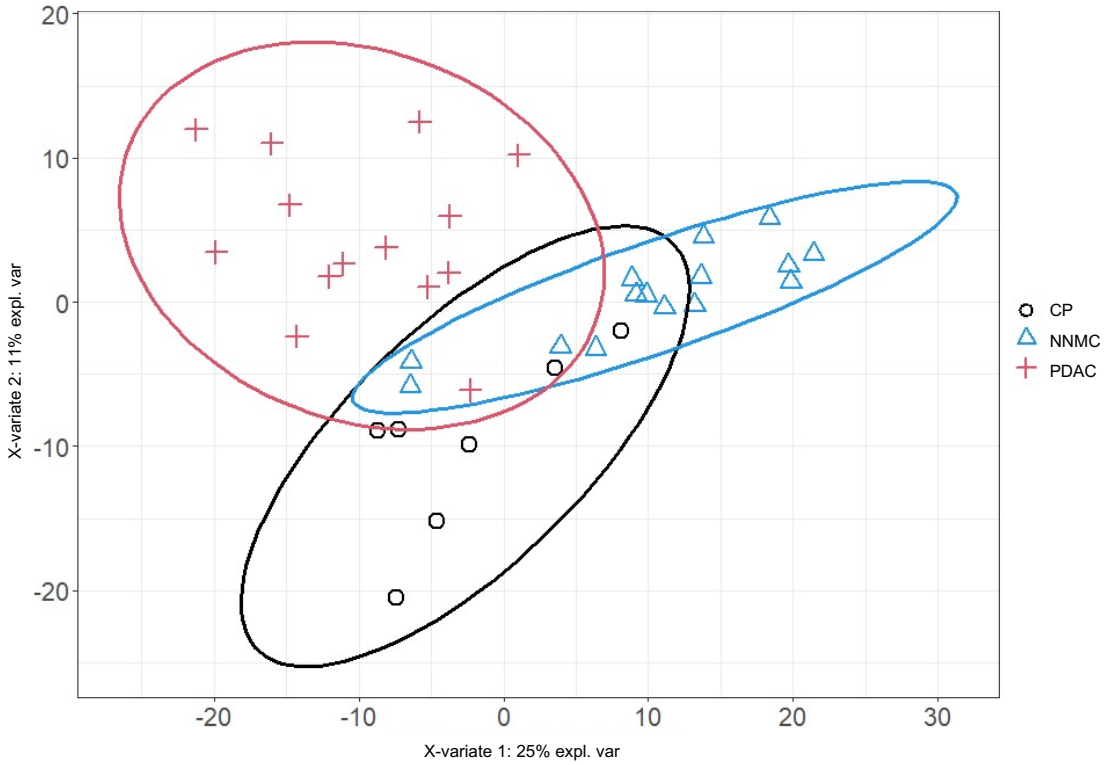

Figure 20: Sparse Least Squares Discriminant Analysis (sPLS-DA) of final DIA dataset. Included are the conditions PDAC, chronic pancreatitis (CP) and normal non-malignant control (NNMC). Ellipses display the calculated confidence interval (95 %). Adapted from figure 3 of Werner et al., 2023 [68].

Since the main objective of this part was to investigate proteome differences between the included conditions, the data from sPLS-DA was further used to extract characteristic protein representatives of each group based on their intensity contribution and explanatory power (see **Table *S 16***). Within this list of characteristic proteins for the respective condition, gene enrichment analysis was performed (see **Table 12**). Protein groups specific for the condition PDAC seem to be involved in cell adhesion, cytoskeleton, and the cytoplasmic energy metabolism. With respect to chronic pancreatitis, the results revealed protein groups participating in the ECM interaction. Lasty, proteins involved in translation and protein targeting and processing in the endoplasmic reticulum (ER) seem to be characteristic for normal pancreatic tissue.

4.3.5 Co-Abundance Clustering

In order to find protein groups showing the same abundance behavior across the considered conditions, a co-abundance cluster analysis using the publicly available Clust algorithm was performed, in order to assign each identified protein to a certain abundance-course with a confidence interval of 95 % [70]. This analysis depicted 8 distinct co-abundance clusters for the present dataset with a total of 1227 assigned proteins (see **Figure *21***). For each of the resulting clusters, gene enrichment analysis was performed in order to identify common biological functions (see **Table 12**). Proteins with the highest relative abundance in PDAC seem to participate in cell adhesion and ECM interaction, whereby with respect to CP, proteins connected to wound healing processes showed the strongest increase in abundance. Regarding characteristic protein groups which are specifically downregulated in PDAC and CP, no enriched GO annotations could be found. This might be due to the very few numbers of proteins which were assigned to the respective cluster (see co-clusters A and B). Regarding cluster 5-8 of the normal non-malignant control (see **Figure *21 C***), it becomes clear that the Clust algorithm did not reveal a clear difference between cluster 5-6 and cluster 7-8, which is illustrated by the similar GO-term results listed below each diagram. Therefore, these four clusters were consequently combined under the heading “major difference to NNMC”. Hereby, proteins participating in translational processes as well as protein targeting and processing in the ER show a high relative abundance change

in the NNMC compared to the other conditions. In contrast, proteins with the least relative abundance in the NNMC include members of the humoral immune response, wound healing, cell adhesion, and cytoskeletal proteins.

Another observation comprises the varying protein numbers, which have been assigned to the respective clusters. It is therefore noticeable that the majority of proteins were assigned to cluster 5-8 (see **Figure *21 C***) which shows the major difference to NNMC. On the other hand, cluster 1-2 (see **Figure *21 A***) and cluster 3-4 (see **Figure *21 B***) dispose a substantially lower number of allocated proteins.

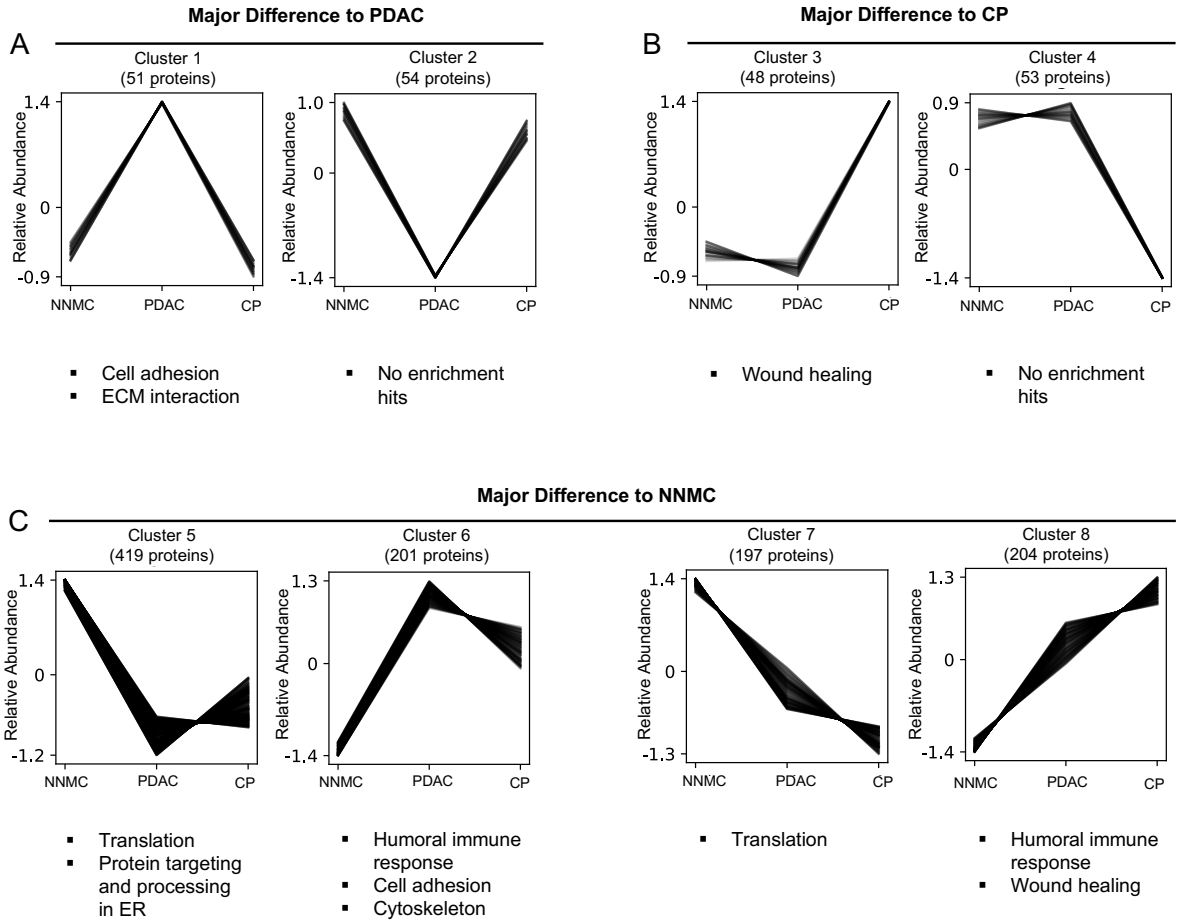

Figure 21: PDAC-, CP-, and NNMC-specific Relative Protein Abundance Change. Co-abundance clusters show specific relative protein abundance changes of the conditions PDAC (A), chronic pancreatitis (CP) (B), and normal non-malignant control (NNMC) (C), with the respective GO-term annotation listed below each cluster diagram. X-axis shows the different conditions PDAC, CP and NNMC, whereas relative abundance is plotted on the y-axis. Numbers of proteins assigned to each cluster are stated above each cluster diagram. Adapted from figure 3 and figure S5 of Werner et al., 2023 [68].

4.3.6 Multigroup Limma Comparison

As the co-abundance clusters only provide a general overview about protein groups which show the same abundance behavior between the different conditions, we further aimed to investigate the individual protein level. At this point, the leading question was which individual proteins changed their abundance significantly compared to the given condition. Therefore, a differential expression analysis using a multigroup limma approach was performed. The results revealed 588 significant hits (adjusted p-value ≤ 0,05) for the comparison CP vs. NNMC, 112 significant hits for PDAC vs CP, and a total of 980 significant hits for PDAC vs. NNMC (see **Figure 22**). For each condition in the respective comparison, gene enrichment analysis was performed (see **Table 12**).

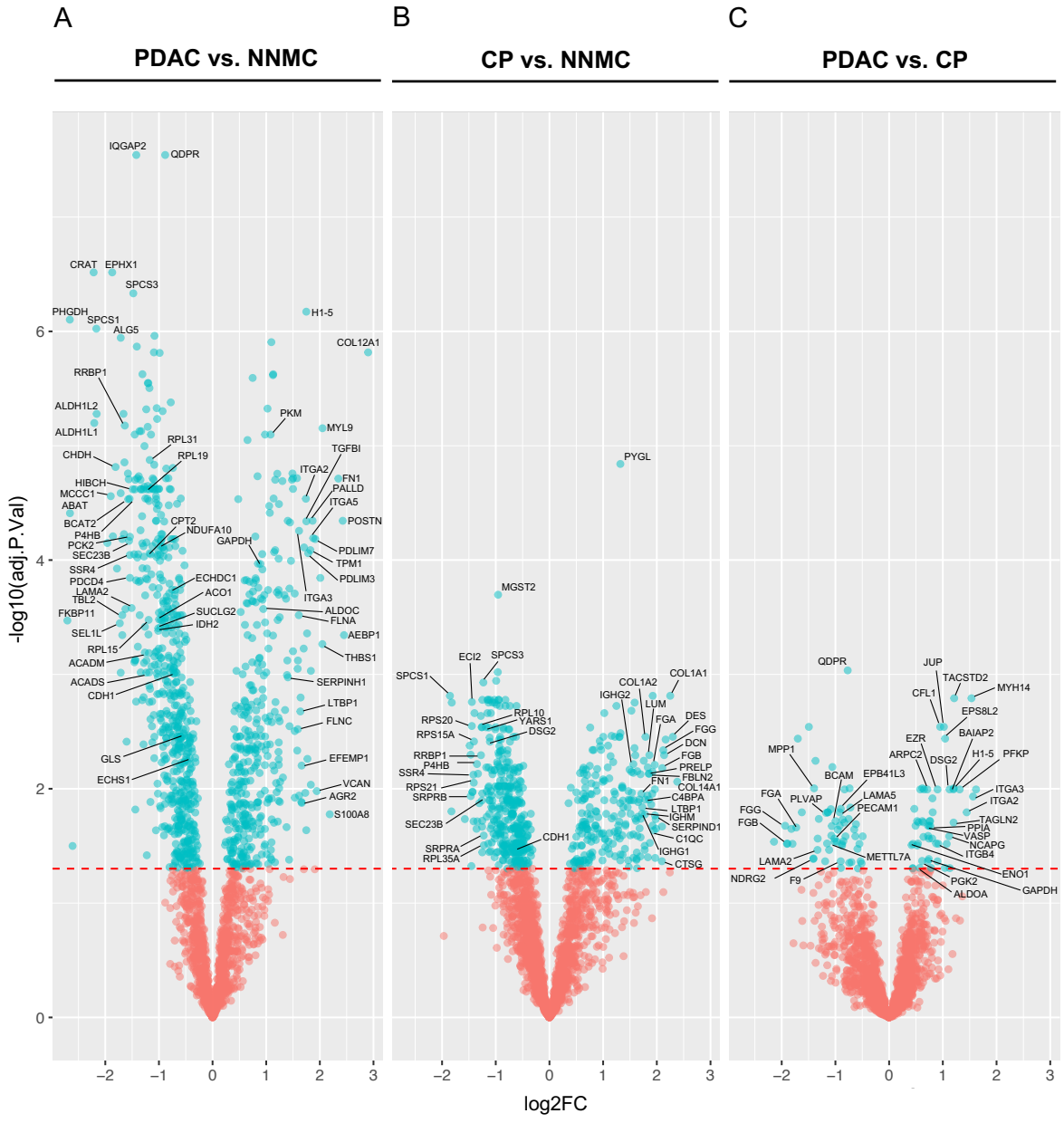

Figure 22: Volcano Plots of CP and PDAC compared to the NNMC using a Multigroup Limma approach. (A) PDAC vs. normal non-malignant control (NNMC) (B) Chronic pancreatitis (CP) vs. NNMC (C) PDAC vs. CP. The fold changes in log2 scale are plotted on the x-axis, y-axis shows the respective

adjusted p-values in -log10 scale. The applied p-value cut-off was set to 0,05, which is depicted as a dashed line. Arrows show a manual selection of significantly up- or downregulated proteins of the respective condition. Adapted from figure 3 of Werner et al., 2023 [68].

Regarding the comparison of PDAC with the normal non-malignant control (see **Figure *22 A***), gene-enrichment analysis revealed proteins involved in translational processes to be downregulated in PDAC compared with normal pancreatic tissue, as for example multiple ribosomal proteins (RPL15, RPL19, RPL31). Furthermore, we observed proteins contributing to the protein targeting and processing in the ER to be downregulated in PDAC, as the signal peptidase complex subunits 1 and 3 (SPCS1, SPCS3), which are important for protein export processes, in addition to the ribosome-binding protein 1 (RRBP1) and protein disulfide-isomerase (P4HB), which are both involved in protein processing in the ER. In addition, proteins being part of the mitochondrial energy metabolism could be shown to be downregulated in PDAC compared to its normal counterpart. Hereby, proteins of the citrate cycle were found, as the isocitrate dehydrogenase (IDH2), cytoplasmic aconitate hydratase (ACO1), succinate--CoA ligase (SUCLG2), as well as members of the fatty acid degradation, pyruvate metabolism and oxidative phosphorylation (see **Table *S 16***). Moreover, proteins involved in the amino acid metabolism seem to be downregulated in PDAC, as for example the branched-chain-amino-acid aminotransferase (BCAT2), and the 4-aminobutyrate aminotransferase (ABAT). Here, proteins particularly seem to be involved in the cysteine and methionine metabolism, valine, leucine and isoleucine degradation as well as beta-alanin metabolism. Another observation comprises the downregulation of the tumor suppressor protein programmed cell death protein 4 (PDCD4) in PDAC compared to normal pancreatic tissue.

Proteins which were found to be upregulated in PDAC compared to the NNMC include members of the ECM interaction, as for example collagens (COL12A1), fibronectin (FN1), and integrins (ITGA2, ITGA3, ITGA5). Furthermore, cytoskeletal proteins like filamin-C (FLNC), and fibronectin (FN1), as well as proteins involved in cell adhesion could be observed to be upregulated in PDAC. The latter group includes proteins as filamin-A (FLNA), transforming growth factor-beta-induced protein ig-h3 (TGFBI) and the versican core protein (VCAN). Moreover, the proto-oncogene protein anterior gradient protein 2 homolog (AGR2) was also found to be upregulated in PDAC compared to normal pancreatic tissue. Besides the proto-oncogene protein and proteins of cell adhesion, cytoskeleton and ECM interaction, the results further

revealed members of the cytoplasmic glycolysis/gluconeogenesis, as the pyruvate kinase (PKM), fructose-bisphosphate aldolase C (ALDOC) and glyceraldehyde-3-phosphate dehydrogenase (GAPDH). However, gene-enrichment analysis did not reveal the term glycolysis/gluconeogenesis.

The comparison of chronic pancreatitis with the NNMC (see **Figure *22 B***) revealed proteins involved in translational processes to be downregulated in CP compared to normal pancreatic tissue. These proteins mainly include ribosomal proteins (RPS20, RPS21, RPS15A, RPL10, RPL35A), among others. Furthermore, proteins involved in protein targeting and processing in the ER were found to be downregulated in CP compared to normal pancreatic tissue, including signal peptidase complex subunits 1 and 3 (SPCS1, SPCS3), and signal recognition particle receptor subunits alpha and beta (SRPRA, SRPRB), which represent important members for protein export processes. Moreover, cell adhesion molecules cadherin-1 (CDH1) and desmoglein-2 (DSG2) could also be observed to be downregulated in CP compared to the NNMC.

Proteins, which were shown to be upregulated in CP compared to NNMC are involved in the humoral immune response, as multiple immunoglobulins (IGHG1, IGHG2, IGHM), as well as c4b-binding protein alpha chain (C4BPA) and complement C1q subcomponent subunit C (C1QC), which are contributing to the complement and coagulation cascades. Furthermore, proteins included in wound healing processes were shown to upregulated in CP, as fibrinogens (FGA, FGB, FGG) contributing to the formation of fibrin blood clots, the serine protease Cathepsin G (CTSG), and heparin cofactor 2 (SERPIND1). In addition, the results revealed proteins of the ECM interaction to be upregulated in CP compared to normal pancreatic tissue, including collagens (COL1A1, COL1A2, COL14A1) and fibronectin (FN1), among others.

Lastly, the proteome of the PDAC entity was compared against chronic pancreatitis (see **Figure *22 C***). Here, proteins involved in wound healing processes were found to be downregulated in PDAC compared to CP, where again multiple fibrinogens (FGA, FGB, FGG) along with the coagulation factor IX (F9) could be identified. Another finding represents the protein methyltransferase-like protein 7A (METTL7A), which is involved in neutrophil degranulation, and 55 kDa erythrocyte membrane protein (MPP1), a regulator for neutrophil chemotaxis. Moreover, two tumor suppressor

proteins (NDRG2, EPB41L3) could be observed to be downregulated in PDAC compared to CP.

On the other hand, proteins which were found to be upregulated in PDAC compared to chronic pancreatitis include members of cell adhesion, as integrins (ITGA3, ITGB4), the tight junction proteins vasodilator-stimulated phosphoprotein (VASP), ezrin (EZR), a member of the cadherin family, namely desmoglein-2 (DSG2), as well as plakoglobin (JUP). We further observed many cytoskeletal proteins to be upregulated in PDAC, as for example integrin alpha-2 (ITGA2), cofilin-1 (CFL1), and ezrin (EZR). In addition, proteins involved in cytoplasmic metabolism additionally seem to be upregulated in PDAC compared to CP, as for example multiple proteins of the glycolysis like the ATP-dependent 6-phosphofructokinase (PFKP), phosphoglycerate kinase 2 (PGK2), fructose-bisphosphate aldolase A (ALDOA), alpha-enolase (ENO1), and glyceraldehyde-3-phosphate dehydrogenase (GAPDH), which all display proteins involved in glycolysis/gluconeogenesis.

Table 12: sPLS-DA, Co-Abundance Cluster and Multigroup Limma analysis of PDAC, CP and NNMC samples. (A) sPLS-DA with representative protein groups for each condition (B) co-abundance clustering of each condition (C) Multigroup Limma analysis of the predetermined comparisons PDAC vs. NNMC and CP vs. NNMC.

A sPLS-DA

PDAC	▪ Cell adhesion ▪ Cytoskeleton ▪ Cytoplasmatic energy metabolism
CP	▪ ECM interaction
NNMC	▪ Translation ▪ Protein targeting and processing in ER

B Co-Abundance Clustering

	Upregulated	Downregulated
PDAC	▪ Cell adhesion ▪ ECM interaction	▪ No enrichment hits
CP	▪ Wound healing	▪ No enrichment hits
NNMC	▪ Translation ▪ Protein targeting and processing in ER	▪ Humoral immune response ▪ Wound healing ▪ Cell adhesion ▪ Cytoskeleton

C Multigroup Limma

	Upregulated	Downregulated
PDAC vs. NNMC	▪ Cell adhesion ▪ Cytoskeleton ▪ ECM interaction	▪ Protein targeting and processing in ER ▪ Translation ▪ Mitochondrial energy metabolism ▪ Amino acid metabolism
CP vs. NNMC	▪ Humoral immune Response ▪ Wound healing ▪ ECM interaction	▪ Protein targeting and processing in ER ▪ Translation
PDAC vs. CP	▪ Cell adhesion ▪ Cytoskeleton ▪ Cytoplasmatic energy metabolism	▪ Wound healing

4.3.7 Pro-Tumorigenic Proteins and Tumor Suppressor Gene (TSG) Abundance

In general, PDAC represents a tumor with commonly recurrent gene abnormalities [71]. Four of the most usually identified oncogenes in PDAC are mutations of KRAS, as well as mutations and deletions of the tumor suppressor genes TP53, SMAD4 and CDKN2A. As most of the literature is referring to oncogenes rather than oncogene proteins, we further aimed to investigate pro-tumorigenic proteins in PDAC. Therefore, the generated DIA data (before sparsity reduction) was matched against a created list including commonly known PDAC oncogenes. The results revealed nine identified PDAC pro-tumorigenic proteins and two tumor suppressor gene proteins (see **Table *13***). Among the identified pro-tumorigenic proteins in PDAC were metalloproteinase domain-containing protein 9 (ADAM9), RAC-beta serine/threonine-protein kinase (AKT2), Receptor tyrosine-protein kinase erbB-2 (ERBB2), GTPase KRas (KRAS), mesothelin (MSLN), and protein S100P (see **Table *13 A***). In normal pancreatic tissue, the identified pro-tumorigenic proteins were significantly less present, whereas MSLN was not present at all. In addition to pro-tumorigenic proteins, two tumor suppressor gene proteins were found in the PDAC condition, namely dual specificity mitogen-activated protein kinase kinase 4 (MAP2K4) and mothers against decapentaplegic homolog 4 (SMAD4), however, they were also present in most samples of the normal control condition (see **Table *13 B***).

Table 13: **Identified Pro-tumorigenic and Tumor Suppressor Gene Proteins in PDAC and Normal Pancreas.** (A) Identified pro-tumorigenic proteins in PDAC (n=14) and normal pancreas (n=15) samples. (B) Identified tumor suppressor gene proteins in PDAC and normal pancreas samples. Adapted from table 2 of Werner et al., 2023 [68].

A

Pro-tumorigenic Protein	**Detected in x PDAC Samples** (n=14)	**Detected in x Normal Pancreas Samples** (n=15)
ADAM9	10 (71,4 %)	1 (6,7 %)
AKT2	8 (57,1 %)	3 (20,0 %)
ERBB2	4 (28,6 %)	2 (13,3 %)
KRAS	13 (92,9 %)	5 (33,3 %)
MSLN	5 (35,7 %)	0 (0 %)
S100P	14 (100 %)	7 (46,7 %)

B

Tumor Suppressor Gene Protein	**Detected in x PDAC Samples** (n=14)	**Detected in x Normal Pancreas Samples** (n=15)
MAP2K4	13 (92,9 %)	14 (93,3 %)
SMAD4	10 (71,4 %)	9 (60,0 %)

5 DISCUSSION

Kallikreins seem to play a major role in pancreatic carcinogenesis, with particular focus on KLK6 and KLK10, as they represent the most upregulated kallikreins in PDAC [17, 19-21]. In the present study, we aimed to investigate KLK6 and KLK10 protein expression in CCM of pancreatic cancer cells as well as in patient-derived FFPE tissues by applying targeted MS analysis. Using the explorative MS approach, we further performed a complete proteome profiling of PDAC and included control tissues.

5.1 Protocol Optimization

For this study, a protocol suitable for sample preparation of both CCM and FFPE tissue was needed. Therefore, we chose the single-pot solid-phase enhanced sample preparation (SP3) method, which enables both sample preparation methods. Since different types of the magnetic beads may vary in their surface hydrophilicity/hydrophobicity, we evaluated their differences in KLK binding. In accordance with testing different bead types, varying bead amounts were investigated and the optimal bead amount for KLK detection was determined. Regarding the targeted analysis with the aim of detecting secreted KLKs in CCM rather than intracellular located proteins, the internal standards GAPDH and tubulin were not appropriate.

Although intracellular GAPDH and Tubulin represent the most commonly used proteins for internal standards [72], they were not appropriate for the present KLK project since we aimed to detect secreted proteins in CCM rather than intracellular located proteins. Since there is no such commonly established internal standard applied as a reference protein in CCM, in this study, we introduce the usage of a commercially available spike-in protein as a novel reference protein for CCM, namely Avidin, a glycoprotein obtained from egg white. Herefore, the optimal amount of avidin as internal standard was determined, to ensure sufficient detectability but prevent shadowing of desired KLK signal.

5.2 Cell Line Comparison

The previously optimized protocol was further used in order to compare the secretion of KLK proteins between different pancreatic cancer cell lines, namely MiaPaCa-2, AsPC-1, PaCaDD-165, PaCaDD-159, and MaPaC-107 (see **Table 8**). Kallikreins

represent, among others, members of the secretome of the pancreatic cancer cell lines. Up to now, several studies have shed some light onto secretome analyses of CCM, particularly in cancer. With respect to pancreatic cancer, proteomic profiling already revealed various promising protein candidates [39, 73, 74]. However, among these detected proteins, no KLKs were identified. Since the performed secretome studies investigated the entirety of secreted proteins in CCM from pancreatic cancer cells rather than a defined set of proteins of interest, in this part of the present study, we evaluated the KLK protein expression and secretion and performed a targeted MS analysis by covering all 15 kallikreins in the established SRM assay.

In our data, KLK3, KLK5, KLK6, KLK7 and KLK10 could be reproducibly detected among CCM of the included cell lines (see **Figure *15***). Interestingly, KLK3/PSA, which actually functions as a biomarker for prostate cancer because of its elevated levels in the patients' serum [10], showed high levels in CCM from the pancreatic cancer cell line MiaPaCa-2 compared to the other cell lines. The fact that KLK3/PSA is secreted by pancreatic tumor cells reinforces the suggestion that kallikreins are likely to play an important role in multiple tumor entities and represent a possible source for therapeutic or diagnostic actions. Apart from KLK3/PSA, highest levels of KLK5, KLK6 and KLK7 could also be observed in CCM of MiaPaCa-2 compared to the other cell lines. This observation goes in line with a previous publication, which reported elevated protein levels of KLK5, KLK6 and to a lesser extent KLK7 in MiaPaCa-2 cells by using ELISAs [54]. Furthermore, as KLK5 could be shown to activate KLK7 and KLK3, these KLKs could act in a similar way or even share the same pathways in pancreatic cancer and/or other tumor entities (see **Figure *1***). On the one hand, a common function of KLK3, KLK5, KLK6 and KLK7 may include the proteolytic cleavage of E-Cadherin and thus promoting pancreatic cancer invasion, since this effect could previously be observed for KLK6 and KLK7 (Klucky et al., 2007, Johnson et al., 2007). On the other hand, another commonality of these kallikreins could persist in the hydrolysis of certain ECM components and thereby promoting tumor progression and invasion, as it was already suggested for KLK3, KLK5 and KLK6 [29, 75-77].

As already mentioned earlier, KLK6 secretion levels revealed to be the highest in MiaPaCa-2. However, KLK6 was additionally detected in CCM of the cell line PaCaDD-159, whereas it was not found in the other cell lines. Since KLK6 protein levels seem

to correlate between MiaPaCa-2 and PaCaDD-159, which both represent cell lines deriving from the primary tumor rather than the metastatic site of the tumor (see **Table *8***), elevated KLK6 secretion may be a specific effect for cell lines deriving from the original tumor of PDAC patients. With respect to KLK10, its highest protein levels were detected in CCM of cell line AsPC-1, and to a smaller extent in PaCaDD-165, PaCaDD-159 and MaPaC-107, whereas no KLK10 was detected in CCM of MiaPaCa-2. This observation goes in line with a previous publication, which reported highest KLK10 mRNA and protein levels in AsPC-1 lysates, whereas MiaPaCa-2 showed none or very few KLK10 [21]. Due to the finding that both KLK10 mRNA and protein levels are upregulated in AsPC-1, it is likely that KLK10 is undergoing translation and subsequent secretion into the extracellular space in AsPC-1 cells. Furthermore, Cao et al. (2018) found that immunohistochemical KLK10 expression of human PDAC tissues was significantly higher in the group of metastatic patients compared to the metastasis-free group, assuming an aberrant expression pattern of KLK10 within malignant transformation of PDAC. Interestingly, metastatic features have also been described for the cell line AsPC-1 [78], which according to our data showed the highest KLK10 secretion. This finding underlines the suggestion that KLK10 may be involved in malignant transformation in PDAC. However, elevated levels of secreted KLK10 does not seem to be a specific effect for metastatic tumor cell lines in general, as KLK10 was additionally detected in PaCaDD-159, which represents a primary cell line (see **Table *8***).

5.3 Targeted (PRM) MS Analysis

FFPE samples represent an important source for medical research [55]. Therefore, a selection of tissue sections of the entities PDAC (n=14), normal pancreas (n=5), non-malignant adjacent pancreas (n=11), chronic pancreatitis (n=7) and ampullary cancer (n=3) was subjected to targeted MS analysis using the PRM approach to investigate the KLK protein expression.

Out of the 15 KLKs included in the first PRM measurement assay, KLK1 was detected in tissues of normal and non-malignant adjacent pancreas. KLK1 is the first human kallikrein, originally found as an abundant protein in the pancreas [16]. Our finding goes in line with several other groups, who observed KLK1 as an abundant protein in the pancreas [79-81]. Interestingly, other studies reported comparable KLK1 expression levels between normal and cancerous pancreatic tissue [17, 18, 24]. In addition to

observing the expression of KLK1 in cancer tissue, it has also been suggested that the protein is involved in invasion, metastasis, and degradation of the ECM when it comes to cancer in general (see **Figure *1***), however, this was not investigated with our experimental setup. We further observed KLK6 and KLK10 expression in tissues of PDAC and ampullary cancer. This finding is in accordance with several other reports, which found KLK6 and KLK10 expression in cancerous pancreatic tissue [17, 20, 22, 24, 82]. With respect to ampullary cancer, it seems that protein profiles of pancreatic cancer and ampullary cancer share multiple similarities [83]. This might be due to the proximity of the ampulla of Vater to the pancreas [84]. Hence, many of the genes upregulated in ampullary cancer were also found in several other cancer entities, including pancreatic cancer [83]. The authors reported several promising overexpressed genes in snap-frozen tissue samples of ampullary cancer, among them proteins involved in calcium homeostasis (S100P), remodeling of the ECM like multiple metalloproteinases and collagens, cell surface adhesion proteins as integrins, as well as several kallikreins, although more detailed information was not disclosed [83]. Therefore, up to now, little is known about KLK protein expression in ampullary cancer. In tissues of non-malignant adjacent pancreas, KLK6 showed expression in three samples (n=14). However, it is important to mention that these three tissues samples were scratched off directly next to the tumor areas, which might explain KLK6 detectability. Moreover, we detected KLK7 in tissues of PDAC (see **Table *10***). KLK7 is proposed to be involved in ECM degradation, invasion, metastasis, and shedding of E-Cadherin (see **Figure *1***). The latter could be observed not only for KLK7 but also in case of KLK6, suggesting that both kallikreins are involved in promoting tumor invasiveness in pancreatic cancer. [31, 32]. KLK7 (mRNA and protein) overexpression in pancreatic cancer on the other hand has already been reported by several authors [24, 32, 33]. Interestingly, KLK7 seems to show no expression in normal pancreatic tissue [23, 34], which goes in line with our results, as we did not find any KLK7 in tissues of benign pancreas (see **Table *10***). Since KLK14 was only detectable in 1/14 PDAC samples (see **Table *10***) and its presence in pancreatic cancer has not yet been described in the literature, it was excluded from the future PRM measurement assay for final analysis. As the results of the first PRM analysis allowed us to obtain a general overview about KLK expression within the included tissue entities, we gained valuable information on the basis on which we were further able to build a final PRM assay including the most promising candidates (KLK6,

KLK7, and KLK10), to confirm consistency with our previously yielded proteomics results.

Regarding the final PRM analysis, KLK6 again showed strong expression in samples of PDAC (11/14) (see **Table *11***). The same applied to KLK10, which was detected in 12/14 PDAC samples. Furthermore, both KLK6 and KLK10 show expression in all ampullary cancer samples (n=3). These findings corroborate the results of the first PRM measurement. Another finding represents the detection of KLK6 in one sample of non-malignant adjacent pancreatic tissues (n=11), as well as the detection of KLK10 in one chronic pancreatitis sample (n=7), which most likely represent outliers. It is interesting that KLK7, which seemed to be a promising candidate according to the first measurement, could not be detected in any of the PDAC samples in the second measurement (see **Table *11***). These differences might be due to any emerged variations during the measurement, such as issues concerning the spray stability or instrument performance. Besides, a larger patient cohort would be necessary to confirm the presence of KLK7 in pancreatic cancer.

Important to note is that all acquired data of the first PRM measurement represent qualitative data rather than quantitative, since data normalization was not possible (varying GAPDH expression among the samples, no stable signals of iRT or heavy reference peptides). Although it was possible to normalize the data of the final PRM analysis to spiked-in heavy peptides (due to stable signals throughout the measurement), a quantitative comparison between the first and final measurement is not intended. However, since only the second measurement allows quantitative statements about KLK upregulation in the included tissues, we performed a quantitative comparison of KLK6 and KLK10 upregulation between the different tissues within the final PRM data.

Hereby, we focused on the comparison between PDAC and the benign conditions chronic pancreatitis, normal and non-malignant adjacent pancreas (see **Figure *17***). KLK6 and KLK10 were significantly overexpressed in PDAC compared to the benign tissues in all three comparisons. This observation of KLK6 and KLK10 being significantly upregulated in PDAC but not in the normal pancreas has also been reported in the literature [24, 82]. Beyond that, high expression levels of KLK6 and KLK10

seem to be associated with a shorter survival [20, 24]. Although both KLK6 and KLK10 seem to be significantly overexpressed within tissues of PDAC, KLK6 in general seems to be higher upregulated in PDAC than KLK10 (see **Figure *17***). This is in line with a publication of Yousef et al., 2004, reporting KLK6 to be the most significant differential expressed gene in pancreatic cancer compared to the normal pancreas, also considering KLK1, KLK7, KLK8, KLK10 and KLK11 [82]. When plotting ampullary cancer against the benign entities, the same effect as for PDAC could be shown, since KLK6 and KLK10 were significantly upregulated in ampullary cancer compared to benign tissues (see **Figure *S 26***). This finding underlines the similarity between pancreatic and ampullary cancer, which has already been suggested [83].

In summary, KLK6 and KLK10 were found to be significantly upregulated in PDAC and ampullary cancer compared to non-neoplastic tissues, i.e. normal pancreas, non-malignant adjacent pancreas, and chronic pancreatitis, as shown by quantitative proteomic analysis. Although one cannot quantitively compare the first and final PRM measurement, we can state that both PRM measurements showed the same effect for KLK6 and KLK10, namely an expression of the two kallikreins in samples of PDAC and ampullary cancer compared to the benign conditions.

Most importantly, our data stands in contrast to the assumption that KLK10 might be a tumor suppressor, which has been suggested for several other tumor entities due to the downregulation of KLK10 [25, 27]. Since we found significantly increased expression levels of KLK10 in PDAC compared to the included control tissues, it can be concluded from our data that KLK10 is most likely not a tumor suppressor for PDAC.

Another remarkable observation which came to light during both the first and final PRM measurement concerns the enzyme glyceraldehyde-3-phosphate dehydrogenase (GAPDH). GAPDH represents a key enzyme in both the glycolysis and gluconeogenesis and is therefore constitutively expressed within many tissues [85]. As it represents an important housekeeping gene, it is commonly used as an internal standard and was included in both PRM measurement assays to serve as a potential reference protein for future data normalization. However, during both measurements, expression of GAPDH varied among the different tissue entities, resulting in higher expression levels in samples of PDAC and ampullary cancer and lower levels in non-neoplastic tissues such as chronic pancreatitis, normal and non-malignant adjacent

pancreas (see **Figure *16***). The finding of elevated GAPDH levels in pancreatic cancer is supported by the results of a study, which found GAPDH (RNA) to belong among the gene with the highest variability in expression within pancreatic cancer compared to normal pancreatic tissue [85].

Typical hallmarks of cancer in general represent rapid proliferation and the ability to metastasize [86]. It is therefore not surprising that GAPDH expression differs between normal and cancerous tissues, as cancer cells require greater amounts of glucose to generate the necessary energy. This effect of increased glucose uptake, followed by enhanced glycolysis and lactate production under aerobic conditions is referred to as the "Warburg effect" [87] and is strongly pronounced within PDAC [86, 88]. Thus, GAPDH as part of the glycolysis could potentially promote growth and metastasis of pancreatic tumors [89].

5.4 Explorative (DIA) MS Analysis

In order to globally evaluate interesting proteins which may be relevant in connection with PDAC and its characteristics rather than looking at the individual KLK expression, we further performed an explorative proteome comparison between the different tissue entities. To ensure high quality results and prevent selection of only the most abundant proteins, the explorative data-independent acquisition (DIA) method was used for this project (see **Figure *18***). This method overcomes the limitation of a maximum number of fragmented and identified peptides, as all ionized peptides are being fragmented [52]. Initially, the generated data was subjected to sPLS-DA, where overlaps of the calculated 95 % confidence intervals indicate that the affected conditions show similarities in their protein profiles. In the first sPLS-DA, the conditions normal pancreas (NP) and non-malignant adjacent pancreas (NMAP) showed an almost complete overlap of their proteomes, suggesting a great commonality between their global proteomic profiles. Since the finding of similar proteomic profiles in cases of normal and adjacent pancreatic tissues has been reported before [58, 90], the two conditions were further combined to the condition normal non-malignant control (NNMC). Furthermore, ampullary cancer and PDAC revealed a complete overlap in their global proteome profile (see **Figure *S 24***). This underlines the assumption that their proteomes resemble each other, which has also been suggested by other groups [83] and could already be demonstrated by the PRM measurements carried out previously, since both KLK6 and KLK10 were detected within the two conditions (see **Table 10** and **Table *11***).

Considering the final sPLS-DA, it reveals an almost distinct clustering of all three conditions (see **Figure *20***). This seems reasonable, as each tissue (normal, inflammatory, and cancerous) comes along with its own characteristics. Nevertheless, their proteomes partially overlap, probably because they originate from the same tissue, namely the pancreas. Since the benign conditions NNMC and CP show a larger overlap compared to PDAC, it suggests that the proteome difference between malignant and non-malignant entities is greater. All aforementioned findings illustrate the difficulty of clearly separating the three conditions CP, PDAC and normal pancreas based on their proteomic profiles. As tissue heterogeneity occurs not only between different tissue types but also among different patients, this difficulty of correct classification is only amplified.

Aiming to further classify the different tissues, gene enrichment analysis of characteristic protein representatives of each group was performed based on the generated sPLS-DA data. With respect to PDAC, entity-characteristic protein groups seem to be involved in cell adhesion processes (see **Table 12 *A***). This finding goes in line with the results of the co-abundance clustering, which additionally revealed upregulated cell adhesion molecules in PDAC compared to CP and the NNMC (see **Figure *21 A***). Cell adhesion molecules in general represent cell-surface molecules which are essential for cell-cell or cell-matrix interaction [91]. As they are of great importance for the maintenance of normal tissue structure, their loss seems to be associated with an increased motility resulting in tumor cell invasion and metastatic spread [92, 93]. This loss of adhesive properties of the epithelial cells results in an epithelial-to-mesenchymal transition (EMT), giving rise to single cell dissemination [94]. EMT has already been described for PDAC and is suggested to contribute to its invasive properties [95]. Contrary to the assumption, that reduced expression or absence of adhesion molecules leads to tumor cell dissemination, our data suggests that their presence seems to be specific for PDAC, which stands in contrast to the EMT theory. As PDAC is well-known for its invasive properties and developing of early metastases [4], the question arises how PDAC should be capable of metastasis despite the presence of adhesion molecules. Surprisingly, it has been noted before that in many tumor types, cell adhesion molecules were maintained, despite a more mesenchymal phenotype of cancer cells [96-100]. In addition, it has already been reported, that the retention of adhesion molecules in cancer could potentially result in a collective cancer cell

invasion rather than single cell dissemination, with groups of multiple cancer cells remaining both physically and functionally connected [92]. Consistent with the fact that pancreatic cancer is well-known for its invasiveness and development of early metastases, cancer cell clusters seem to show an increased metastatic potential compared to individual cells [92, 101]. Collectively, our data could possibly suggest a cell-cluster-like migration process in pancreatic cancer leading to metastases, although this hypothesis would need to be confirmed by further research.

This suggestion is further underlined by our results of the multigroup limma analysis, which also revealed cell adhesion proteins to be significantly upregulated within PDAC compared to both the normal control and pancreatitis. One certain protein seems to show particular relevance in the progress of a cluster-like cell invasion, namely plakoglobin (JUP). This specific cell adhesion protein was recently found to be significantly overexpressed within PDAC compared to normal pancreatic tissue, besides, it was reported to be crucial for cell-cluster formation [92, 102]. Our study is in agreement with these previous reports, as we found JUP as a characteristic protein for the PDAC condition according to the final sPLS-DA (see **Table *S 16***), as well as significantly overexpressed in the multigroup limma comparison PDAC compared to CP (see **Figure *22 C***). Other proteins that have already been associated with collective cell migration are integrins [92], which mediate cell-cell and cell-matrix binding. In our data, multiple members of the integrin family (ITGA2, ITGA3, ITGA5) showed a significant overexpression in PDAC compared to the NNMC (see **Figure *22 A***). This finding goes in line with the literature, as for example ITGA2 could be observed to be significantly upregulated in pancreatic cancer compared to normal pancreatic tissue [103]. Since several integrins are differentially expressed in PDAC and are strongly suggested to play a key role in collective cell migration, their blockage was even proposed as novel therapeutic targets for pancreatic cancer [92, 104-106]. Furthermore, Filamin-A (FLNA), a cytoskeletal protein which is involved in the regulation of cell adhesion, has been observed to be strongly expressed in PDAC [107, 108]. Within the framework of this study, FLNA turned out to be significantly upregulated in PDAC compared to the NNMC (see **Figure *22 A***). Besides FLNA, we observed a significant overexpression of the versican core protein (VCAN) in PDAC compared to the normal control, which is also implicated in cell adhesion. Interestingly, multiple other studies found VCAN to be differentially expressed in PDAC and some even reported a

significant upregulation in PDAC compared to the normal pancreas [105, 106, 109]. In contrast to upregulated cell adhesion molecules in PDAC, we found a significant downregulation of cell adhesion proteins cadherin-1 (CDH1) and desmoglein-2 (DSG2) in CP compared to the normal control (see **Figure *22 B***), although gene enrichment analysis did not officially define the term. This finding suggests that cell adhesion proteins appear to be only preserved in PDAC, supporting the potential hypothesis of a collection cell migration in pancreatic cancer but not in inflammatory tissues of pancreatitis.

An important prerequisite for cell migration and thus formation of metastases is the dynamics of the cytoskeleton within a cell, which enables the cells movement [110]. Therefore, it seems not surprising that gene enrichment analysis of the sPLS-DA further revealed cytoskeletal proteins being a specific group for PDAC, which is supported by a significant upregulation of cytoskeletal proteins in PDAC compared to both the NNMC and CP in the multigroup limma analysis. One particular protein involved in the regulation of the actin cytoskeleton, namely cofilin-1 CFL1, was observed to be significantly upregulated in PDAC compared to CP, which goes in line with our data of the sPLS-DA (see **Table *S 16***) and the literature [111]. Consistent with the above findings of upregulated cytoskeletal and cell adhesion molecules in PDAC, these protein groups appeared to be downregulated in the normal pancreas compared to PDAC and CP (see **Figure *21 C***).

The finding of both cytoskeletal and cell adhesion molecules being characteristic for PDAC further corresponds well with a study, which investigated the phosphoproteomes of PDAC [112]. The results revealed proteins involved in cell adhesion and the cytoskeleton to be differentially phosphorylated in PDAC. As post-translational phosphorylation represents an important way to regulate the function of proteins and can therefore affect protein localization, stability, as well as its catalytic activity, phosphorylation of cell adhesion and structural proteins may result in changes of signal transduction in PDAC [112]. These changes may for example lead to the maintenance of proliferative signaling, and/or the activation of invasion and metastasis, which represent, among others, two crucial hallmarks of cancer [113].

Another key hallmark of cancer comprises the ability to reprogram cellular metabolism [113]. Notably, in many cancers including pancreatic cancer, glycolytic processes in the cytosol seem to be upregulated, whereas oxidative phosphorylation in the mitochondria is downregulated [88]. This metabolic switch to enhanced glycolysis in cancer cells, the so-called “Warburg effect”, can be observed by both our results of gene enrichment analysis of the sPLS-DA and multigroup limma analysis. The latter revealed a significant upregulation of glycolytic proteins in PDAC compared to the normal pancreas, although gene enrichment analysis did not indicate this term. These proteins include pyruvate kinase (PKM), fructose-bisphosphate aldolase C (ALDOC) and glyceraldehyde-3-phosphate dehydrogenase (GAPDH) (see **Figure *22 A***). In addition, we found a significant upregulation of several key proteins of the glycolysis within PDAC compared to chronic pancreatitis, (PFKP, PGK2, ALDOA, ENO1, GAPDH), whereas enzymes PFKP, ENO1 and GAPDH were additionally detected as specific proteins for PDAC in the sPLS-DA (see **Table *S 16***). Interestingly, the finding of upregulated GAPDH in malignant entity PDAC vs. both benign tissues of normal pancreas and pancreatitis coincides with the previous PRM analyses, where higher levels of GAPDH expression were detected in PDAC and ampullary cancer compared to the benign entities (see **Figure *16***). On the other hand, one would expect that the upregulated glycolytic processes in PDAC should also be accompanied by a downregulation of mitochondrial energy production. This effect is indeed observed, with proteins of the citrate cycle, as for example IDH2, ACO1, and SUCLG2 being significantly downregulated in PDAC compared to the NNMC (see **Figure *22 A***).

In addition to the downregulated mitochondrial energy metabolism, we also observed a significant downregulation of amino acid metabolism in tissues of pancreatic cancer, which is consistent with the literature [103]. Hereby, particularly the cysteine and methionine metabolism, beta-alanin metabolism, as well as the valine, leucine, and isoleucine degradation seem to be downregulated in PDAC compared to the NNMC (see **Table 12 *C***). The amino acids valine, leucine, and isoleucine, summarized as branched-chain amino acids (BCAAs), represent essential amino acids for protein synthesis and molecular signaling and have recently been linked to an increased risk of pancreatic cancer [114]. Interestingly, we report a significant downregulation of the branched-chain-amino-acid aminotransferase (BCAT2) within PDAC compared to the NNMC, which plays a crucial role in the BCAA catabolism (see **Figure *22 A***). Furthermore, the mitochondrial enzyme 4-aminobutyrate aminotransferase (ABAT)

shows a significant downregulation in PDAC compared to normal pancreatic tissue. Its reduced expression has already been observed in most tumors and has even been associated with a significantly worse prognosis of tumor patients [115]. Since ABAT plays a key role in gamma-aminobutyric acid (GABA) catabolism, its downregulation should be associated with increased levels of GABA. In fact, it has already been reported that PDAC tissues seem to possess higher levels of GABA than normal pancreatic tissues, albeit its exact function in PDAC is not fully elucidated until now [116]. In addition, it has been reported that the glutamine metabolism plays a crucial role in pancreatic cancers invasiveness [117]. Consistent with this hypothesis, we found the mitochondrial glutaminase kidney isoform (GLS), which contributes to the renal catabolism of glutamine [117], to be significant downregulated in both PDAC and CP compared to non-neoplastic pancreatic tissue. The additional downregulation of GLS in tissues of chronic pancreatitis illustrates the need of amino acids not only in tumorous, but also in inflammatory pancreatic tissues. In summary, we can conclude that processes such as reduced valine, leucine, and isoleucine degradation, as well as downregulation of catabolic amino acid enzymes like BCAT2, ABAT and GLS provide the tumor with important sources for cancer growth and may likely represent approaches for novel therapeutic targets in pancreatic cancer.

A prerequisite for the growth and progression of cancer is, among other things, the ability of cancer cells to move around the tumor microenvironment, which in turn enables the cells to metastasize. Since this process requires degradation of the ECM, it comes unexpected that ECM interaction seems to be significantly upregulated in PDAC compared to the normal pancreas (see **Figure *22 A***), which is in line with our results of the co-abundance clustering (see **Figure *21 A***). One major component of the ECM, fibronectin (FN1), which is involved in both cell-ECM interaction and the regulation of the actin cytoskeleton [118], has been reported to be diffusely distributed and overexpressed within the stroma of both chronic pancreatitis and PDAC [105, 106, 119]. Our study strengthens this statement, as fibronectin could be shown to be significantly overexpressed in PDAC compared to the NNMC (see **Figure *22 A***). Since fibronectin is also important for wound healing processes and its presence has already been reported in chronic pancreatitis [120], its significant overexpression in CP compared to normal tissue is not surprising (see **Figure *22 B***). Cleavage of fibronectin as a component of the ECM could therefore facilitate the spread of tumor metastases. Since KLK6, for example, has also been shown to cleave rat plasma fibronectin [30], it is

suspected that KLK6 itself contributes to the degradation of the ECM in PDAC and thus supports its invasive properties.

Other key proteins involved in the ECM interaction are collagens. In this study, numerous collagens (COL1A1, COL1A2, COL14A1, COL12A1) were found to be significantly overexpressed in both PDAC and CP compared to the normal control (see **Figure *22 A and B***). These findings are compatible with previous reports and may possibly mirror the role of ECM protein interaction in the context of tissue remodeling during cancer progression as well as chronic inflammation [119, 121].

Since it appears that ECM remodeling is crucial for wound healing processes [122], it does not seem surprising that besides ECM interaction, also proteins involved in wound healing processes were found to be upregulated in CP compared to the normal pancreas (see **Table 12 *C***), which is in accordance with our data of the co-cluster abundance analysis (see **Figure *21 B***) and the literature [123]. Crucial for healing processes is, among other things, the correct formation of blood clots [122], which is for example achieved by fibrinogens. In the present study, we found multiple fibrinogens (FGA, FGB, FGG) to be significantly upregulated in CP compared to the NNMC, which may possibly indicate an early activation of wound healing processes in highly inflammatory tissues of chronic pancreatitis. Besides the strong upregulation of proteins involved in wound healing in CP compared to normal tissue, the impact of wound healing processes even seems to have a greater significance in CP than in the malignant entity PDAC, as we found FGA, FGB and FGG, along with the coagulation factor IX (F9) to be strongly downregulated in PDAC compared to CP (see **Figure *22 C***). Therefore, it does not seem surprising, that when comparing normal pancreatic tissue to pancreatitis and PDAC, wound healing processes appear to be downregulated in the normal control (see **Figure *21 C***).

Regarding the final comparison between malignant and inflammatory pancreatic tissue (see **Figure *22 C***), it becomes clear that despite several fundamental differences, their proteomes appear to resemble within certain aspects. For example, when looking at the previous analyses and comparisons, EMC interaction seems to be a characteristic feature for both PDAC and CP. Consequently, ECM interaction seems to be equally represented in both inflammatory and cancerous pancreatic tissue, suggesting both diseases requiring a distinct exchange with the ECM. Another common feature in the

proteome of PDAC and CP is the neglect of pancreatic exocrine function. Importantly, both pancreatic cancer and pancreatitis originate from the exocrine part of the pancreas [124]. Under physiological conditions, the exocrine pancreas shows strong expression of translational and ER-related proteins, highlighting the overall increased gene expression in healthy exocrine pancreatic tissue. This effect can be seen in our data both in the sPLS-DA and co-cluster abundance analysis (see **Table 12** ***A*** and **Figure** ***21 C***). Since inflammation as well as cancer of the pancreas lead to destruction of normal pancreatic tissue, this change in tissue structure results in an impairment of the pancreatic exocrine function. The latter is illustrated by our data, in which proteins involved in the pancreatic exocrine function show a significant downregulation in both PDAC and CP compared to normal pancreatic tissue. These downregulated proteins in PDAC vs. the NNMC include translational members as many ribosomal proteins (RPL15, RPL19, RPL31), members of protein export mechanisms (SPCS1, SPCS3) and protein processing molecules (RRBP1, P4HB). Interestingly, similar proteins were shown to be downregulated within inflammatory tissues of CP compared to the NNMC, again including multiple ribosomal proteins (RPS20, RPS21, RPS15A, RPL10, RPL35A), in addition to the protein export members SPCS1 and SPCS3.

One of the most important drivers of the inflammatory response are assumed to be coagulation and complement cascades. Moreover, both cascades are additionally considered to be parts of a global serine protease system [125]. Since the kallikrein family represents secreted serine proteases, their participation and contribution to the inflammatory response is likely, however, we did not find any KLK proteins in our explorative data. Regarding the complement cascade, it represents a major part of the humoral immune response [125]. It is already known that pancreatitis is linked to the humoral immune response through systemic activation of the complement system. Pancreatic cancer on the other hand is also suggested to be associated with the classical complement pathway, as this tumor entity is well known to create a pro-inflammatory microenvironment [125]. It is therefore not surprising that the co-abundance clustering analysis revealed proteins involved in the humoral immune response to be downregulated in normal compared to inflammatory and malignant pancreatic tissue (see **Figure** ***21 C***). Furthermore, our data revealed multiple components of immunoglobulins (IGHG1, IGHG2, IGHM) as representatives of the upregulated humoral immune response in inflammatory tissues of CP compared to the normal pancreas. Since the classical pathway of the complement system includes

immunoglobulins, it can therefore be assumed that the activation of the complement system in chronic pancreatitis is triggered via the classical pathway [125]. However, to avoid hyperinflammation, the complement system is tightly controlled and regulated. One of these regulators of the classical pathway of the complement system is C4b-binding protein (C4BP), whose blood levels can increase extremely during an inflammatory response [126]. In this study, we report significantly increased levels of C4b-binding protein alpha chain (C4BPA) in tissues of CP compared to the normal pancreas (see **Figure *22 B***), which is associated with the enhanced inflammatory response in chronic pancreatitis and reinforces the suggestion that CP utilizes the classical complement system pathway as part of the humoral immune response. Nevertheless, the exact physiological role and activation of the humoral immune response in chronic pancreatitis is still not fully understood until now [125].

Another interesting result of our study comprises the detection of up-regulated pro-tumorigenic and downregulated tumor suppressor proteins in PDAC. Hereby, the proto-oncogene protein anterior gradient protein 2 homolog (AGR2) was found to be significantly overexpressed in PDAC compared to the normal pancreas (see **Figure *22 A***). AGR2 was already reported to be highly expressed in PDAC compared to tissues of normal pancreas and pancreatitis and has previously been linked to enhanced metastatic potential in pancreatic cancer [127, 128]. Our results therefore support the hypothesis that the protein AGR2 may contribute to PDAC's aggressive nature and invasiveness. On the other hand, downregulation of tumor suppressor proteins in PDAC compared to normal pancreatic tissue can be illustrated by tumor suppressor protein programmed cell death protein 4 (PDCD4) (see **Figure *22 A***). Strongly downregulated PDCD4 mRNA and protein expression in PDAC compared to normal adjacent tissues has recently been reported and was even linked to a significantly poorer survival [129, 130]. Interestingly, other tumor suppressor proteins (NDRG2 and EPB41L3) which we observed to be significantly downregulated in PDAC compared to CP are also assumed to result in much poorer overall survival of PDAC patients [131, 132]. This suggests that downregulation of tumor suppressor proteins PDCD4, NDRG2 and EPB41L3 has a positive impact on the progression of pancreatic cancer, leading to a poorer prognosis for cancer patients.

5.5 Pro-Tumorigenic Proteins

Another core component and hallmark of cancer development represents its genomic instability and mutation [113]. In PDAC, most frequent oncogenic mutations involve KRAS and SMAD4, among others [71, 133]. Oncogenic KRAS mutation enables the tumor to consequently maintain cellular processes like cell proliferation, migration, and survival, and its presence has been associated with a worse prognosis of pancreatic cancer patients [134]. Previously, Cao et al. detected KRAS (mRNA and protein levels) in both PDAC and normal adjacent tissues, however, the latter group showed significantly ($p < 0,001$) lower amounts of KRAS than the tumorous tissue [90]. This finding goes in line with our results, as we observed substantially higher KRAS protein expression in PDAC (92,9 %) than in the NNMC (33,3 %). Furthermore, we observed strong expression (71,4 %) of matrix metalloprotease ADAM9 in tissues of PDAC (see **Table *13 A***). This finding is in accordance with previous reports, which found both elevated mRNA and protein levels of ADAM9 within tissues of pancreatic cancer compared to adjacent tissues, whilst higher levels of ADAM9 even correlated with a lower survival of patients [71, 135]. Since metalloproteinases enable the remodeling of the ECM through proteolytic activity generating space for multicellular movement [92], the strong appearance of ADAM9 in our data underlines our previous hypothesis that PDAC could possibly use a cell-cluster like migration method. Moreover, the oncogenic protein ERBB2 was detected in 28,6 % of PDAC tissues, while it was present in 13,3 % of normal tissues. ERBB2 has already been attributed a key role in the carcinogenesis of PDAC and was also found to be overexpressed within PDAC tissues [71]. Its overexpression in the exocrine pancreas has additionally been linked to a more inflammatory phenotype [136], which may possibly lead to pancreatic cancer in the future. One might therefore speculate that current inflammatory processes are underway in the normal pancreatic tissues in which ERBB2 has been detected in our study. In addition, pro-tumorigenic AKT2 frequently shows overexpression in PDAC [133], which is in accordance with our results, as we detected its presence in 57,1 % of PDAC tissues. In the present study, the calcium-binding protein S100P further showed expression in 100 % of PDAC tissues (see **Table *13 A***) and was already proposed to contribute to the aggressiveness and growth of pancreatic cancer [137]. It has been established before, that S100P, as well as mesothelin, which we observed in 35 % in PDAC tissues, are overexpressed within pancreatic cancer compared to normal tissues [19, 71, 90, 103]. Interestingly, both S100P and Mesothelin were also found to be

highly expressed within tissues of ampullary cancer, along with several KLKs [83]. The above-mentioned finding that both KLK6 and KLK10 could be detected in ampullary and pancreatic cancer, combined with the simultaneous detection of pro-tumorigenic proteins, suggests that these two cancer entities also share similarities in terms of genomic mutations.

Within many cancer types, including pancreatic cancer, tumor suppressor genes or genes exhibiting a tumor-suppression function are silenced [138]. Interestingly, in PDAC, we report strong expression of two tumor suppressors in both PDAC and the normal pancreas, namely SMAD4 and MAP2K4. These results are consistent with previous reports that found MAP2K4 proteins to be highly expressed in PDAC tissue (97,3 %) compared to normal pancreatic tissue. Regarding the tumor suppressor SMAD4, it is inactivated in 55 % of carcinomas [71]. In the present data, we found a slightly lower value of about 30 % SMAD4 deletion in PDAC, which would need to be re-examined with a larger cohort.

6 CONCLUSION

Within the scope of this project, a robust and reproducible sample preparation workflow for both conditioned pancreatic cancer cells media and pancreatic formalin-fixed paraffin-embedded tissue was established, optimized for the best possible enrichment and detection of kallikreins.

Our data of the targeted selected reaction monitoring analysis revealed detection of secreted proteins kallikrein 6 and 10, among several other kallikreins, in conditioned media of pancreatic cancer cells. Besides verified kallikrein secretion of cancer cells, targeted parallel reaction monitoring analysis showed a significant upregulation of kallikrein 6 and kallikrein 10 in pancreatic and ampullary cancer compared to the included controls, which supports the suggestion that kallikreins play an important role in pancreatic cancer and are involved in its tissue malignancy. Moreover, both targeted (parallel reaction monitoring) and explorative analysis highlight the Warburg effect in pancreatic ductal adenocarcinoma, with a significant upregulation of glycolytic proteins and downregulation of the mitochondrial energy metabolism. Furthermore, since pancreatic ductal adenocarcinoma as well as pancreatitis lead to a destruction of the exocrine tissue of the pancreas, we observed an impairment of the normal exocrine function with a significantly decreased overall gene expression. With respect to inflammatory tissues of chronic pancreatitis, analyses revealed signs of inflammatory reactions such as significantly upregulated wound healing and humoral immune response. Furthermore, our data suggest that pancreatic ductal adenocarcinoma maintains its cell-cell connections, possibly indicating collective invasion of cancer cells, which would directly contradict the epithelial-to-mesenchymal transition theory. In summary, our data of the targeted analyses suggest that kallikrein 6 and kallikrein 10 may be potential biomarkers for pancreatic ductal adenocarcinoma, while the explorative analysis revealed interesting up- and downregulated proteins within the different conditions, which need to be further validated together in larger patient cohorts.

7 OUTLOOK

A robust workflow for sample processing of conditioned pancreatic cancer cell medium and pancreatic FFPE tissue for MS analysis is now established, providing us with valuable information on the relative quantification of kallikreins. For future analyses, it would be interesting to further determine the amounts of KLKs by absolute quantification, which would allow us to compare different proteins. This could be achieved with so-called absolute quantification standards, which are, however, very expensive and extremely difficult to handle. Furthermore, since we were able to detect several KLKs in the SRM analysis, it would be of interest to perform Western Blot analyses to confirm the consistency of the MS results. Nevertheless, as no suitable and reliable KLK antibodies were available, we had to neglect this idea.

Secreted proteins will further appear in tissues and bodily fluids (e.g. blood), therefore they represent a potential source for the discovery of novel biomarkers and new therapeutic strategies [139]. Since we have already demonstrated that KLK6 and KLK10 are secreted by pancreatic cancer cells and further investigated their protein expression levels in PDAC tissues, the next step would be to apply targeted MS of KLK6 and KLK10 in blood samples from PDAC patients. By ELISA, KLK levels in sera from PDAC patients do not seem to differ compared to healthy donors [20], however, so far little is known about the mass spectrometric detection of KLK6 and KLK10 in sera from PDAC patients.

It is a well-known fact that the secretome plays an important role in the tumor microenvironment and is thus suggested to contribute to the regulation of cancer development and metastasis [74]. Therefore, it would be interesting to further perform an explorative secretome analysis of CCM of the pancreatic cancer cell lines included in this study and see if KLKs can be detected here. Unfortunately, this was not possible due to time constraints.

Moreover, too little is known so far about the correlation between ampullary cancer and kallikreins. As our data showed high expression levels of KLK6 and KLK10 in this cancer entity, and kallikreins have been detected in ampullary cancer before [83], it would be worth to further explore KLK expression in ampullary cancer. Nevertheless, a larger

patient cohort would be necessary to confirm KLK6 and KLK10 overexpression in ampullary cancer.

A recent study of Candido et al. found out, that KLK6 expression was higher in tumor invasive areas, whereas noninvasive tumor areas were represented by lower KLK6 mRNA levels [24]. Therefore, it would be interesting to investigate the exact sites of KLK overexpression in an FFPE section, which would be achieved, for example, by Matrix-assisted laser desorption/ionization (MALDI) imaging. With respect to KLK10, it was found that its immunohistochemical expression of human PDAC tissue was significantly higher in the group of patients with metastasis as in the metastasis-free group, suggesting KLK10 expression levels to correlate with malignant transformation in PDAC [21]. Hence, it would be worth further investigating whether KLK10 expression increases in PDAC tissues from already metastasized patients. Unfortunately, both ideas were not feasible due to time constraints.

Furthermore, sPLS-DA of the DIA approach shows a clear clustering of all three conditions CP, PDAC and normal pancreas with a partial overlap of their proteomes. This highlights the difficulty of clearly separating these diseases based on their proteome profiles. As tissue heterogeneity occurs not only between different tissue types but also between different patients, this difficulty of correct classification is only amplified. Therefore, personalized novel therapeutic strategies may represent a new approach for PDAC patients. Since our explorative data revealed specific up- and downregulated proteins for each condition, as well as several potential proto-oncogene proteins and pro-tumorigenic proteins, proteomic analyses could provide such a potential source for novel therapeutic approaches.

In closing, semi-tryptic analysis (detection of the proteolytic activity of the protein) and proteogenomics (expansion of the peptide library with transcripts) display potential additional experiments for further exploration of our data.

8 REFERENCES

1. Sarantis, P, Koustas, E, Papadimitropoulou, A, Papavassiliou, AG, Karamouzis, MV: Pancreatic ductal adenocarcinoma: Treatment hurdles, tumor microenvironment and immunotherapy. *World J Gastrointest Oncol,* 12**:** 173-181, 2020. https://doi.org/10.4251/wjgo.v12.i2.173

2. Vujasinovic, M, Dugic, A, Maisonneuve, P, Aljic, A, Berggren, R, Panic, N, Valente, R, Pozzi Mucelli, R, Waldthaler, A, Ghorbani, P, Kordes, M, Hagstrom, H, Lohr, JM: Risk of Developing Pancreatic Cancer in Patients with Chronic Pancreatitis. *J Clin Med,* 9, 2020. https://doi.org/10.3390/jcm9113720

3. Rawla, P, Sunkara, T, Gaduputi, V: Epidemiology of Pancreatic Cancer: Global Trends, Etiology and Risk Factors. *World J Oncol,* 10**:** 10-27, 2019. https://doi.org/10.14740/wjon1166

4. McGuigan, A, Kelly, P, Turkington, RC, Jones, C, Coleman, HG, McCain, RS: Pancreatic cancer: A review of clinical diagnosis, epidemiology, treatment and outcomes. *World J Gastroenterol,* 24**:** 4846-4861, 2018. https://doi.org/10.3748/wjg.v24.i43.4846

5. Casolino, R, Braconi, C, Malleo, G, Paiella, S, Bassi, C, Milella, M, Dreyer, SB, Froeling, FEM, Chang, DK, Biankin, AV, Golan, T: Reshaping preoperative treatment of pancreatic cancer in the era of precision medicine. *Ann Oncol,* 32**:** 183-196, 2021. https://doi.org/10.1016/j.annonc.2020.11.013

6. Neoptolemos, JP, Palmer, DH, Ghaneh, P, Psarelli, EE, Valle, JW, Halloran, CM, Faluyi, O, O'Reilly, DA, Cunningham, D, Wadsley, J, Darby, S, Meyer, T, Gillmore, R, Anthoney, A, Lind, P, Glimelius, B, Falk, S, Izbicki, JR, Middleton, GW, Cummins, S, Ross, PJ, Wasan, H, McDonald, A, Crosby, T, Ma, YT, Patel, K, Sherriff, D, Soomal, R, Borg, D, Sothi, S, Hammel, P, Hackert, T, Jackson, R, Buchler, MW, European Study Group for Pancreatic, C: Comparison of adjuvant gemcitabine and capecitabine with gemcitabine monotherapy in patients with resected pancreatic cancer (ESPAC-4): a multicentre, open-label, randomised, phase 3 trial. *Lancet,* 389**:** 1011-1024, 2017. https://doi.org/10.1016/S0140-6736(16)32409-6

7. Vincent, A, Herman, J, Schulick, R, Hruban, RH, Goggins, M: Pancreatic cancer. *Lancet,* 378**:** 607-620, 2011. https://doi.org/10.1016/S0140-6736(10)62307-0

8. Seufferlein, T, Ettrich, TJ: Treatment of pancreatic cancer-neoadjuvant treatment in resectable pancreatic cancer (PDAC). *Transl Gastroenterol Hepatol,* 4**:** 21, 2019. https://doi.org/10.21037/tgh.2019.03.05

9. Huang, Z, Liu, F: Diagnostic value of serum carbohydrate antigen 19-9 in pancreatic cancer: a meta-analysis. *Tumour Biol,* 35**:** 7459-7465, 2014. https://doi.org/10.1007/s13277-014-1995-9

10. Hong, SK: Kallikreins as biomarkers for prostate cancer. *Biomed Res Int,* 2014**:** 526341, 2014. https://doi.org/10.1155/2014/526341

11. Yousef, GM, Diamandis, EP: The new human tissue kallikrein gene family: structure, function, and association to disease. *Endocr Rev,* 22**:** 184-204, 2001. https://doi.org/10.1210/edrv.22.2.0424

12. Borgono, CA, Michael, IP, Diamandis, EP: Human tissue kallikreins: physiologic roles and applications in cancer. *Mol Cancer Res,* 2**:** 257-280, 2004.

13. Sotiropoulou, G, Pampalakis, G, Diamandis, EP: Functional roles of human kallikrein-related peptidases. *J Biol Chem,* 284**:** 32989-32994, 2009. https://doi.org/10.1074/jbc.R109.027946

14. Yoon, H, Laxmikanthan, G, Lee, J, Blaber, SI, Rodriguez, A, Kogot, JM, Scarisbrick, IA, Blaber, M: Activation profiles and regulatory cascades of the human kallikrein-related peptidases. *J Biol Chem,* 282**:** 31852-31864, 2007. https://doi.org/10.1074/jbc.M705190200

15. Figueroa, CD, Molina, L, Bhoola, KD, Ehrenfeld, P: Overview of tissue kallikrein and kallikrein-related peptidases in breast cancer. *Biol Chem,* 399**:** 937-957, 2018. https://doi.org/10.1515/hsz-2018-0111

16. Kraut, H, Frei, EK, Wehrle, E: Über die Inaktivierung des Kallikreins. (VI. Mitteilung über dieses Kreislaufhormon.). 1930.

17. Yousef, GM, Borgono, CA, White, NM, Robb, JD, Michael, IP, Oikonomopoulou, K, Khan, S, Diamandis, EP: In silico analysis of the human kallikrein gene 6. *Tumour Biol,* 25**:** 282-289, 2004. https://doi.org/10.1159/000081393

18. Dong, Y, Matigian, N, Harvey, TJ, Samaratunga, H, Hooper, JD, Clements, JA: Tissue-specific promoter utilisation of the kallikrein-related peptidase genes, KLK5 and KLK7, and cellular localisation of the encoded proteins suggest roles in exocrine pancreatic function. *Biol Chem,* 389**:** 99-109, 2008. https://doi.org/10.1515/BC.2008.013

19. Iacobuzio-Donahue, CA, Ashfaq, R, Maitra, A, Adsay, NV, Shen-Ong, GL, Berg, K, Hollingsworth, MA, Cameron, JL, Yeo, CJ, Kern, SE, Goggins, M, Hruban, RH: Highly expressed genes in pancreatic ductal adenocarcinomas: a comprehensive characterization and comparison of the transcription profiles obtained from three major technologies. *Cancer Res,* 63**:** 8614-8622, 2003.

20. Ruckert, F, Hennig, M, Petraki, CD, Wehrum, D, Distler, M, Denz, A, Schroder, M, Dawelbait, G, Kalthoff, H, Saeger, HD, Diamandis, EP, Pilarsky, C, Grutzmann, R: Co-expression of KLK6 and KLK10 as prognostic factors for survival in pancreatic ductal adenocarcinoma. *Br J Cancer,* 99**:** 1484-1492, 2008. https://doi.org/10.1038/sj.bjc.6604717

21. Cao, XY, Zhang, XX, Yang, MW, Hu, LP, Jiang, SH, Tian, GA, Zhu, LL, Li, Q, Sun, YW, Zhang, ZG: Aberrant upregulation of KLK10 promotes metastasis via enhancement of EMT and FAK/SRC/ERK axis in PDAC. *Biochem Biophys Res Commun,* 499**:** 584-593, 2018. https://doi.org/10.1016/j.bbrc.2018.03.194

22. Hustinx, SR, Cao, D, Maitra, A, Sato, N, Martin, ST, Sudhir, D, Iacobuzio-Donahue, C, Cameron, JL, Yeo, CJ, Kern, SE, Goggins, M, Mollenhauer, J, Pandey, A, Hruban, RH: Differentially expressed genes in pancreatic ductal adenocarcinomas identified through serial analysis of gene expression. *Cancer Biol Ther,* 3**:** 1254-1261, 2004. https://doi.org/10.4161/cbt.3.12.1238

23. Iakovlev, V, Siegel, ER, Tsao, MS, Haun, RS: Expression of kallikrein-related peptidase 7 predicts poor prognosis in patients with unresectable pancreatic ductal adenocarcinoma. *Cancer Epidemiol Biomarkers Prev,* 21**:** 1135-1142, 2012. https://doi.org/10.1158/1055-9965.EPI-11-1079

24. Candido, JB, Maiques, O, Boxberg, M, Kast, V, Peerani, E, Tomas-Bort, E, Weichert, W, Sananes, A, Papo, N, Magdolen, V, Sanz-Moreno, V, Loessner, D: Kallikrein-Related Peptidase 6 Is Associated with the Tumour Microenvironment of Pancreatic Ductal Adenocarcinoma. *Cancers (Basel),* 13, 2021. https://doi.org/10.3390/cancers13163969

25. Pepin, D, Shao, ZQ, Huppe, G, Wakefield, A, Chu, CW, Sharif, Z, Vanderhyden, BC: Kallikreins 5, 6 and 10 differentially alter pathophysiology and overall survival in an ovarian cancer xenograft model. *PLoS One,* 6**:** e26075, 2011. https://doi.org/10.1371/journal.pone.0026075

26. Zhang, Y, Bhat, I, Zeng, M, Jayal, G, Wazer, DE, Band, H, Band, V: Human kallikrein 10, a predictive marker for breast cancer. *Biol Chem,* 387**:** 715-721, 2006. https://doi.org/10.1515/BC.2006.090

27. Goyal, J, Smith, KM, Cowan, JM, Wazer, DE, Lee, SW, Band, V: The role for NES1 serine protease as a novel tumor suppressor. *Cancer Res,* 58**:** 4782-4786, 1998.

28. Chen, H, Sells, E, Pandey, R, Abril, ER, Hsu, CH, Krouse, RS, Nagle, RB, Pampalakis, G, Sotiropoulou, G, Ignatenko, NA: Kallikrein 6 protease advances colon tumorigenesis via induction of the high mobility group A2 protein. *Oncotarget,* 10**:** 6062-6078, 2019. https://doi.org/10.18632/oncotarget.27153

29. Magklara, A, Mellati, AA, Wasney, GA, Little, SP, Sotiropoulou, G, Becker, GW, Diamandis, EP: Characterization of the enzymatic activity of human kallikrein 6: Autoactivation, substrate specificity, and regulation by inhibitors. *Biochem Biophys Res Commun,* 307**:** 948-955, 2003. https://doi.org/10.1016/s0006-291x(03)01271-3

30. Bernett, MJ, Blaber, SI, Scarisbrick, IA, Dhanarajan, P, Thompson, SM, Blaber, M: Crystal structure and biochemical characterization of human kallikrein 6 reveals

that a trypsin-like kallikrein is expressed in the central nervous system. *J Biol Chem,* 277**:** 24562-24570, 2002. https://doi.org/10.1074/jbc.M202392200

31. Klucky, B, Mueller, R, Vogt, I, Teurich, S, Hartenstein, B, Breuhahn, K, Flechtenmacher, C, Angel, P, Hess, J: Kallikrein 6 induces E-cadherin shedding and promotes cell proliferation, migration, and invasion. *Cancer Res,* 67**:** 8198-8206, 2007. https://doi.org/10.1158/0008-5472.CAN-07-0607

32. Johnson, SK, Ramani, VC, Hennings, L, Haun, RS: Kallikrein 7 enhances pancreatic cancer cell invasion by shedding E-cadherin. *Cancer,* 109**:** 1811-1820, 2007. https://doi.org/10.1002/cncr.22606

33. Du, JP, Li, L, Zheng, J, Zhang, D, Liu, W, Zheng, WH, Li, XS, Yao, RC, Wang, F, Liu, S, Tan, X: Kallikrein-related peptidase 7 is a potential target for the treatment of pancreatic cancer. *Oncotarget,* 9**:** 12894-12906, 2018. https://doi.org/10.18632/oncotarget.24132

34. Kishi, T, Soosaipillai, A, Grass, L, Little, SP, Johnstone, EM, Diamandis, EP: Development of an immunofluorometric assay and quantification of human kallikrein 7 in tissue extracts and biological fluids. *Clin Chem,* 50**:** 709-716, 2004. https://doi.org/10.1373/clinchem.2003.029538

35. Cho, WC: Proteomics technologies and challenges. *Genomics Proteomics Bioinformatics,* 5**:** 77-85, 2007. https://doi.org/10.1016/S1672-0229(07)60018-7

36. Wilkins, MR, Pasquali, C, Appel, RD, Ou, K, Golaz, O, Sanchez, J-C, Yan, JX, Gooley, AA, Hughes, G, Humphery-Smith, I, Williams, KL, Hochstrasser, DF: From Proteins to Proteomes: Large Scale Protein Identification by Two-Dimensional Electrophoresis and Arnino Acid Analysis. *Bio/Technology,* 14**:** 61-65, 1996. https://doi.org/10.1038/nbt0196-61

37. Mishra, N: *Introduction to Proteomics. Principles and Applications.*, 2010.

38. Domon, B, Aebersold, R: Mass Spectrometry and Protein Analysis. *Science,* 312**:** 212-217, 2006. https://doi.org/doi:10.1126/science.1124619

39. Liu, P, Weng, Y, Sui, Z, Wu, Y, Meng, X, Wu, M, Jin, H, Tan, X, Zhang, L, Zhang, Y: Quantitative secretomic analysis of pancreatic cancer cells in serum-containing conditioned medium. *Scientific Reports,* 6**:** 37606, 2016. https://doi.org/10.1038/srep37606

40. Yates, JR, Ruse, CI, Nakorchevsky, A: Proteomics by mass spectrometry: approaches, advances, and applications. *Annu Rev Biomed Eng,* 11**:** 49-79, 2009. https://doi.org/10.1146/annurev-bioeng-061008-124934

41. Aebersold, R, Mann, M: Mass spectrometry-based proteomics. *Nature,* 422**:** 198-207, 2003. https://doi.org/10.1038/nature01511

42. Gillet, LC, Leitner, A, Aebersold, R: Mass Spectrometry Applied to Bottom-Up Proteomics: Entering the High-Throughput Era for Hypothesis Testing. *Annu Rev Anal Chem (Palo Alto Calif),* 9**:** 449-472, 2016. https://doi.org/10.1146/annurev-anchem-071015-041535

43. Escher, C, Reiter, L, MacLean, B, Ossola, R, Herzog, F, Chilton, J, MacCoss, MJ, Rinner, O: Using iRT, a normalized retention time for more targeted measurement of peptides. *PROTEOMICS,* 12**:** 1111-1121, 2012. https://doi.org/https://doi.org/10.1002/pmic.201100463

44. Grebe, SK, Singh, RJ: LC-MS/MS in the Clinical Laboratory - Where to From Here? *Clin Biochem Rev,* 32**:** 5-31, 2011.

45. Angel, TE, Aryal, UK, Hengel, SM, Baker, ES, Kelly, RT, Robinson, EW, Smith, RD: Mass spectrometry-based proteomics: existing capabilities and future directions. *Chem Soc Rev,* 41**:** 3912-3928, 2012. https://doi.org/10.1039/c2cs15331a

46. Wells, JM, McLuckey, SA: Collision-induced dissociation (CID) of peptides and proteins. *Methods Enzymol,* 402**:** 148-185, 2005. https://doi.org/10.1016/S0076-6879(05)02005-7

47. Steen, H, Mann, M: The abc's (and xyz's) of peptide sequencing. *Nature Reviews Molecular Cell Biology,* 5**:** 699-711, 2004. https://doi.org/10.1038/nrm1468

48. Yates, JR, 3rd: Mass spectral analysis in proteomics. *Annu Rev Biophys Biomol Struct,* 33**:** 297-316, 2004. https://doi.org/10.1146/annurev.biophys.33.111502.082538

49. Borras, E, Sabido, E: What is targeted proteomics? A concise revision of targeted acquisition and targeted data analysis in mass spectrometry. *Proteomics,* 17, 2017. https://doi.org/10.1002/pmic.201700180

50. Banerjee, SL, Dionne, U, Lambert, JP, Bisson, N: Targeted proteomics analyses of phosphorylation-dependent signalling networks. *J Proteomics,* 189**:** 39-47, 2018. https://doi.org/10.1016/j.jprot.2018.02.004

51. Aebersold, R, Bensimon, A, Collins, BC, Ludwig, C, Sabido, E: Applications and Developments in Targeted Proteomics: From SRM to DIA/SWATH. *PROTEOMICS,* 16**:** 2065-2067, 2016. https://doi.org/https://doi.org/10.1002/pmic.201600203

52. Bilbao, A, Varesio, E, Luban, J, Strambio-De-Castillia, C, Hopfgartner, G, Müller, M, Lisacek, F: Processing strategies and software solutions for data-independent acquisition in mass spectrometry. *PROTEOMICS,* 15**:** 964-980, 2015. https://doi.org/https://doi.org/10.1002/pmic.201400323

53. Tsai, TH, Choi, M, Banfai, B, Liu, Y, MacLean, BX, Dunkley, T, Vitek, O: Selection of Features with Consistent Profiles Improves Relative Protein Quantification in Mass Spectrometry Experiments. *Mol Cell Proteomics,* 19**:** 944-959, 2020. https://doi.org/10.1074/mcp.RA119.001792

54. Shaw, JL, Diamandis, EP: Regulation of human tissue kallikrein-related peptidase expression by steroid hormones in 32 cell lines. *Biol Chem,* 389**:** 1409-1419, 2008. https://doi.org/10.1515/bc.2008.158

55. Coscia, F, Doll, S, Bech, JM, Schweizer, L, Mund, A, Lengyel, E, Lindebjerg, J, Madsen, GI, Moreira, JM, Mann, M: A streamlined mass spectrometry-based proteomics workflow for large-scale FFPE tissue analysis. *J Pathol,* 251**:** 100-112, 2020. https://doi.org/10.1002/path.5420

56. Grillo, F, Bruzzone, M, Pigozzi, S, Prosapio, S, Migliora, P, Fiocca, R, Mastracci, L: Immunohistochemistry on old archival paraffin blocks: is there an expiry date? *J Clin Pathol,* 70**:** 988-993, 2017. https://doi.org/10.1136/jclinpath-2017-204387

57. Takadate, T, Onogawa, T, Fukuda, T, Motoi, F, Suzuki, T, Fujii, K, Kihara, M, Mikami, S, Bando, Y, Maeda, S, Ishida, K, Minowa, T, Hanagata, N, Ohtsuka, H, Katayose, Y, Egawa, S, Nishimura, T, Unno, M: Novel prognostic protein markers of resectable pancreatic cancer identified by coupled shotgun and targeted proteomics using formalin-fixed paraffin-embedded tissues. *Int J Cancer,* 132**:** 1368-1382, 2013. https://doi.org/10.1002/ijc.27797

58. Cui, Y, Tian, M, Zong, M, Teng, M, Chen, Y, Lu, J, Jiang, J, Liu, X, Han, J: Proteomic analysis of pancreatic ductal adenocarcinoma compared with normal adjacent pancreatic tissue and pancreatic benign cystadenoma. *Pancreatology,* 9**:** 89-98, 2009. https://doi.org/10.1159/000178879

59. Demichev, V, Messner, CB, Vernardis, SI, Lilley, KS, Ralser, M: DIA-NN: neural networks and interference correction enable deep proteome coverage in high throughput. *Nat Methods,* 17**:** 41-44, 2020. https://doi.org/10.1038/s41592-019-0638-x

60. Ruckert, F, Aust, D, Bohme, I, Werner, K, Brandt, A, Diamandis, EP, Krautz, C, Hering, S, Saeger, HD, Grutzmann, R, Pilarsky, C: Five primary human pancreatic adenocarcinoma cell lines established by the outgrowth method. *J Surg Res,* 172**:** 29-39, 2012. https://doi.org/10.1016/j.jss.2011.04.021

61. Hughes, CS, Moggridge, S, Muller, T, Sorensen, PH, Morin, GB, Krijgsveld, J: Single-pot, solid-phase-enhanced sample preparation for proteomics experiments. *Nat Protoc,* 14**:** 68-85, 2019. https://doi.org/10.1038/s41596-018-0082-x

62. MacLean, B, Tomazela, DM, Shulman, N, Chambers, M, Finney, GL, Frewen, B, Kern, R, Tabb, DL, Liebler, DC, MacCoss, MJ: Skyline: an open source document editor for creating and analyzing targeted proteomics experiments.

Bioinformatics, 26**:** 966-968, 2010. https://doi.org/10.1093/bioinformatics/btq054

63. Searle, BC, Pino, LK, Egertson, JD, Ting, YS, Lawrence, RT, MacLean, BX, Villen, J, MacCoss, MJ: Chromatogram libraries improve peptide detection and quantification by data independent acquisition mass spectrometry. *Nat Commun,* 9**:** 5128, 2018. https://doi.org/10.1038/s41467-018-07454-w

64. Balotf, S, Wilson, R, Tegg, RS, Nichols, DS, Wilson, CR: Optimisation of Sporosori Purification and Protein Extraction Techniques for the Biotrophic Protozoan Plant Pathogen Spongospora subterranea. *Molecules,* 25, 2020. https://doi.org/10.3390/molecules25143109

65. Cleland, TP: Human Bone Paleoproteomics Utilizing the Single-Pot, Solid-Phase-Enhanced Sample Preparation Method to Maximize Detected Proteins and Reduce Humics. *J Proteome Res,* 17**:** 3976-3983, 2018. https://doi.org/10.1021/acs.jproteome.8b00637

66. Hughes, CS, Foehr, S, Garfield, DA, Furlong, EE, Steinmetz, LM, Krijgsveld, J: Ultrasensitive proteome analysis using paramagnetic bead technology. *Mol Syst Biol,* 10**:** 757, 2014. https://doi.org/10.15252/msb.20145625

67. Muller, T, Kalxdorf, M, Longuespee, R, Kazdal, DN, Stenzinger, A, Krijgsveld, J: Automated sample preparation with SP3 for low-input clinical proteomics. *Mol Syst Biol,* 16**:** e9111, 2020. https://doi.org/10.15252/msb.20199111

68. Werner, J, Bernhard, P, Cosenza-Contreras, M, Pinter, N, Fahrner, M, Pallavi, P, Eberhard, J, Bronsert, P, Ruckert, F, Schilling, O: Targeted and explorative profiling of kallikrein proteases and global proteome biology of pancreatic ductal adenocarcinoma, chronic pancreatitis, and normal pancreas highlights disease-specific proteome remodelling. *Neoplasia,* 36**:** 100871, 2023. https://doi.org/10.1016/j.neo.2022.100871

69. Rückert, F, Werner, K, Aust, D, Hering, S, Saeger, H, Grützmann, R, Pilarsky, C: Establishment and characterization of six primary pancreatic cancer cell lines. *Austin J Cancer Clin Res,* 2**:** 1055, 2015.

70. Abu-Jamous, B, Kelly, S: Clust: automatic extraction of optimal co-expressed gene clusters from gene expression data. *Genome Biol,* 19**:** 172, 2018. https://doi.org/10.1186/s13059-018-1536-8

71. Bosman, FT, World Health Organization., International Agency for Research on Cancer.: *WHO classification of tumours of the digestive system,* Lyon, International Agency for Research on Cancer, 2010.

72. Li, R, Shen, Y: An old method facing a new challenge: re-visiting housekeeping proteins as internal reference control for neuroscience research. *Life Sci,* 92**:** 747-751, 2013. https://doi.org/10.1016/j.lfs.2013.02.014

73. Makawita, S, Smith, C, Batruch, I, Zheng, Y, Ruckert, F, Grutzmann, R, Pilarsky, C, Gallinger, S, Diamandis, EP: Integrated proteomic profiling of cell line conditioned media and pancreatic juice for the identification of pancreatic cancer biomarkers. *Mol Cell Proteomics,* 10**:** M111 008599, 2011. https://doi.org/10.1074/mcp.M111.008599

74. Liu, P, Kong, L, Jin, H, Wu, Y, Tan, X, Song, B: Differential secretome of pancreatic cancer cells in serum-containing conditioned medium reveals CCT8 as a new biomarker of pancreatic cancer invasion and metastasis. *Cancer Cell International,* 19**:** 262, 2019. https://doi.org/10.1186/s12935-019-0980-1

75. Webber, MM, Waghray, A, Bello, D: Prostate-specific antigen, a serine protease, facilitates human prostate cancer cell invasion. *Clin Cancer Res,* 1**:** 1089-1094, 1995.

76. Borgono, CA, Diamandis, EP: The emerging roles of human tissue kallikreins in cancer. *Nat Rev Cancer,* 4**:** 876-890, 2004. https://doi.org/10.1038/nrc1474

77. Michael, IP, Sotiropoulou, G, Pampalakis, G, Magklara, A, Ghosh, M, Wasney, G, Diamandis, EP: Biochemical and enzymatic characterization of human kallikrein 5 (hK5), a novel serine protease potentially involved in cancer progression. *J Biol Chem,* 280**:** 14628-14635, 2005. https://doi.org/10.1074/jbc.M408132200

78. Chen, WH, Horoszewicz, JS, Leong, SS, Shimano, T, Penetrante, R, Sanders, WH, Berjian, R, Douglass, HO, Martin, EW, Chu, TM: Human pancreatic adenocarcinoma: in vitro and in vivo morphology of a new tumor line established from ascites. *In Vitro,* 18**:** 24-34, 1982. https://doi.org/10.1007/BF02796382

79. Daikichi Fukushima, NK, and Shigetada Nakanish: Nucleotide Sequence of Cloned cDNA for Human Pancreatic Kainkrein. *Biochemistry*, 1985.

80. ole-MoiYoi, OK, Pinkus, GS, Spragg, J, Austen, KF: Identification of human glandular kallikrein in the beta cell of the pancreas. *N Engl J Med,* 300**:** 1289-1294, 1979. https://doi.org/10.1056/NEJM197906073002301

81. Pinkus, GS, Maier, M, Seldin, DC, ole-MoiYoi, OK, Austen, KF, Spragg, J: Immunohistochemical localization of glandular kallikrein in the endocrine and exocrine human pancreas. *J Histochem Cytochem,* 31**:** 1279-1288, 1983. https://doi.org/10.1177/31.11.6194204

82. Yousef, GM, Borgono, CA, Popalis, C, Yacoub, GM, Polymeris, ME, Soosaipillai, A, Diamandis, EP: In-silico analysis of kallikrein gene expression in pancreatic and colon cancers. *Anticancer Res,* 24**:** 43-51, 2004.

83. Van Heek, NT, Maitra, A, Koopmann, J, Fedarko, N, Jain, A, Rahman, A, Iacobuzio-Donahue, CA, Adsay, V, Ashfaq, R, Yeo, CJ, Cameron, JL, Offerhaus, JA, Hruban, RH, Berg, KD, Goggins, M: Gene expression profiling

identifies markers of ampullary adenocarcinoma. *Cancer Biol Ther,* 3**:** 651-656, 2004. https://doi.org/10.4161/cbt.3.7.919

84. Paluri, R, Kasi, A: Ampullary Cancer. In: *StatPearls.* Treasure Island (FL), 2021.

85. Rubie, C, Kempf, K, Hans, J, Su, T, Tilton, B, Georg, T, Brittner, B, Ludwig, B, Schilling, M: Housekeeping gene variability in normal and cancerous colorectal, pancreatic, esophageal, gastric and hepatic tissues. *Mol Cell Probes,* 19**:** 101-109, 2005. https://doi.org/10.1016/j.mcp.2004.10.001

86. Bose, S, Zhang, C, Le, A: Glucose Metabolism in Cancer: The Warburg Effect and Beyond. *Adv Exp Med Biol,* 1311**:** 3-15, 2021. https://doi.org/10.1007/978-3-030-65768-0_1

87. Warburg, O: Über den Stoffwechsel der Carcinomzelle. *Naturwissenschaften,* 12**:** 1131-1137, 1924. https://doi.org/10.1007/BF01504608

88. Yang, J, Ren, B, Yang, G, Wang, H, Chen, G, You, L, Zhang, T, Zhao, Y: The enhancement of glycolysis regulates pancreatic cancer metastasis. *Cell Mol Life Sci,* 77**:** 305-321, 2020. https://doi.org/10.1007/s00018-019-03278-z

89. Guo, C, Liu, S, Sun, MZ: Novel insight into the role of GAPDH playing in tumor. *Clin Transl Oncol,* 15**:** 167-172, 2013. https://doi.org/10.1007/s12094-012-0924-x

90. Cao, L, Huang, C, Cui Zhou, D, Hu, Y, Lih, TM, Savage, SR, Krug, K, Clark, DJ, Schnaubelt, M, Chen, L, da Veiga Leprevost, F, Eguez, RV, Yang, W, Pan, J, Wen, B, Dou, Y, Jiang, W, Liao, Y, Shi, Z, Terekhanova, NV, Cao, S, Lu, RJ, Li, Y, Liu, R, Zhu, H, Ronning, P, Wu, Y, Wyczalkowski, MA, Easwaran, H, Danilova, L, Mer, AS, Yoo, S, Wang, JM, Liu, W, Haibe-Kains, B, Thiagarajan, M, Jewell, SD, Hostetter, G, Newton, CJ, Li, QK, Roehrl, MH, Fenyo, D, Wang, P, Nesvizhskii, AI, Mani, DR, Omenn, GS, Boja, ES, Mesri, M, Robles, AI, Rodriguez, H, Bathe, OF, Chan, DW, Hruban, RH, Ding, L, Zhang, B, Zhang, H, Clinical Proteomic Tumor Analysis, C: Proteogenomic characterization of pancreatic ductal adenocarcinoma. *Cell,* 184**:** 5031-5052 e5026, 2021. https://doi.org/10.1016/j.cell.2021.08.023

91. Makrilia, N, Kollias, A, Manolopoulos, L, Syrigos, K: Cell adhesion molecules: role and clinical significance in cancer. *Cancer Invest,* 27**:** 1023-1037, 2009. https://doi.org/10.3109/07357900902769749

92. Janiszewska, M, Primi, MC, Izard, T: Cell adhesion in cancer: Beyond the migration of single cells. *J Biol Chem,* 295**:** 2495-2505, 2020. https://doi.org/10.1074/jbc.REV119.007759

93. Cavallaro, U, Christofori, G: Multitasking in tumor progression: signaling functions of cell adhesion molecules. *Ann N Y Acad Sci,* 1014**:** 58-66, 2004. https://doi.org/10.1196/annals.1294.006

94. Aiello, NM, Maddipati, R, Norgard, RJ, Balli, D, Li, J, Yuan, S, Yamazoe, T, Black, T, Sahmoud, A, Furth, EE, Bar-Sagi, D, Stanger, BZ: EMT Subtype Influences Epithelial Plasticity and Mode of Cell Migration. *Dev Cell,* 45**:** 681-695 e684, 2018. https://doi.org/10.1016/j.devcel.2018.05.027

95. Luu, T: Epithelial-Mesenchymal Transition and Its Regulation Mechanisms in Pancreatic Cancer. *Front Oncol,* 11**:** 646399, 2021. https://doi.org/10.3389/fonc.2021.646399

96. Wolf, K, Wu, YI, Liu, Y, Geiger, J, Tam, E, Overall, C, Stack, MS, Friedl, P: Multi-step pericellular proteolysis controls the transition from individual to collective cancer cell invasion. *Nat Cell Biol,* 9**:** 893-904, 2007. https://doi.org/10.1038/ncb1616

97. Bergmann, F, Wandschneider, F, Sipos, B, Moldenhauer, G, Schniewind, B, Welsch, T, Schirrmacher, P, Kloppel, G, Altevogt, P, Schafer, H, Sebens Muerkoster, S: Elevated L1CAM expression in precursor lesions and primary and metastastic tissues of pancreatic ductal adenocarcinoma. *Oncol Rep,* 24**:** 909-915, 2010. https://doi.org/10.3892/or.2010.909

98. Tsutsumi, S, Morohashi, S, Kudo, Y, Akasaka, H, Ogasawara, H, Ono, M, Takasugi, K, Ishido, K, Hakamada, K, Kijima, H: L1 Cell adhesion molecule (L1CAM) expression at the cancer invasive front is a novel prognostic marker of pancreatic ductal adenocarcinoma. *J Surg Oncol,* 103**:** 669-673, 2011. https://doi.org/10.1002/jso.21880

99. Tempia-Caliera, AA, Horvath, LZ, Zimmermann, A, Tihanyi, TT, Korc, M, Friess, H, Buchler, MW: Adhesion molecules in human pancreatic cancer. *J Surg Oncol,* 79**:** 93-100, 2002. https://doi.org/10.1002/jso.10053

100. Kuehn, R, Lelkes, PI, Bloechle, C, Niendorf, A, Izbicki, JR: Angiogenesis, angiogenic growth factors, and cell adhesion molecules are upregulated in chronic pancreatic diseases: angiogenesis in chronic pancreatitis and in pancreatic cancer. *Pancreas,* 18**:** 96-103, 1999. https://doi.org/10.1097/00006676-199901000-00012

101. Maddipati, R, Stanger, BZ: Pancreatic Cancer Metastases Harbor Evidence of Polyclonality. *Cancer Discov,* 5**:** 1086-1097, 2015. https://doi.org/10.1158/2159-8290.CD-15-0120

102. Nweke, E, Ntwasa, M, Brand, M, Devar, J, Smith, M, Candy, G: Increased expression of plakoglobin is associated with upregulated MAPK and PI3K/AKT signalling pathways in early resectable pancreatic ductal adenocarcinoma. *Oncol Lett,* 19**:** 4133-4141, 2020. https://doi.org/10.3892/ol.2020.11473

103. Zhou, YY, Chen, LP, Zhang, Y, Hu, SK, Dong, ZJ, Wu, M, Chen, QX, Zhuang, ZZ, Du, XJ: Integrated transcriptomic analysis reveals hub genes involved in diagnosis and prognosis of pancreatic cancer. *Mol Med,* 25**:** 47, 2019. https://doi.org/10.1186/s10020-019-0113-2

104. Ryschich, E, Khamidjanov, A, Kerkadze, V, Buchler, MW, Zoller, M, Schmidt, J: Promotion of tumor cell migration by extracellular matrix proteins in human pancreatic cancer. *Pancreas,* 38**:** 804-810, 2009. https://doi.org/10.1097/MPA.0b013e3181b9dfda

105. Wu, J, Li, Z, Zeng, K, Wu, K, Xu, D, Zhou, J, Xu, L: Key genes associated with pancreatic cancer and their association with outcomes: A bioinformatics analysis. *Mol Med Rep,* 20**:** 1343-1352, 2019. https://doi.org/10.3892/mmr.2019.10321

106. Lei, X, Chen, G, Li, J, Wen, W, Gong, J, Fu, J: Comprehensive analysis of abnormal expression, prognostic value and oncogenic role of the hub gene FN1 in pancreatic ductal adenocarcinoma via bioinformatic analysis and in vitro experiments. *PeerJ,* 9**:** e12141, 2021. https://doi.org/10.7717/peerj.12141

107. Kim, H, McCulloch, CA: Filamin A mediates interactions between cytoskeletal proteins that control cell adhesion. *FEBS Lett,* 585**:** 18-22, 2011. https://doi.org/10.1016/j.febslet.2010.11.033

108. Zhou, AX, Toylu, A, Nallapalli, RK, Nilsson, G, Atabey, N, Heldin, CH, Boren, J, Bergo, MO, Akyurek, LM: Filamin a mediates HGF/c-MET signaling in tumor cell migration. *Int J Cancer,* 128**:** 839-846, 2011. https://doi.org/10.1002/ijc.25417

109. Chen, Q, Yu, D, Zhao, Y, Qiu, J, Xie, Y, Tao, M: Screening and identification of hub genes in pancreatic cancer by integrated bioinformatics analysis. *J Cell Biochem,* 120**:** 19496-19508, 2019. https://doi.org/10.1002/jcb.29253

110. Friedl, P, Alexander, S: Cancer invasion and the microenvironment: plasticity and reciprocity. *Cell,* 147**:** 992-1009, 2011. https://doi.org/10.1016/j.cell.2011.11.016

111. Ger, M, Žalytė, E, Kaupinis, A, Kurlinkus, B, Petrulionis, M, Šileikis, A, Strupas, K, Valius, M: Primary pancreatic ductal adenocarcinoma cell cultures represent the features of native tumours. *Biologija,* 65, 2019.

112. Zhou, W, Capello, M, Fredolini, C, Racanicchi, L, Piemonti, L, Liotta, LA, Novelli, F, Petricoin, EF: Phosphoproteomic analysis of pancreatic ductal adenocarcinoma cells reveals differential phosphorylation of cell adhesion, cell junction and structural proteins. *J Proteomics Bioinform,* 4**:** 170-178, 2011.

113. Hanahan, D: Hallmarks of Cancer: New Dimensions. *Cancer Discov,* 12**:** 31-46, 2022. https://doi.org/10.1158/2159-8290.CD-21-1059

114. Lei, MZ, Li, XX, Zhang, Y, Li, JT, Zhang, F, Wang, YP, Yin, M, Qu, J, Lei, QY: Acetylation promotes BCAT2 degradation to suppress BCAA catabolism and pancreatic cancer growth. *Signal Transduct Target Ther,* 5**:** 70, 2020. https://doi.org/10.1038/s41392-020-0168-0

115. Xinyu, W, Yi, j, Zhe, L, Hui, Y, Anqin, D: The Oncogenic Role of γ-Aminobutyrate Aminotransferase in Human Tumor: A Pan-Cancer Analysis. *Scientific Reports*, 2022. https://doi.org/10.21203/rs.3.rs-1177474/v1

116. Takehara, A, Hosokawa, M, Eguchi, H, Ohigashi, H, Ishikawa, O, Nakamura, Y, Nakagawa, H: Gamma-aminobutyric acid (GABA) stimulates pancreatic cancer growth through overexpressing GABAA receptor pi subunit. *Cancer Res,* 67**:** 9704-9712, 2007. https://doi.org/10.1158/0008-5472.CAN-07-2099

117. Xu, R, Yang, J, Ren, B, Wang, H, Yang, G, Chen, Y, You, L, Zhao, Y: Reprogramming of Amino Acid Metabolism in Pancreatic Cancer: Recent Advances and Therapeutic Strategies. *Front Oncol,* 10**:** 572722, 2020. https://doi.org/10.3389/fonc.2020.572722

118. Mao, Y, Schwarzbauer, JE: Fibronectin fibrillogenesis, a cell-mediated matrix assembly process. *Matrix Biol,* 24**:** 389-399, 2005. https://doi.org/10.1016/j.matbio.2005.06.008

119. Shouji Shimoyama, tFG, t, Susanne Gansauge, TO, 2and Hans. G. Beget *,1: Altered Expression of Extracellular Matrix Molecules and Their Receptors in Chronic Pancreatitis and Pancreatic Adenocarcinoma in Comparison with Normal Pancreas. *International Journal of Pancreatology*, 1995.

120. Topalovski, M, Brekken, RA: Matrix control of pancreatic cancer: New insights into fibronectin signaling. *Cancer Lett,* 381**:** 252-258, 2016. https://doi.org/10.1016/j.canlet.2015.12.027

121. Tian, C, Clauser, KR, Ohlund, D, Rickelt, S, Huang, Y, Gupta, M, Mani, DR, Carr, SA, Tuveson, DA, Hynes, RO: Proteomic analyses of ECM during pancreatic ductal adenocarcinoma progression reveal different contributions by tumor and stromal cells. *Proc Natl Acad Sci U S A,* 116**:** 19609-19618, 2019. https://doi.org/10.1073/pnas.1908626116

122. Thomas, D, Radhakrishnan, P: Tumor-stromal crosstalk in pancreatic cancer and tissue fibrosis. *Mol Cancer,* 18**:** 14, 2019. https://doi.org/10.1186/s12943-018-0927-5

123. Whittle, MC, Hingorani, SR: Fibroblasts in Pancreatic Ductal Adenocarcinoma: Biological Mechanisms and Therapeutic Targets. *Gastroenterology,* 156**:** 2085-2096, 2019. https://doi.org/10.1053/j.gastro.2018.12.044

124. Zhou, Q, Melton, DA: Pancreas regeneration. *Nature,* 557**:** 351-358, 2018. https://doi.org/10.1038/s41586-018-0088-0

125. Bettac, L, Denk, S, Seufferlein, T, Huber-Lang, M: Complement in Pancreatic Disease-Perpetrator or Savior? *Front Immunol,* 8**:** 15, 2017. https://doi.org/10.3389/fimmu.2017.00015

126. Markiewski, MM, Nilsson, B, Ekdahl, KN, Mollnes, TE, Lambris, JD: Complement and coagulation: strangers or partners in crime? *Trends Immunol,* 28**:** 184-192, 2007. https://doi.org/10.1016/j.it.2007.02.006

127. Tiemann, K, Garri, C, Lee, SB, Malihi, PD, Park, M, Alvarez, RM, Yap, LP, Mallick, P, Katz, JE, Gross, ME, Kani, K: Loss of ER retention motif of AGR2 can impact mTORC signaling and promote cancer metastasis. *Oncogene,* 38**:** 3003-3018, 2019. https://doi.org/10.1038/s41388-018-0638-9

128. Ramachandran, V, Arumugam, T, Wang, H, Logsdon, CD: Anterior gradient 2 is expressed and secreted during the development of pancreatic cancer and promotes cancer cell survival. *Cancer Res,* 68**:** 7811-7818, 2008. https://doi.org/10.1158/0008-5472.CAN-08-1320

129. Bao, J, Li, Z: miR-499a promotes PANC-1 cell proliferation by down-regulating PDCD4 expression in pancreatic ductal adenocarcinoma. *Int J Clin Exp Pathol,* 13**:** 1390-1396, 2020.

130. Nagao, Y, Hisaoka, M, Matsuyama, A, Kanemitsu, S, Hamada, T, Fukuyama, T, Nakano, R, Uchiyama, A, Kawamoto, M, Yamaguchi, K, Hashimoto, H: Association of microRNA-21 expression with its targets, PDCD4 and TIMP3, in pancreatic ductal adenocarcinoma. *Modern Pathology,* 25**:** 112-121, 2012. https://doi.org/10.1038/modpathol.2011.142

131. Yamamura, A, Miura, K, Karasawa, H, Morishita, K, Abe, K, Mizuguchi, Y, Saiki, Y, Fukushige, S, Kaneko, N, Sase, T, Nagase, H, Sunamura, M, Motoi, F, Egawa, S, Shibata, C, Unno, M, Sasaki, I, Horii, A: Suppressed expression of NDRG2 correlates with poor prognosis in pancreatic cancer. *Biochem Biophys Res Commun,* 441**:** 102-107, 2013. https://doi.org/10.1016/j.bbrc.2013.10.010

132. Li, S, Wang, L, Zhao, Q, Wang, Z, Lu, S, Kang, Y, Jin, G, Tian, J: Genome-Wide Analysis of Cell-Free DNA Methylation Profiling for the Early Diagnosis of Pancreatic Cancer. *Front Genet,* 11**:** 596078, 2020. https://doi.org/10.3389/fgene.2020.596078

133. Orth, M, Metzger, P, Gerum, S, Mayerle, J, Schneider, G, Belka, C, Schnurr, M, Lauber, K: Pancreatic ductal adenocarcinoma: biological hallmarks, current status, and future perspectives of combined modality treatment approaches. *Radiat Oncol,* 14**:** 141, 2019. https://doi.org/10.1186/s13014-019-1345-6

134. Buscail, L, Bournet, B, Cordelier, P: Role of oncogenic KRAS in the diagnosis, prognosis and treatment of pancreatic cancer. *Nat Rev Gastroenterol Hepatol,* 17**:** 153-168, 2020. https://doi.org/10.1038/s41575-019-0245-4

135. Long, NP, Jung, KH, Anh, NH, Yan, HH, Nghi, TD, Park, S, Yoon, SJ, Min, JE, Kim, HM, Lim, JH, Kim, JM, Lim, J, Lee, S, Hong, SS, Kwon, SW: An Integrative Data Mining and Omics-Based Translational Model for the Identification and Validation of Oncogenic Biomarkers of Pancreatic Cancer. *Cancers (Basel),* 11, 2019. https://doi.org/10.3390/cancers11020155

136. Algul, H, Wagner, M, Lesina, M, Schmid, RM: Overexpression of ErbB2 in the exocrine pancreas induces an inflammatory response but not increased proliferation. *Int J Cancer,* 121**:** 1410-1416, 2007. https://doi.org/10.1002/ijc.22779

137. Arumugam, T, Simeone, DM, Van Golen, K, Logsdon, CD: S100P promotes pancreatic cancer growth, survival, and invasion. *Clin Cancer Res,* 11**:** 5356-5364, 2005. https://doi.org/10.1158/1078-0432.CCR-05-0092

138. Qiu, C, Bu, X, Jiang, Z: Protocadherin-10 acts as a tumor suppressor gene, and is frequently downregulated by promoter methylation in pancreatic cancer cells. *Oncol Rep,* 36**:** 383-389, 2016. https://doi.org/10.3892/or.2016.4793

139. Lai, ZW, Nice, EC, Schilling, O: Glycocapture-based proteomics for secretome analysis. *PROTEOMICS,* 13**:** 512-525, 2013. https://doi.org/https://doi.org/10.1002/pmic.201200414

140. e.V., DGfrP: Abstractband zur 105. Jahrestagung der Deutschen Gesellschaft für Pathologie, 2022. https://www.pathologie-dgp.de/media/Dgp/Jahrestagung-2022/DGP2022_Abstractband_final_Web.pdf. Retrieved 24.02.2023.

9 OWN PUBLICATIONS

Results of the present work were partially published in the Journal "Neoplasia" (Impact Factor 6,218) in January 2023:

Werner, J, Bernhard, P, Cosenza-Contreras, M, Pinter, N, Fahrner, M, Pallavi, P, Eberhard, J, Bronsert, P, Ruckert, F, Schilling, O: Targeted and explorative profiling of kallikrein proteases and global proteome biology of pancreatic ductal adenocarcinoma, chronic pancreatitis, and normal pancreas highlights disease-specific proteome remodelling. *Neoplasia,* 36**:** 100871, 2023. https://doi.org/10.1016/j.neo.2022.100871

Published congress contributions:

Werner, J, Bernhard, P, Fröhlich, K, Fahrner, M, Eberhard, J, Bronsert, P, Ruckert, F, Schilling, O: Targeted and explorative mass spectrometry show kallikrein 6 and 10 overexpression in PDAC and suggest a collective cell migration for pancreatic cancer. Published in "Abstractband zur 105. Jahrestagung der Deutschen Gesellschaft für Pathologie" [140].

Presentations and posters:

Werner, J, Bernhard, P, Fröhlich, K, Fahrner, M, Eberhard, J, Bronsert, P, Ruckert, F, Schilling, O: Proteome profiling of PDAC and specific detection of kallikrein proteases -6 and -10 by targeted and shotgun mass spectrometry. Flash talk and poster presentation at the 41st Annual Meeting of the German Pancreas Club, February 10-12, 2022, in Lübeck.

Werner, J, Bernhard, P, Fröhlich, K, Fahrner, M, Eberhard, J, Bronsert, P, Ruckert, F, Schilling, O: Targeted and explorative mass spectrometry show kallikrein 6 and 10 overexpression in PDAC and suggest a collective cell migration for pancreatic cancer. Oral presentation at the 105. Jahrestagung der Deutschen Gesellschaft für Pathologie e. V., June 09-11, 2022, in Münster.

Werner, J, Bernhard, P, Cosenza-Contreras, M, Pinter, N, Fahrner, M, Pallavi, P, Eberhard, J, Bronsert, P, Ruckert, F, Schilling, O: Targeted mass spectrometry shows detection of kallikrein proteases in pancreatic ductal adenocarcinoma and explorative profiling provides novel disease-specific insights into proteomic characteristics between cancerous, inflammatory, and normal pancreas. Oral presentation at the 42nd Annual Meeting of the German Pancreas Club, March 02-04, 2023, in Munich.

10 SUPPLEMENTS

Table S 14. Detailed chromatographic gradient information for peptide separation prior to SRM Measurement. The table shows the proportion of buffer B (50 % (v/v) ACN in 0,1 % (v/v) FA in H2O) in buffer A (0,1 % (v/v) FA) over time at a constant flow rate. Adapted from table S1 of Werner et al., 2023 [68].

Time [min]	Duration	Flow [nl/min]	% B
0	Start	250	8
60	60	250	56
70	10	250	90
71	1	250	100
72	1	250	100
73	1	250	5
83	10	250	5

Table S 15. Detailed chromatographic gradient information for peptide separation prior to PRM and DIA Measurement. The table shows the proportion of buffer B 80 % (v/v) ACN in 0,1 % (v/v) FA, 1 % (v/v) MEG) in buffer A (0,1 % (v/v) FA) over time at a constant flow rate. Adapted from table S2 of Werner et al., 2023 [68].

Time [min]	Duration	Flow [nl/min]	% B
0	Start	700	8
2	2	700	10
24	22	350	20
70	46	350	40
80	10	350	55
82	2	350	100
120	38	350	100


PDAC
Adjacent Pancreas
Chronic Pancreatitis
Normal Pancreas
Ampullary Cancer

Figure S 23. Exemplary Endogenous KLK6 Detection in FFPE Tissue Samples of Patient Cohort. X-axis shows the retention time of the eluting peptides and y-axis represents the intensity of detected peptides. The dotted frames represent the expected retention time window of the eluting peptides.

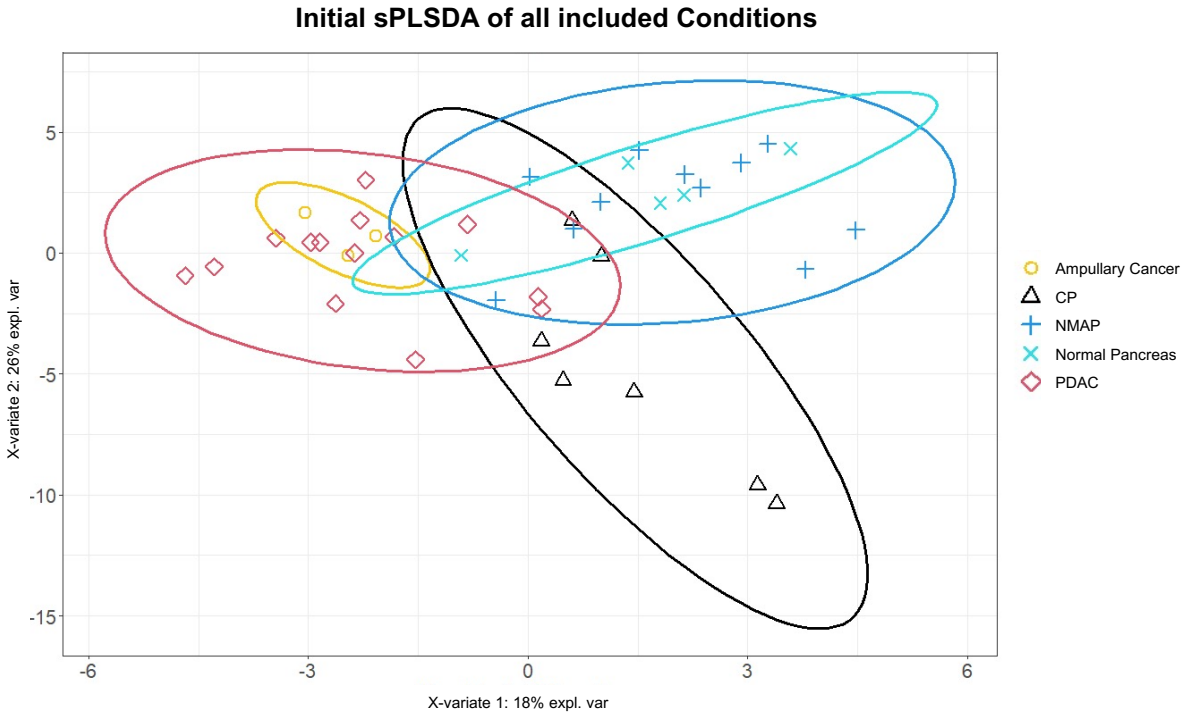

Figure S 24. Sparse Least Squares Discriminant Analysis (sPLS-DA) of generated DIA data. Included are the conditions PDAC, chronic pancreatitis (CP), ampullary cancer, non-malignant adjacent pancreas, and normal pancreas. Ellipses display the calculated confidence interval (95 %). Adapted from figure S2 of Werner et al., 2023 [68].

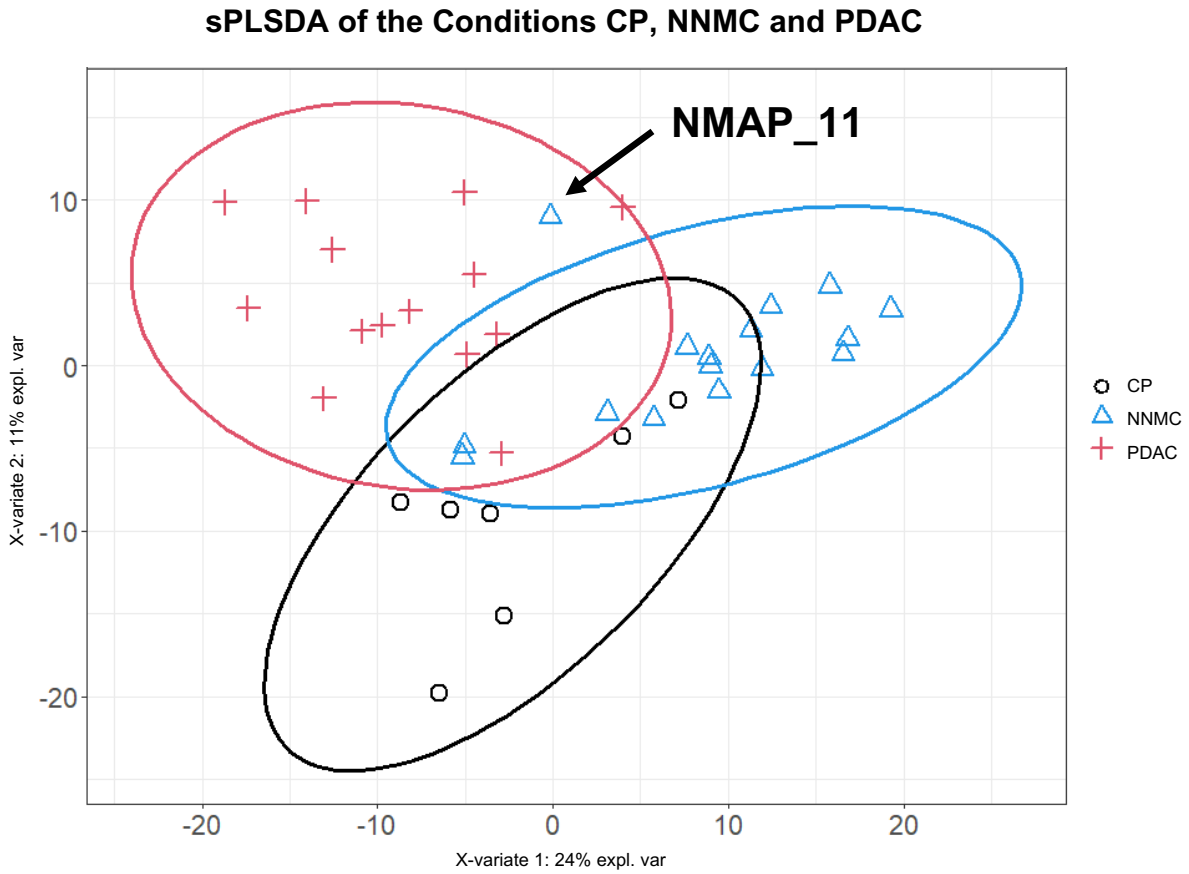

Figure S 25. Sparse Least Squares Discriminant Analysis (sPLS-DA) of generated DIA data only including the three final conditions. Included are the conditions PDAC, chronic pancreatitis (CP), and normal non-malignant control (NNMC). Ellipses display the calculated confidence interval (95 %). Sample NMAP_11 is located outside the calculated confidence interval for the NNMC condition (red arrow). Adapted from figure S3 of Werner et al., 2023 [68].

Table S 16. Characteristic proteins for the respective conditions from sPLS-DA.

Tissue Entity	Protein Names				
CP					
	A2M	COL14A1	FGG	MYO1C	TTR
	ADD1	COL15A1	FYCO1	NES	VAT1
	ADD3	COL1A1	GNAO1	NID1	VIM
	ADH5	COL1A2	GNAS	NID2	
	AKAP12	COL6A1	GNB1	OGN	
	ALDH4A1	COL6A2	GNB2	OLFML1	
	APOA1	COL6A3	GNG2	OLFML3	
	APOB	CYB5R3	HRG	PAFAH1B1	
	APOH	DCN	HSPA12A	PECAM1	
	ASPH	DDAH2	HSPB6	PLG	
	BCAM	DPT	HSPG2	POTEI	

C4BPA	DPYSL2	KANK2	PTGFRN
C7	EHD2	KCTD12	RCN1
CAT	EPB41L2	LAMA5	SELENBP1
CAVIN1	EPB41L3	LAMB2	SLC9A3R2
CAVIN2	ESD	LAMC1	SNTB2
CD81	FAH	LRP1	STOM
CLIC2	FASN	MPP1	TINAGL1
CLU	FGB	MTPN	TNXB

NNMC

AARS1	DECR1	MAT2A	PSMC5	SLC25A13
AARSD1	DPM1	MCCC1	RACK1	SLIRP
ABHD10	ECHDC1	MCCC2	RDH11	SND1
ACADM	ECI1	METTL7A	RDX	SPCS3
ACADVL	EEF1B2	MIA3	RNPS1	SPR
ACAT1	EEF1D	MLEC	RPL10	SRP54
ACO1	EFHD2	MMUT	RPL10A	SRP68
ACO2	EHD4	MPI	RPL12	SRP72
AIFM1	EIF4A2	MYO6	RPL15	SRPRA
AIMP2	EPHX1	NADK2	RPL18	SRPRB
AKR1A1	EPRS1	NAGK	RPL21	SSR1
ALDH1A1	FARSA	NANS	RPL23	SSR4
ALDH1L2	FECH	NARS1	RPL3	TBC1D15
ALDH3A2	FKBP2	NCLN	RPL30	TBL2
ALDH6A1	FN3K	NDUFA5	RPL4	TKT
ALDH7A1	FNDC3A	NDUFB9	RPL5	TM9SF3
ALDH9A1	GART	NDUFS1	RPL7A	TMEM205
ALG2	GCDH	NDUFV2	RPN1	TPD52
ALG5	GFPT1	NIBAN1	RPN2	TRAP1
APPL1	GMPPA	NONO	RPS17	TRIM25
ATP13A1	GMPPB	NSF	RPS2	TTC37
ATP1B1	GSTZ1	NUCB2	RPS26	UBA5
ATP5F1A	HDLBP	OS9	RPS3	UFL1
ATP5F1B	HIBCH	OSBP	RPS4X	UFM1
BCKDHA	HMOX2	P4HB	RPS6	UGGT1
C11orf54	HSD17B10	PAPSS1	RPS7	USO1
CARS1	HSDL2	PCCA	RPS8	UTRN
CCDC47	HSP90B1	PCCB	RPSA	VARS1
CD2AP	HSPA5	PCK2	RRBP1	WDR61
CDK5RAP3	HSPD1	PDCD4	RSL1D1	
COPG1	HSPE1	PDHB	SAMM50	
CPT2	HYOU1	PDIA4	SARS1	
CRAT	IARS2	PDIA6	SCFD1	
CRYZ	IQGAP2	PEBP1	SEC22B	

CSDE1	ISYNA1	PGM1	SEC23B	
CYB5A	IVD	PGM3	SEC24A	
DBT	KARS1	PLPBP	SEC24C	
DDOST	LARS1	PRDX4	SEC31A	
DDRGK1	LMAN1	PREB	SEC63	
DDX46	LRRC47	PRKAR2A	SF3B2	

PDAC

ACTG1	CORO1C	GAPDH	NUP210	SRSF7
ACTN1	CSE1L	GLRX3	PALLD	TAGLN
ACTR3	CSK	GSTK1	PDLIM1	TGFBI
AHSA1	CSRP1	HK1	PFKP	TLN1
ALDOC	CSTF2	HNRNPF	PKM	TPD52L2
ANXA1	DNM1L	HSPA8	PLEC	TUBA4A
AP2B1	DNM2	HSPH1	PLS3	TWF1
ARFIP1	DPYSL3	IFI16	PPP1R12A	UBA6
ARHGAP1	DSG2	JUP	PRPF4	WDR1
ARPC3	EFTUD2	LDHA	PRPF6	
BUB3	EHD1	LGALS1	PSME3	
CALD1	EIF2AK2	LMCD1	PUF60	
CAP1	EIF6	LNPEP	PYCARD	
CAPG	ENO1	MAT2B	RBM14	
CAPZA1	ERMP1	MSN	RCC2	
CAPZB	ERO1A	MVP	S100A11	
CFL1	EZR	MYH14	SEPTIN9	
CHMP4B	FLNA	MYH9	SERPINH1	
CNN2	FN1	MYOF	SFXN1	
CORO1A	G3BP1	NSUN2	SQOR	

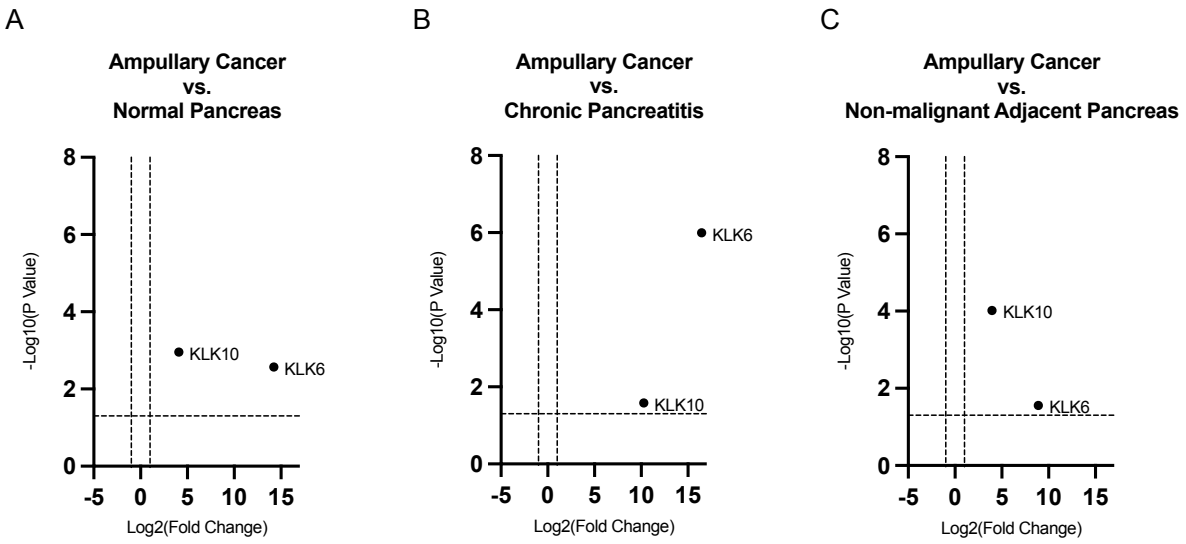

Figure S 26: Volcano Plots on KLK protein level comparing Ampullary Cancer with tissues of Normal Pancreas, Non-malignant Adjacent Pancreas, and Chronic Pancreatitis. The data is normalized to heavy labelled reference peptides. Black dots represent KLK6 or KLK10 protein. X-axis shows the Log2 Fold Chance in protein expression and y-axis represents the adjusted p-value in -log10 scale. Horizontal dashed line represents the adjusted p-value threshold of P value=0,05, whereas the vertical dashed line represents a Fold Change threshold for 2-fold abundance change.

11 ACKNOWLEDGEMENTS

First and foremost, I would like to thank Professor Dr. Felix Rückert for the opportunity to perform my doctoral thesis on this very exciting and interesting topic and for his detailed introduction to the kallikrein biology. I would like to express my sincere thanks to Professor Dr. Oliver Schilling for the opportunity to perform my work at his laboratory, where he warmly welcomed me into his working group. I am very grateful for his excellent guidance and support over the entire time. I have learned a lot from all our talks and discussions which have inspired my scientific work.

I would especially like to thank my supervisor Patrick Bernhard. I am very grateful for his excellent introduction to the laboratory work, the active support in the bioinformatic evaluation of the data and guidance at all times, never losing patience. He always had an open ear for my ideas and questions, which I very much appreciate. I really enjoyed learning from and working with him and I thank him for everything he has taught me.

I also want to gratefully thank the entire AG Schilling for all the mutual motivation talks and the positive working atmosphere around the laboratory, it was a lot of fun and an honor to be part of your group.

Finally, I would like to thank my family and friends for their never-ending support and encouragement throughout the whole time of my thesis.